Atg21 functions during autophagy as a scaffold for the E3 ubiquitin-like complex in Atg8 lipidation

Dissertation

for the award of the degree
"Doctor rerum naturalium"
of the Georg-August-University Göttingen

within the doctoral program "Molecular Biology of Cells"
of the Georg-August-University School of Science (GAUSS)

submitted by
Lisa Angelika Juris
from Hamm (Westf.)

Göttingen, 2013

Member of the Thesis Committee (First Reviewer):
Prof. Dr. Michael Thumm
Department of Molecular Cellbiology
Center for Biochemistry and Molecular Cell Biology
Georg-August-Universität, Göttingen

Member of the Thesis Committee (Second Reviewer):
Prof. Dr. Volker Lipka
Department of Plant Cell Biology
Schwann-Schleiden Centre
Georg-August-Universität, Göttingen

Member of the Thesis Committee:
Dr. Karin Kühnel
Department of Neurobiology
Max Planck Institute for Biophysical Chemistry, Göttingen

Date of oral examination: 05.02.2014

Affidavit:

Herewith I declare, that I prepared this thesis on my own and with no other sources and aids than quoted.

Lisa Angelika Juris

Contents

1 SUMMARY **1**

2 INTRODUCTION **4**

2.1 The yeast *Saccharomyces cerevisiae* as a model organism **4**

2.2 Autophagy **5**

2.2.1 Microautophagy 5

2.2.2 Macroautophagy 6

2.2.3 The Cytoplasm-to-Vacuole (Cvt) Pathway 7

2.2.4 The pre-autophagosomal structure (PAS) 8

2.2.4.1 The Atg1 kinase complex 9

2.2.4.2 The Atg9-containing vesicles 10

2.2.4.3 The Atg14-containing phosphoinositide 3-kinase complex 13

2.2.4.4 The Atg12- and Atg8-conjugating system 14

2.2.4.5 The Atg2-Atg18 complex 17

3 MATERIALS AND METHODS **21**

3.1 Material **21**

3.1.1 *Saccharomyces cerevisiae* strains 21

3.1.2 *Escherichia coli* strains 23

3.1.3 Plasmids 23

3.1.4 Oligonucleotides 26

3.1.5 Media 30

3.1.5.1 YPD-medium, pH 5.5 30

3.1.5.2 CM-medium, pH 5.6 30

3.1.5.3 SD(-N)-medium 31

3.1.5.4 LB-medium, pH 7.5 31

3.1.5.5 SOC-medium, pH 7.5 31

3.1.6 Antibodies 31

3.1.7 Commercial available Kits 32

3.1.8 Chemicals and consumables 32

3.1.9 Equipment 34

3.2 Cultivation of *S. cerevisiae* **35**

3.2.1 Growth of liquid yeast cultures 35

3.2.2 Short-term storage 35
3.2.3 Long-term storage 36
3.2.4 Cell density determination 36
3.2.5 Split-ubiquitin assay 36

3.3 Cultivation of *E. coli* cultures 36
3.3.1 Growth of liquid *E. coli* cultures 36
3.3.2 *E. coli* short-term storing 36
3.3.3 *E. coli* long-term storing 37
3.3.4 Preparation of electrocompetent *E. coli* cells 37

3.4 Microscopy 37
3.4.1 Fluorescence microscopy 37
3.4.2 Bimolecular Fluorescence Complementation (BiFC) 38
3.4.3 Determination of colocalization rates 39

3.5 Molecular biology methods 39
3.5.1 Isolation of chromosomal DNA 39
3.5.2 High efficiency transformation of DNA in yeast 40
3.5.3 "Quick and Dirty" transformation of plasmid-DNA in yeast 40
3.5.4 Transformation of plasmid-DNA into *E. coli* 41
3.5.5 Plasmid-DNA isolation from *E. coli* 41
3.5.6 DNA agarose gel electrophoresis 41
3.5.7 DNA gel extraction (Gel Extraction Kit) 42
3.5.8 Polymerase chain reaction 42
3.5.9 Molecular cloning 42
3.5.10 Plasmid construction 43
3.5.10.1 Plasmid constructs used in split-ubiquitin assay 43
3.5.10.2 Plasmid constructs for BiFC 44
3.5.10.3 Atg16 plasmid constructs 45
3.5.11 Site-directed mutagenesis of plasmids 46
3.5.12 Sequencing of DNA 46
3.5.13 Gene deletion using homologous recombination 46

3.6 Biochemical methods 47
3.6.1 SDS-Polyacrylamide-Gel-Electrophorese (SDS-PAGE) 47
3.6.2 Western Blot analysis 48
3.6.3 Colloidal Coomassie staining 49
3.6.4 Determination of protein concentrations 50
3.6.5 Alkaline lysis of yeast cells 50
3.6.6 Cell lysis for detection of Atg8-PE 50

3.6.7 Preparation of whole cell extracts – the mild cell lysis procedure 51
3.6.8 GFP-TRAP® 51
3.6.9 Gelfiltration chromatography 52
3.6.10 Density gradient centrifugation 53
3.6.11 Pull down of His-SUMO-Atg21 53
3.6.11.1 Purification of recombinant 6xHis-SUMO-Atg21 and 6xHis-SUMO 53
3.6.11.2 6xHis-SUMO-Atg21 pull down with crude yeast cell extract 54
3.6.11.3 Purification of GST-Atg16 55
3.6.11.4 6xHis-SUMO-Atg21 pull down with recombinant proteins 55
3.6.12 Mass spectrometry analysis 56
3.6.12.1 Materials 56
3.6.12.2 In-gel digestion 56
3.6.12.3 Peptide extraction 56
3.6.12.4 Mass spectrometric analysis 57
3.6.12.5 Database Searching 57

4 RESULTS 58

4.1 Aim of the study 58

4.2 Localization studies of Atg21 58
4.2.1 Part of Atg21-YFP was detected at the PAS 58
4.2.2 Atg21 is not transported into the vacuole 63

4.3 Identification of interaction partner of Atg21 65
4.3.1 Atg21 is part of a high molecular weight complex 65
4.3.1.1 Gelfiltration analysis of Atg21 65
4.3.1.2 Sorbitol density gradient centrifugation 69
4.3.2 Pull down und mass spectrometry analysis to identify potential Atg21 interaction partner 72
4.3.3 Split-ubiquitin analysis of Atg21 75
4.3.4 Interaction studies of Atg21 und At27 76
4.3.4.1 Atg27 and Atg21 interact with each other in split-ubiquitin assay 77
4.3.4.2 Atg21 and Atg27 colocalized in direct fluorescence microscopy 80
4.3.4.3 Analysis of the potential interaction of Atg21 and Atg27 by pull down and GFP-TRAP® 82
4.3.5 Interaction studies of Atg21 und Atg8 84
4.3.5.1 Bimolecular Fluorescence Complementation (BiFC) analysis 85
4.3.5.2 Is Atg8 part of the Atg21 high molecular weight complex detected in gelfiltration? 92

4.3.6 Interaction studies of Atg21 und Atg16 94
4.3.6.1 Atg21 and Atg16 interact with each other in the split-ubiquitin assay 94
4.3.6.2 Fluorescence microscopy analysis of Atg5 and Atg16 96
4.3.6.3 Interaction studies of Atg16 and Atg21 using pull down and GFP-TRAP® analysis 100
4.3.6.4 Determination of the Atg21- interacting domain of Atg16 102

5 DISCUSSION 111

5.1 Part of Atg21 localizes to the PAS 112

5.2 Atg21 is located on the outer autophagosomal membrane 118

5.3 Atg21 is part of a high molecular weight complex 120

5.4 Identification of Atg21 interaction partner 122

5.5 Interaction studies of Atg21 and Atg27 124

5.6 Interaction studies of Atg21 and Atg8 127

5.7 Interaction studies of Atg21 and Atg16 130

6 BIBLIOGRAPHY 141

7 ACKNOWLEDGEMENT 151

8 CURRICULUM VITAE ERROR! BOOKMARK NOT DEFINED.

List of Figures

Figure 1: Life cycle of *Saccharomyces cerevisiae* **4**
Figure 2: Scheme of macroautophagy and the Cvt-pathway **7**
Figure 3: Scheme of the Atg1 kinase complex **10**
Figure 4: Atg9-containing vesicles contribute in membrane dynamics in autophagy **11**
Figure 5: Model of the Atg23-Atg9-Atg27 complex **12**
Figure 6: Vps34 is present in two complexes required for different cellular processes **13**
Figure 7: The two ubiquitin-like protein conjugation machineries in autophagy **14**
Figure 8: Structure of *Kluyveromyces lactis* Hsv2 **18**
Figure 9: Scheme of semi dry Western Blot setting **48**
Figure 10: Scheme of Wet Western Blot settings **49**
Figure 11: Part of Atg21 is localized at the PAS **60**
Figure 12: Additional analysis of the PAS localization of Atg21-YFP **61**
Figure 13: Complementation study of mCherry-Atg21 by monitoring ApeI maturation and determination of its PAS rate. **62**
Figure 14: mCherry-Atg21 is not transported into the vacuole **64**
Figure 15: Atg21-TAP was present in a sensitive high molecular weight complex in gelfiltration **66**
Figure 16: Alternative mild cell lysis procedure keeps the sensitive high molecular weight Atg21 complex intact **68**
Figure 17: The high molecular weight Atg21 complex could not be detected after glycerol density gradient centrifugation **69**
Figure 18: mCherry-Atg21 is present as a high molecular weight complex in sorbitol density gradient centrifugation **71**
Figure 19: Pull down analysis of SUMO-Atg21 **73**
Figure 20: Scheme of the principle of the split-ubiquitin assay **75**
Figure 21: An interaction of Atg27 and Atg21 in split-ubiquitin assay was detected **77**
Figure 22: Interaction analysis of truncated Atg27 in split-ubiquitin assay **79**
Figure 23: mCherry-Atg21 and Atg27-GFP colocalized in direct fluorescence microscopy **81**
Figure 24: Atg27 does not specifically interact with Atg21 in pull down and GFP-TRAP® experiments **83**
Figure 25: Atg21 and Atg8 interact with each other in split-ubiquitin assay **85**
Figure 26: Bimolecular Fluorescence Complementation (BiFC) analysis of Atg8 and Atg21 **87**
Figure 27: BiFC study of MET25-Atg21 C-YC and ADH-N-YN Atg8 **89**
Figure 28: BiFC study of MET25 Atg21 C-YC and MET25 N-YN Atg8 **91**
Figure 29: Atg8 distribution in gelfiltration was not changed in the absence of Atg21 **93**
Figure 30: Atg16 and Atg21 interact in the split-ubiquitin assay **95**
Figure 31: Atg5 and Atg16 are absent from the PAS in growing *atg8Δ atg21Δ* cells **97**

Figure 32: Atg16 and Atg21 colocalize in the absence of Atg5 99
Figure 33: Interaction studies of Atg16 and Atg21 using GFP-TRAP® and pull down experiments 101
Figure 34: Atg21 interacts with the coiled-coil domain of Atg16 103
Figure 35: Fluorescence microscopic analysis of the Atg16-GFP point mutants 105
Figure 36: Amino acids D101 and E102 of Atg16 mediate the interaction with Atg21 107
Figure 37: Functional analysis of the Atg16 point mutants 109

List of Tables

Table 1: Yeast strains used in this study 21
Table 2: *E. coli* strains used in this study 23
Table 3: Plasmids used in this study 23
Table 4: Oligonucleotides used in this study 26
Table 5: Antibodies used in this study 31
Table 6: Commercial available Kits used in this study 32
Table 7: Special chemicals 33
Table 8: Equipment used in this study 34
Table 9: Overview of the used filter sets in fluorescence microscopy 38
Table 10: Contents of the separating gel 47
Table 11: Contents of the stacking gel 47
Table 12: Densities of the glycerol or sorbitol solutions used in density gradient centrifugation 53

List of Equations

Equation 1: Equation to calculate optimal plasmid-insert ratio in ligation mix 43

Abbreviation	
-	without
°C	Degree in Celsius
A	Ampere
aa	Amino acid(s)
ade	Adenine
ADH	Alcohol dehydrogenase
AIM	Atg8-interacting motif
Arg	Arginine
ApeI	Aminopeptidase I
APS	Ammonium persulfate
Atg	Autophagy-related protein
BiFC	Bimolecular Fluorescence Complementation
ccd	coiled-coil domain
CM medium	Complete minimal medium
CPY	Carboxypeptidase C
Cub	C-terminal part of ubiquitin
Cvt	Cytoplasm-to-Vacuole
DNA	Desoxyribonucleic acid
DTT	Dithiothreitol
E. coli	*Escherichia coli*
EDTA	Ethylenediamintetraacetate-disodium salt
eYFP	enhanced YFP
FOA	5-Fluoroorotic Acid
g	gram
g	Gravity
GFP	Green fluorescent protein
Gly	Glycine
GST	Glutathione-S-transferase
h	hour
HA	Human influenza hemagglutinin
His	Histidine
HRPO	Horsereddish peroxidase

IPTG	Isopropyl-α-D-thiogalactopyranoside
KAN	Kanamycin
kDa	kilodalton
l	liter
LB	Lysogeny broth
Leu	Leucine
LIR	LC3-interacting region
Lys	Lysine
M	molar
m	mature
m	meter
m	milli
mCherry	monomeric Cherry
met	Methionine
min	minute
N	Nitrogen
n	nano
NatNT2	Nourseotricine
Nui	N-terminal part of ubiquitin
OD_{600}	Optical density (600 nm)
PAS	Pre-autophagosomal structure
PE	Phosphatidylethanolamine
PGK	Phosphoglycerate kinase
pH	negative logarithm of H^+ concentration
Phe	Phenylalanine
PI3P	Phosphatidylinositol 3-phosphate
$PI(3,5)P_2$	Phosphatidylinositol 3,5-bisphosphate
PMN	Piecemeal Microautophagy of the Nucleus
PMSF	Phenylmethylsulfonylfluoride
pr	Precursor
PROPPIN	β-propeller that binds polyphosphoinositides
RFP	Red fluorescent protein
rpm	round per minute

RT	Room temperature
s	second
S. cerevisiae	*Saccharomyces cerevisiae*
SD	Synthetic defined
SDS	Sodium dodecyl sulfate
TAP	Tandem Affinity Purification
TCA	Trichloroacetic acid
TORC1	Target of Rapamycin Complex 1
Trp	Tryptophan
Ura	Uracile
v/v	volume per volume
V	volt
w/v	weight per volume
WT	Wild type
YC	C-terminal part of eYFP
YFP	Yellow fluorescent protein
YN	N-terminal part of eYFP
YPD	Yeast peptone dextrose
µ	micro
β-ME	Beta mercaptoethanol

1 Summary

Autophagy summarizes a family of intracellular lysosomal (vacuolar) degradative transport process. It is used for the removal and recycling of cytoplasm, protein aggregates and organelles to maintain cellular homeostasis. During macroautophagy in yeast, the double membrane layered transport vesicles (autophagosomes) are formed at the pre-autophagosomal structure (PAS). They finally fuse with the vacuole for degradation and recycling of their contents. Beside this unselective degradation of bulk cytoplasm including organelles, there are several selective types of autophagy. In yeast, the Cytoplasm-to-vacuole (Cvt) pathway selectively transports the hydrolases α-mannosidase, proaminopeptidase I and aspartyl aminopeptidase to the vacuole under nutrient rich conditions.

A hallmark of autophagy is the use of two ubiquitin-like conjugation systems. One covalently couples the ubiquitin-like Atg12 to Atg5. The resulting Atg12-Atg5 conjugate forms a complex with Atg16 that acts as an E3-like enzyme in the second ubiquitin-like conjugation reaction, which couples Atg8 to the head group of the membrane lipid phosphatidylethanolamine (PE). Atg16 specifies the lipidation site, but how it selectively recognizes and binds to the PI3P-positive PAS remained unclear.

In this study, the localization and function of Atg21 was investigated using the model organism *Saccharomyces cerevisiae*. Atg21 forms a WD40 propeller that is peripherally membrane associated by binding to PI3P and PI(3,5)P_2. So far, Atg21 has only been detected at endosomal compartments and at vertices of vacuolar junctions. Atg21 is required for selective types of autophagy as the Cvt pathway and efficient bulk macroautophagy. In the absence of Atg21 no Cvt vesicles are formed, suggesting a fundamental role for Atg21 in the PAS assembly especially during selective types of autophagy. Indeed, growing *atg21Δ* cells fail to efficiently lipidate Atg8 and to recruit Atg8 and Atg5 to the PAS. Since Atg21 has not been detected at the PAS so far, its precise molecular function during autophagy remained elusive.

Using direct fluorescence microscopy, this study revealed, for the first time, that part of Atg21 is also present at the PAS. The presence of Atg21 at the PAS is dependent on Atg14 and therefore on the PAS-specific PI3P pool. Moreover, it could be shown in this study, that Atg21 recruits the Atg12-Atg5/Atg16 complex to the PAS via direct interaction with Atg16. Two conserved surface residues within the coiled-coil domain of Atg16 (D101 and E102) were identified to specifically bind Atg21. Thereby the underlying mechanism of Atg16-mediated recruitment of the Atg12-Atg5/Atg16 complex to autophagosomal membranes has been elucidated in this study. More importantly, it was shown, that the interaction of Atg21 and Atg16 was not only a prerequisite for the proper PAS localization of the Atg12-Atg5/Atg16 complex but also for its autophagic function. Consequently, interaction of Atg16 and Atg21 is needed for efficient Atg8 lipidation.

Importantly, this study also revealed that Atg21 and Atg8 probably interact with each other. This interaction occurred with unlipidated Atg8, suggesting, that Atg21 not only mediates the membrane association of the E3 enzyme Atg12-Atg5/Atg16, but also acts as a scaffold for Atg8 lipidation reaction. Therefore, Atg21 represents the missing link that mediates PI3P-dependent PAS association of the lipidation machinery by recruiting the activated substrate Atg8 and the E3 enzyme required for the transfer of Atg8 to PE. Atg21 thus represents a key factor to specify the lipidation site. This model provides a reasonable explanation for the elementary function of Atg21 in Cvt vesicle formation.

By using gelfiltration chromatography and sorbitol gradient density centrifugation Atg21 was identified as part of a high molecular weight complex. This Atg21 complex is very sensitive to the cell lysis procedure and buffer conditions. Therefore, a mild cell lysis procedure was established to keep the sensible complex intact as a prerequisite not only for further analysis of the complex but also for the identification and verification of additional potential Atg21 interacting proteins.

Pull down experiments and following mass spectrometry analysis identified the target of rapamycin complex I (TORC1) as potential interaction partner of Atg21.

It is already known, that the kinase activity of TORC1 negatively regulates autophagy.

A specific interaction of Atg21 with the type I membrane protein Atg27 but with no other member of the trimeric Atg27-Atg9-Atg23 complex was detected using the split-ubiquitin system. Moreover, it could be suggested that Atg21 interacted with the cytosol-facing C-terminal part of Atg27. In addition, using direct fluorescent microscopy it could be shown here that a considerable part of Atg21 colocalized with Atg27, supporting a potential interaction. The relevance of this putative interaction will be topic of further studies.

2 Introduction

2.1 The yeast *Saccharomyces cerevisiae* as a model organism

The eukaryotic organism *Saccharomyces cerevisiae* belongs to the family of the budding yeasts. It is a unicellular organism and has a round to oval shape with 5 to 10 µm in diameter. *S. cerevisiae* has a simple life cycle (Figure 1). It can exist in a either haploid or diploid form. Both forms grow by mitosis and budding and are able to double in about 100 min, when exposed to sufficient nutrients. Under nutrient-deficient conditions, diploid cells undergo meiosis to produce an ascus containing four haploid spores. After a change in nutrient conditions, the spores can grow as haploid cells. Two haploid cells with different mating type (a and α) can mate to form a diploid cell.

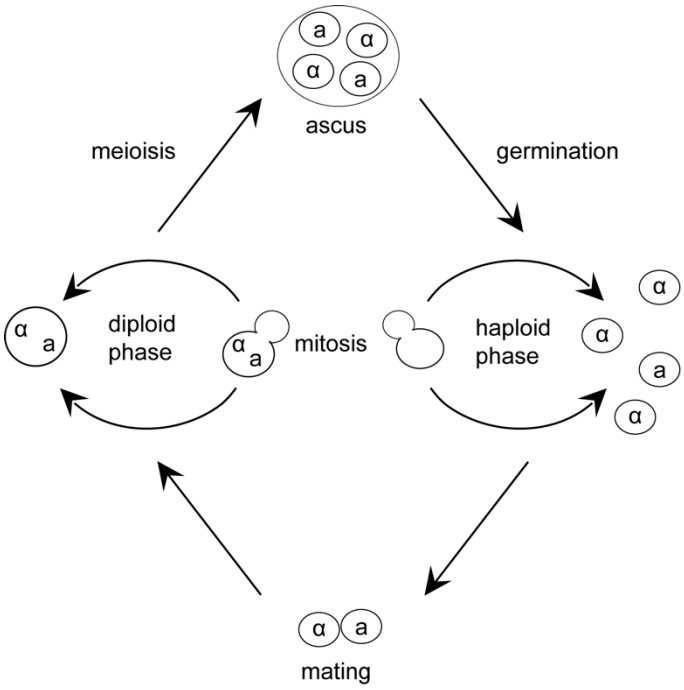

Figure 1: Life cycle of *Saccharomyces cerevisiae*

Using *S. cerevisiae* as a model organism, it can be grown on defined media to control its chemical and physical environment. The *S. cerevisiae* genome is fully sequenced. A haploid cell harbors a set of 16 chromosomes coding for about 6000 genes (Goffeau et al., 1996). In the last decades, efficient techniques have been developed, that easily enable a modification or deletion of a target allele

with absolute precision (Goffeau et al., 1996; Janke et al., 2004; Knop et al., 1999; Longtine et al., 1998; Wach et al., 1997; Wach et al., 1994). Most of the proteins in *S. cerevisiae* are highly conserved and information obtained in yeast can often be transferred to higher eukaryotes making the baker`s yeast *S. cerevisiae* to an ideal and favored model organism in genetic and biochemical research.

2.2 Autophagy

Autophagy describes a specific transport mechanism to the degradative organelle within a cell. It is highly conserved among all eukaryotes and primarily protects cells under stress conditions. Under starvation conditions, the unspecific degradation of cytoplasm and organelles produces free amino and fatty acids, which are subsequently used for the synthesis of new proteins or as energy source. In addition to cellular homeostasis, autophagy plays a crucial role in several physiological processes as autophagic programmed cell death, organelle homeostasis, developmental processes, ageing, immunity and defense against microbial invasion (Chen and Klionsky, 2011). Autophagy is also involved in several human pathophysiologies such as cancer, myopathies, neurodegeneration, heart and liver diseases and gastrointestinal disorders (Choi et al., 2013). In yeast, autophagy can be divided into two major groups: microautophagy and macroautophagy.

2.2.1 Microautophagy

During microautophagy a cargo is directly engulfed by the vacuolar membrane. In *S. cerevisiae*, micronucleophagy or piecemeal microautophagy of the nucleus (PMN) is one specific variant of microautophagy (Krick et al., 2008b). During PMN non-essential portions of the nucleus are directly sequestrated and degraded by the vacuole. PMN occurs at nucleus-vacuole (NV) junctions, which are generated by the interaction of the vacuolar membrane protein Vac8 and the outer nuclear membrane protein Nvj1 (Pan et al., 2000; Roberts et al., 2003). Nvj1 additionally recruits Tsc13 and Osh1, both involved in lipid metabolism, to the NV junctions (Kvam and Goldfarb, 2007). Upon starvation, the NV junctions bud into invaginations at the vacuolar membrane to create a PMN vesicle. This PMN vesicle is released into the vacuolar lumen after fusion of the nuclear and the vacuole membrane and finally degraded by vacuolar hydrolases (Krick et al.,

2008b). Three membranes limit a PMN vesicle; the two inner membranes originate from the nuclear envelope, the outermost membrane from the vacuole membrane (Krick et al., 2008b). PMN requires both, core components of the macroautophagic machinery and components of the selective autophagic machinery, defining PMN as a novel variant of selective microautophagy (Krick et al., 2008b; Roberts et al., 2003). Interestingly, PMN does not require the homotypic vacuole fusion machinery, suggesting a crucial role for the autophagic machinery in the terminal engulfment and fusion stages of PMN (Krick et al., 2008b).

2.2.2 Macroautophagy

In contrast to microautophagy, macroautophagy is characterized by the formation of double-membrane layered transport vesicles at the pre-autophagosomal structure (PAS). In yeast, the formation of the transport vesicles starts with a cup-shaped membrane, the phagophore, which expands and finally closes to form a double-membrane layered transport vesicle, named autophagosome (Yorimitsu and Klionsky, 2005) (Figure 2). The origin of the membranes for autophagosome biogenesis is still under debate and there are several organelles discussed as possible sources such as the plasma membrane, the endoplasmatic reticulum, the Golgi apparatus, endosomes or mitochondria (Lynch-Day et al., 2010; Mari et al., 2010; Taylor et al., 2012; Yamamoto et al., 2012). Due to the extensive need of membranes during autophagy, most probably different rather than one single organelle might serve as a membrane source.

The outer membrane of the autophagosome fuses with the vacuolar membrane to release a still one membrane-layered vesicle, the autophagic body, into the vacuole (Baba et al., 1994). This fusion event depends on the homotypic vacuolar fusion machinery (Ishihara et al., 2001). Within the vacuole, the membrane of the autophagic body is lysed and the cargoes are subsequently degraded or processed by vacuolar hydrolases. Under normal growth conditions macroautophagy acts as constitutive process at a low level, but it is strongly upregulated under stress conditions as nutrient or energy starvation (Parzych and Klionsky, 2013; Yorimitsu and Klionsky, 2005).

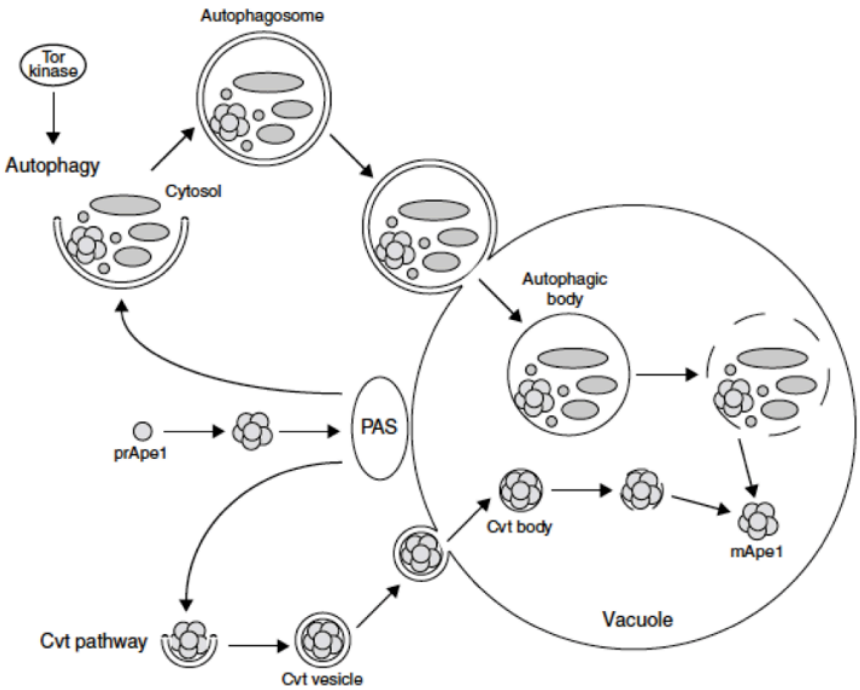

Figure 2: Scheme of macroautophagy and the Cvt-pathway (Yorimitsu and Klionsky, 2005)

The term macroautophagy is often used for the unselective degradation of bulk cytoplasm including organelles. There are also several selective variants of autophagy for the specific degradation of superfluous or damaged organelles as mitochondria (mitophagy), peroxisomes (pexophagy), endoplasmatic reticulum (reticulophagy) and ribosomes (ribophagy) (He and Klionsky, 2009). In general, selective macroautophagy is characterized by the use of a receptor protein, which links the cargo to the autophagic machinery (Mijaljica et al., 2012). In addition, the transport vesicles are specifically formed around a particular cargo und exclude therefore cytoplasm or unspecific components (Reggiori and Klionsky, 2013).

2.2.3 The Cytoplasm-to-Vacuole (Cvt) Pathway

In yeast, the Cytoplasm-to-Vacuole (Cvt) pathway displays another selective variant of autophagy and represents the constitutive transport of the hydrolases α-mannosidase I (AmsI), the aspartyl aminopeptidase (Ape4) and aminopeptidase I (ApeI) to the vacuole (Harding et al., 1995; Hutchins and Klionsky, 2001; Yuga et al., 2011). ApeI is synthesized as a precursor form with a N-terminal propeptide (prApeI) in the cytosol, where it forms a dodecameric complex. The propeptide mediates the formation of prApeI dodecamers into a

large oligomeric structure (ApeI-complex) and also binds to the cargo receptor Atg19, which links the ApeI-complex to the autophagic machinery at the PAS (Chang and Huang, 2007; Morales Quinones et al., 2012; Scott et al., 2001; Shintani and Klionsky, 2004; Yorimitsu and Klionsky, 2005). In addition, Atg19 binds to the additional cargoes AmsI and Ape4, allowing them to use the ApeI transport system (Shintani et al., 2002; Yuga et al., 2011). prApeI, Atg19, AmsI and Ape4 are packed into a sequestering vesicle called Cvt vesicle, that is significantly smaller in size compared to autophagosomes and exclude cytoplasm. The Cvt vesicle is transported to the vacuole, where prApeI is processed by cleavage of its propeptide to generate the matured and active form of ApeI (mApeI) (Klionsky et al., 1992; Morales Quinones et al., 2012; Scott et al., 1997; Scott et al., 1996; Shintani et al., 2002; Suzuki, 2012) (Figure 2). mApeI still forms dodecamers, but due to the lack of the propeptide, does not form the ApeI complex in the vacuole (Morales Quinones et al., 2012). The Cvt pathway is a constitutive transport mechanism and takes place under growing conditions (Scott et al., 1997). As a selective form of autophagy, it relies on the same core autophagy related proteins like macroautophagy and additionally requires some specific proteins. Therefore, information obtained in selective types of autophagy, can often be transferred to other autophagic pathways (Lynch-Day and Klionsky, 2010; Morales Quinones et al., 2012).

2.2.4 The pre-autophagosomal structure (PAS)

The pre-autophagosomal structure (PAS) is defined as that site within a cell, where the formation of the autophagosomes and Cvt vesicles is initiated (Suzuki et al., 2001; Suzuki et al., 2007). Yeast cells usually have one PAS, located near the vacuole under both normal and starvation conditions. Most of the autophagy-related proteins, termed Atg, are at least partially localized to the PAS (Klionsky et al., 2003; Suzuki et al., 2007) In yeast, more than 30 Atgs are known. Among them, 18 proteins belong to the core autophagic machinery, characterizing those proteins required for both macroautophagy and its selective variants (Araki et al., 2013; Motley et al., 2012; Suzuki, 2012; Suzuki and Ohsumi, 2010). These proteins are recruited to the PAS in a specific hierarchy (Suzuki et al., 2007) and are commonly classified into six functional groups: I) the Atg1 kinase complex

II) the Atg9-containing vesicles III) the Atg14-containing phosphoinositides 3-kinase complex IV) the Atg12-conjugating system V) the Atg8-conjugating system and VI) the Atg2-Atg18 complex.

2.2.4.1 The Atg1 kinase complex

The Atg1 kinase complex serves as a basic scaffold structure for the PAS assembly and is required for the recruitment of further autophagy-related proteins. Atg1 is the solely serine/threonine kinase involved in autophagy (Matsuura et al., 1997). Besides Atg1 itself, no other target for the kinase has been identified so far. Atg1 directly interacts with its regulator Atg13, what enhances its kinase activity (Kamada et al., 2000). Atg1 and Atg13 probably exhibit a core regulator function at an early step in autophagy induction (Reggiori and Klionsky, 2013). The Atg13-Atg1 complex itself is regulated by nutrients. Under nutrient-rich conditions, Atg13 and Atg1 are highly hyperphosphorylated (Scott et al., 2000). The phosphorylation is partly mediated by the nutrient sensors Target of rapamycin complex 1 (TORC1) and/or protein kinase A (PKA) (Budovskaya et al., 2005; Kamada et al., 2010; Yorimitsu et al., 2009). The kinase TORC1 acts as a negative regulator of autophagy. It is active under nutrient-rich conditions and inhibits autophagy. Upon starvation it is inactivated and autophagy is induced. Since TORC regulates Atg13 phosphorylation, Atg13 becomes rapidly dephosphorylated upon autophagy induction (Loewith and Hall, 2011; Scott et al., 2000). For yeast, it was originally reported that the phosphorylation of Atg13 leads to a reduced Atg1 binding affinity, preventing the Atg1 kinase activity under nutrient-rich conditions (Kamada et al., 2000). However, recent studies revealed, that Atg1 and Atg13 might interact constitutively with each other, independent of the nutrient conditions (Kraft et al., 2012). This model would fit nicely with results from higher eukaryotes and indicates that the phosphorylation of yeast Atg1 and most likely Atg13 rather than their interaction is essential for Atg1 activity (Kraft et al., 2012). In general, Atg1 has a dual role in autophagy. Atg1 mutants defective in Atg13 binding, fail to efficiently assemble the PAS under starvation conditions, suggesting a scaffold function for Atg1 at the PAS. In contrast, Atg1 kinase mutants assemble the PAS but are defective in Atg protein dissociation

kinetics (Cheong et al., 2008). Thus, the Atg1 kinase activity is probably involved in later steps of autophagy.

In addition to Atg1 and Atg13, the Atg1 kinase complex includes the ternary Atg17-Atg31-Atg29 complex and also Atg11, Atg20 and Atg24 (Figure 3).

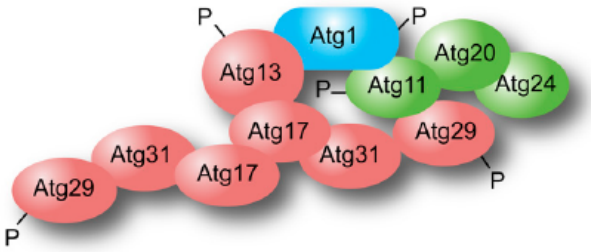

Figure 3: Scheme of the Atg1 kinase complex (Reggiori and Klionsky, 2013)

So far, it is not known, if all of these proteins are present in the complex at the same time or if there are subcomplexes that vary in their composition depending on nutrient conditions (Inoue and Klionsky, 2010). Atg17 acts as a central component in PAS assembly under autophagy-inducing conditions (Cheong et al., 2008; Suzuki et al., 2007). It forms a constitutive complex with Atg29 and Atg31 (Kabeya et al., 2009; Kawamata et al., 2008). In addition, self-interaction of Atg17 leads to a stable dimeric Atg17-Atg29-Atg31 complex, which is probably recruited to the PAS under both, nutrient-rich condition and starvation (Chew et al., 2013; Ragusa et al., 2012). Atg17 also enhances the Atg1 kinase activity by an unknown mechanism (Kamada et al., 2000). Atg17 is essential for PAS assembly during macroautophagy, but not for selective types of autophagy. For selective types of autophagy, Atg11 adopts the function of Atg17 and acts as a scaffold protein that directs further Atg proteins to the PAS (Suzuki et al., 2007). However, though involved in the formation of the starvation-specific PAS, Atg11 is not required for bulk autophagy. Atg11 also serves as an adaptor for selective autophagic cargoes at the PAS by binding receptor proteins involved in selective autophagy such as Atg19 (Cvt pathway) and Atg32 (mitophagy) (Mijaljica et al., 2012).

2.2.4.2 The Atg9-containing vesicles

Among the core autophagy machinery, Atg9 is the sole integral membrane protein. It contains six membrane-spanning domains, its C- and N-terminus

facing the cytosol (Legakis et al., 2007). Atg9 is one of the first proteins recruited to the PAS (Suzuki et al., 2007). It cycles between the PAS and a non-PAS pool and was reported to directly participate in the phagophore formation (Legakis et al., 2007; Mari et al., 2010; Yamamoto et al., 2012). At the non-PAS pool, Atg9 resides in tubular and vesicular structures. These Atg9 reservoirs consist of clustered 20-30 nm vesicles and are often located close to mitochondria. In yeast, they derive from Golgi-related secretory and endosomal pathways, but their origin is still under debate (Mari et al., 2010; Ohashi and Munro, 2010; Yamamoto et al., 2012). At the PAS, Atg9 interacts with the Atg1 kinase complex by direct interaction with the scaffold proteins Atg17 and/or Atg11 (He et al., 2006; Sekito et al., 2009). In addition, Atg1 contains a C-terminal EAT (early autophagosome targeting/tethering) region that has been reported to selectively bind highly curved 20-30 nm vesicles and to be capable of tethering them (Ragusa et al., 2012). In the current model, the Atg9 containing vesicles are brought together at the PAS mediated by lipid binding of Atg1 and additional protein interaction with Atg17. The vesicles then fuse in a probably SNARE- and the tethering proteins Ypt1 and Trs85-dependent manner to form the phagophore, that finally expands to an autophagosome (Kakuta et al., 2012; Lipatova et al., 2012; Lynch-Day et al., 2010; Ragusa et al., 2012) (Figure 4).

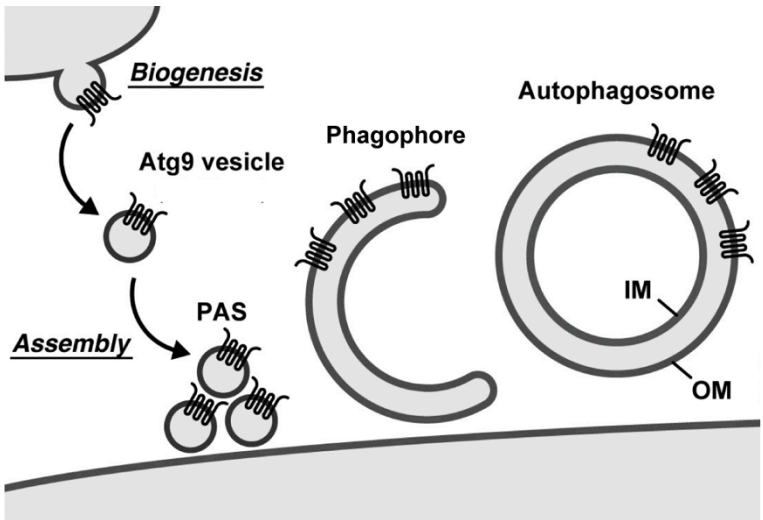

Figure 4: Atg9-containing vesicles contribute in membrane dynamics in autophagy

(IM=inner autophagosomal membrane; OM=outer autophagosomal membrane) ((Yamamoto et al., 2012); modified)

However, quantitative fluorescence microscopy revealed that only three Atg9 vesicles contribute to the formation of a single autophagosome during starvation (Yamamoto et al., 2012). Based on the reported small diameter of these vesicles, most likely essential amounts of the phagophore lipids derive from other membrane sources (Stanley et al., 2013). Atg9 vesicles are translocated to the PAS immediately after assembly of the scaffold complex, but before recruitment of further Atg protein. Therefore, Atg9 may play a crucial role in a very early step of autophagosome formation such as nucleation of the phagophore or recruitment of other Atg proteins to the PAS (Yamamoto et al., 2012).

The peripherally membrane associated protein Atg23 and the type I membrane protein Atg27 form a trimeric complex with Atg9 that links both proteins (Legakis et al., 2007) (Figure 5). Interestingly, Atg9 belongs to the core autophagy machinery, but Atg27 is only essential for the Cvt pathway (Legakis et al., 2007; Yen et al., 2007).

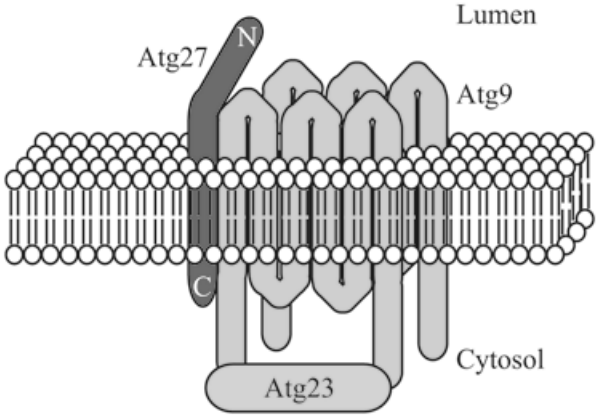

Figure 5: Model of the Atg23-Atg9-Atg27 complex ((Legakis et al., 2007); modified)

As Atg9, Atg23 and Atg27 cycle between the non-PAS pool and the PAS and the cycling of all three proteins depends upon one another. Atg23 and Atg27 are essential for both, transport of Atg9 vesicles from the Golgi to its reservoir (Ragusa et al., 2012; Stanley et al., 2013; Yamamoto et al., 2012) and from its reservoir to the PAS (Legakis et al., 2007). After autophagosome formation, Atg9 clusters on the outer membrane of the autophagosomes and recruits the Atg2-Atg18 complex, which mediates together with Atg1 the Atg9 recycling by an unknown mechanism (Ragusa et al., 2012; Stanley et al., 2013; Yamamoto et al., 2012).

2.2.4.3 The Atg14-containing phosphoinositide 3-kinase complex

The yeast *S. cerevisiae* has only one phosphoinositide 3-kinase, named Vps34, which specifically phosphorylates phosphoinositides at the D-3 position of the inositol ring to create phosphatidylinositol-3-phosphate (PI3P) (Schu et al., 1993). Vps34 is present in two distinct complexes, which share the subunits Vps34, Vps15 and Atg6. Each complex additionally contains a unique factor, which specifies the localization and cellular function of the respective complex (Kihara et al., 2001) (Figure 6).

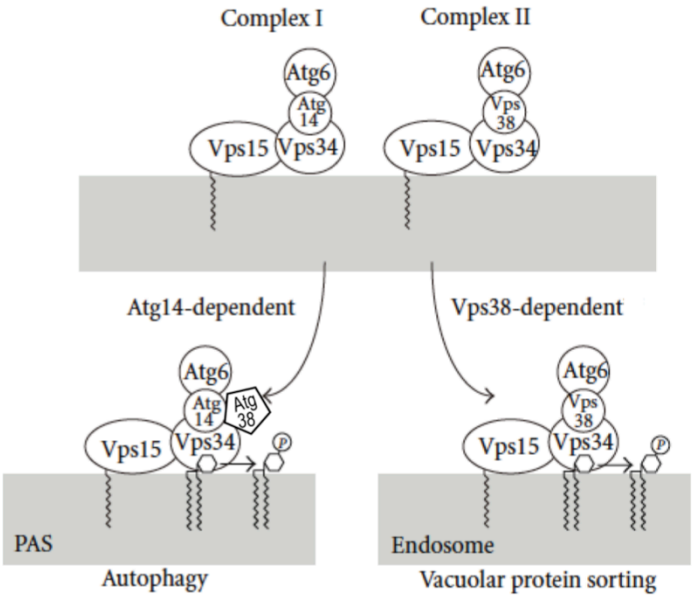

Figure 6: Vps34 is present in two complexes required for different cellular processes ((Obara et al., 2011); modified)

Complex II, containing Vps38, localizes to endosomes and acts in the vacuolar protein sorting pathway (Kihara et al., 2001; Obara et al., 2006). Complex I specifically integrates Atg14 and Atg38 and is essential for autophagy (Araki et al., 2013; Kihara et al., 2001). Atg14 links complex I to the PAS, where it generates the PAS-specific PI3P pool (Jao et al., 2013; Obara et al., 2006). PI3P is essential for autophagy since it recruits autophagy relevant PI3P effectors to the PAS. Deletion of *ATG14* and therefore the PI3P pool at the PAS, affects the recruitment of Atg8, the Atg12-Atg5/Atg16 complex and the Atg2-Atg18 complex (see below) to the PAS leading to a complete block in the autophagic process (Suzuki et al., 2007). Consequently, the deletion of *VPS38* does not affect autophagy, whereas in the absence of Atg14 the vacuolar protein sorting is unaffected (Kihara et al., 2001). This provides a suitable tool to distinguish

between the two Vps34 complexes. Furthermore, the influence of the PAS-specific PI3P pool on the localization of particular proteins can be specifically investigated.

2.2.4.4 The Atg12- and Atg8-conjugating system

With the Atg12- and Atg8-conjugating systems, autophagy uses two unique ubiquitin-like protein conjugation procedures, which involve approximately half of the core autophagy machinery. The primary sequence of both, Atg12 and Atg8, has low similarity to ubiquitin, but the crystal structure of the mammalian Atg8 homologue (LC3) revealed a C-terminal ubiquitin-like domain for LC3/Atg8. Compared to ubiquitin they additionally contain a N-terminal helical domain (Sugawara et al., 2004). Similarly, based on the plant Atg12 homologue (ATG12b), Atg12 is proposed to contain a ubiquitin-like fold at its C-terminus (Suzuki et al., 2005). Furthermore, Atg12 and Atg8 are conjugated to their specific targets in a manner similar to protein ubiquitination (Figure 7 A).

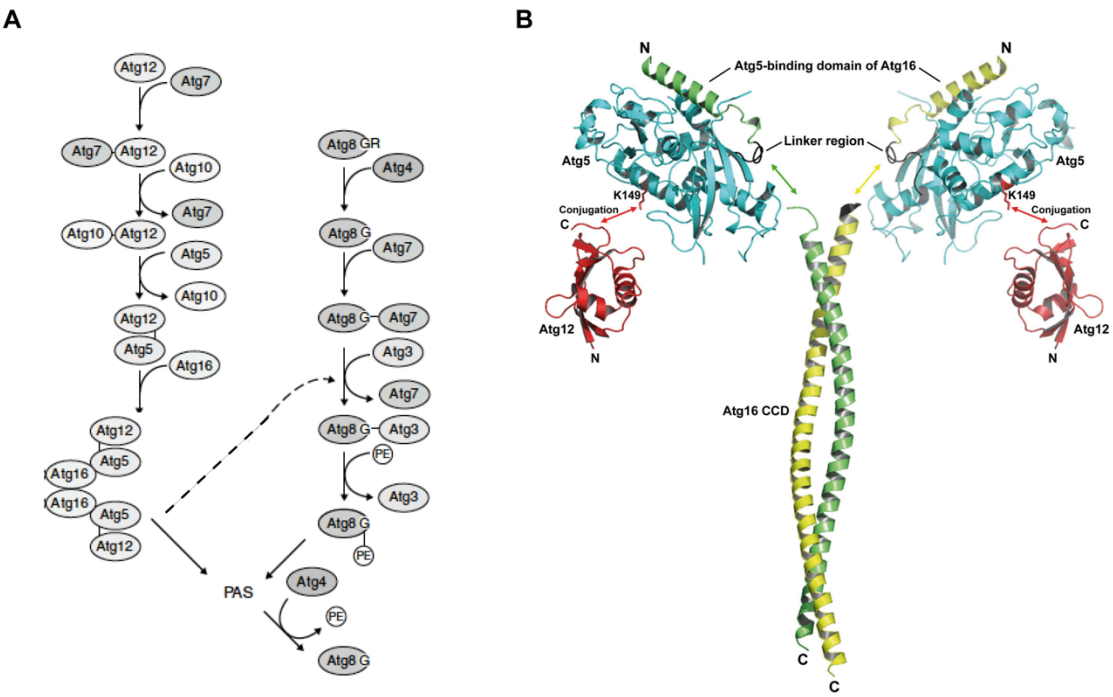

Figure 7: The two ubiquitin-like protein conjugation machineries in autophagy

(A) Scheme of both ubiquitin-like conjugation reactions ((Yorimitsu and Klionsky, 2005); modified)
(B) Model of the Atg12-Atg5/Atg16 complex; CCD: coiled-coil domain (Fujioka et al., 2010)

The C-terminal glycine of Atg12 is activated by the E1 enzyme Atg7, transferred to the E2 enzyme Atg10 and finally covalently attached to an internal lysine of the target protein Atg5 (Kuma et al., 2002; Mizushima et al., 1998; Shintani et al., 1999; Tanida et al., 1999). Remarkably, no E3 enzyme is involved in the conjugation reaction. The substrate specificity is mediated by direct recognition of the target protein Atg5 by the E2 enzyme Atg10 (Yamaguchi et al., 2012). Atg5, preferentially as Atg12-Atg5 conjugate, non-covalently binds to the N-terminus of Atg16 (Atg12-Atg5/Atg16 complex) (Mizushima et al., 1999). Atg12-Atg5/Atg16 is most likely a dimeric complex mediated by dimerization of the C-terminal coiled-coil domain of Atg16 (Fujioka et al., 2010; Kuma et al., 2002) (Figure 7 B). The dimerization of Atg16 is crucial for the Atg12-Atg5/Atg16 complex activity as an E3-like enzyme in the Atg8 conjugation reaction (Kuma et al., 2002).

Atg8 is synthesized with an additional arginine at its C-terminus. Before conjugation reaction, the cysteine protease Atg4 cleaves this arginine resulting in an exposed C-terminal glycine (Kirisako et al., 2000). This glycine is also activated by the E1 enzyme Atg7, transferred to the unique E2 enzyme Atg3 and finally covalently attached to the head group of the membrane lipid phosphatidylethanolamine (PE) (Ichimura et al., 2000; Kim et al., 1999; Kirisako et al., 2000; Shintani et al., 1999; Tanida et al., 1999). The conjugation reaction of Atg8 represents a unique mechanism different to ubiquitination as it results in a covalent membrane anchoring of Atg8 via conjugation to a lipid and not a protein.

As mentioned before, the Atg12-Atg5/Atg16 complex promotes this conjugation as an E3-like enzyme. Atg12 directly binds and probably activates Atg3, so that the Atg12-Atg5/Atg16 complex may act as a platform to bring the Atg8-carrying E2 enzyme Atg3 into close proximity to the substrate PE (Noda et al., 2012; Romanov et al., 2012; Sakoh-Nakatogawa et al., 2013). The Atg12-Atg5 conjugate alone was shown to accelerate the Atg8-PE conjugation *in vitro*, revealing that Atg16 is dispensable for the E3-like function of the Atg12-Atg5 conjugate. However, as a prerequisite for the conjugation of Atg8 to PE, Atg16 directs the Atg12-Atg5/Atg16 complex to autophagy-related membranes *in vivo* (Hanada et al., 2007). The Atg16-mediated PAS localization of the Atg12-Atg5/Atg16

complex is dependent on Atg14 respectively the PAS-specific PI3P pool. Because Atg16 has no obvious PI3P binding motif, the mechanism of membrane association remains still elusive (Cebollero et al., 2012; Matsushita et al., 2007; Suzuki et al., 2001).

Atg8-PE is found on all autophagy-related membranes (Kabeya et al., 2000; Kirisako et al., 1999). At the forming autophagosomes, it is located on the inner and outer membrane (Kirisako et al., 2000). The part, present on the inner membrane of the expanding phagophore, is trapped inside the matured autophagosome and transported to the vacuole, where it is finally degraded (Huang et al., 2000; Kabeya et al., 2000; Kirisako et al., 1999). In contrast, the part of Atg8, located on the outer membrane of the forming autophagosome, is cleaved off by the protease Atg4 and subsequently used for another round of lipidation (Kirisako et al., 2000). Beside the recycling aspect, the release of Atg8 from the outer membrane of the expanding phagophore is crucial to facilitate the maturation into a fusion-capable autophagosome (Nair et al., 2012; Yu et al., 2012).

The expression of Atg8 is highly upregulated upon autophagy induction (Huang et al., 2000; Kirisako et al., 1999) and the amount of Atg8 directly correlates with the size of the autophagosomes, suggesting that Atg8 plays a role in autophagosome expansion (Nakatogawa et al., 2007; Xie et al., 2008). In addition, the part of Atg8, which is present on the inner membrane of the forming autophagosome, binds receptor proteins in selective types of autophagy and serves therefore as an adaptor to link the specific cargoes to the forming autophagosomes (Chang and Huang, 2007; Mijaljica et al., 2012; Motley et al., 2012; Shintani et al., 2002). Almost all of the Atg8-interacting proteins bind to a certain region within Atg8 via a particular binding motif, called AIM (Atg8-interacting motif) or, with regard to the mammalian Atg8 homologue, LIR (LC3-interacting region). The AIM typically consists of a four amino acid motif, beginning with a tryptophan, followed by two, often acidic amino acids and ending with a lysine (WXXL) (Alemu et al., 2012; Mijaljica et al., 2012; Noda et al., 2008). This binding motif is specific for Atg8 homologues, since the side chains of the tryptophan and the lysine within the AIM bind to hydrophobic pockets in

Atg8, which are conserved among all Atg8 homologues but not among other ubiquitin-like proteins (Noda et al., 2009).

2.2.4.5 The Atg2-Atg18 complex

The Atg18-family proteins belong to the family of β-propellers that bind polyphosphoinositides (PROPPINs). PROPPINs are conserved from yeast to humans. With Atg18, Atg21 and Hsv2, yeast contains three PROPPINs (Dove et al., 2009; Dove et al., 2004; Krick et al., 2006; Michell et al., 2006; Stromhaug et al., 2004). Mammalia exhibits four PROPPIN orthologs, called WIPIs (WD40 repeat-containing protein that interacts with PtdIns) (Jeffries et al., 2004; Proikas-Cezanne et al., 2004). WIPI1 and WIPI2 share common ancestry with Atg18, whereas WIPI3 and WIPI4 form a clade with Hsv2 (Krick et al., 2012; Polson et al., 2010). Atg21 orthologs, however, have been only found in yeast species so far (Meijer et al., 2007).

Atg18 and its homologues contain seven WD-40 repeats, each consisting of around 40 amino acids and ending with a tryptophan (W) and an aspartate (D) residue. They fold into a seven-bladed β-propeller. The blades are comprised of four-stranded antiparallel β-sheets, and are interconnected through six loops (Barth et al., 2001; Dove et al., 2004). Like members of the PROPPIN family from other species, they contain a conserved lipid binding motif, consisting of the four amino acid Phe-Arg-Arg-Gly (FRRG) (Dove et al., 2004; Krick et al., 2006; Nair et al., 2010; Stromhaug et al., 2004). Recent studies revealed, that this motif participate in two different lipid binding sites (Baskaran et al., 2012; Krick et al., 2012; Watanabe et al., 2012), which preferentially bind to PI3P and PI(3,5)P_2 and mediate their peripheral membrane association (Dove et al., 2004; Krick et al., 2006) (Figure 8).

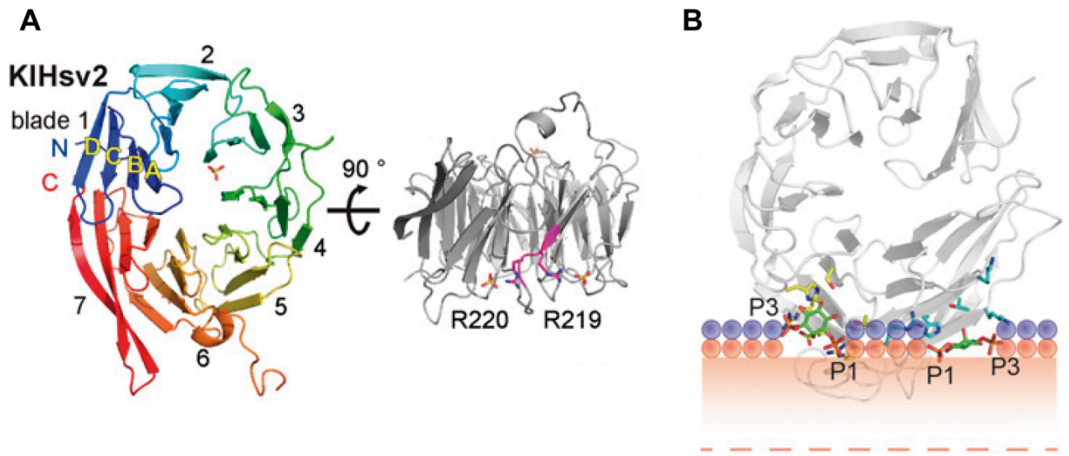

Figure 8: Structure of *Kluyveromyces lactis* Hsv2

(A) KlHsv2 forms a seven-bladed β-propeller scaffold. Each blade consists of a four-stranded antiparallel β-sheet (A-D). The lipid binding motif (FRRG) is located within the fifth loop between blade 5 and 6 and participate in two different lipid-binding pockets. **(B)** Model of membrane recognition of PROPPINs. The headgroup groups of the two PI3P molecules are indicated in green. ((Krick et al., 2012); modified)

WD-40 domain containing proteins commonly serve as a stable protein-protein interaction platform to coordinate the assembly of protein complexes (Xu and Min, 2011).

Atg18, Atg21 and Hsv2 are highly homologues, but they are required for different types of autophagy. Atg18 as a member of the core autophagy machinery is essential for all types of autophagy, whereas Hsv2 only affects efficient PMN (Barth et al., 2001; Guan et al., 2001; Krick et al., 2008b; Stromhaug et al., 2004). Bulk macroautophagy is severely impaired in the absence of Atg21. In contrast, Atg21 is required for selective types of autophagy as the Cvt pathway or PMN. Consequently, the biogenesis of Cvt vesicles is blocked in the absence of Atg21. In detail, Atg21 is essential for the recruitment of Atg8 and Atg5 to the PAS under nutrient-rich conditions and efficient lipidation of Atg8, suggesting a crucial role for Atg21 in PAS organization during the Cvt pathway. Though, Atg21 has not been detected at the PAS so far (Barth et al., 2002; Krick et al., 2008b; Meiling-Wesse et al., 2004; Stromhaug et al., 2004).

All three homologues localize at endosomal compartments in a PI3P-dependent manner, but their function there remains elusive (Krick et al., 2008a).

Atg18 also localizes PI(3,5)P_2- and PI3P-dependent at the vacuolar membrane and the PAS, where it exhibits autophagic and non-autophagic functions (Dove et al., 2004; Guan et al., 2001). At the vacuolar membrane it is involved in retrograde vesicular transport from the vacuole to the Golgi and in vacuole homeostasis by regulating the PI3P 5-kinase Fab1 (Dove et al., 2004; Efe et al., 2007; Jin et al., 2008; Michell and Dove, 2009). Atg21 is also found at vertices of vacuolar junctions. However, Atg21 is not required for the retrograde transport from the vacuole as its homolog Atg18 (Dove et al., 2004; Krick et al., 2006; Meiling-Wesse et al., 2004). At the PAS, Atg18 in a complex with Atg2 is required for the retrograde transport of Atg9 from the PAS to its non-PAS pool, but the underlying mechanism remains elusive so far (Legakis et al., 2007; Reggiori et al., 2004). In addition to PI3P, the protein interaction partner Atg2 is required for proper PAS localization of Atg18 (Obara et al., 2008b; Rieter et al., 2013). Atg2 interacts with the transmembrane protein Atg9, thereby mediating the membrane association of the Atg18-Atg2 complex (Obara et al., 2008b; Reggiori et al., 2004). The proper PAS localization of Atg18 requires both, PI3P and the protein interaction partner Atg2. The absence of only one of the components leads to a cytosolic localization and as a consequence to a block in autophagosome biogenesis at an early step (Rieter et al., 2013). Atg18 and Atg2 have been reported to constitutively form a complex in the cytosol, which is subsequently recruited to the PAS dependent on the PI3P binding ability of Atg18 (Obara et al., 2008b). In contrast, recent studies revealed, that Atg2 is recruited to the PAS independently from Atg18 and that the presence of both, Atg2 and PI3P, cooperatively mediates Atg18 PAS recruitment (Rieter et al., 2013). Furthermore, the Atg2-binding site within Atg18 has been located in the loop connecting blade 2 and 3 of the β-propeller and therefore on the opposite side to the PIP binding region located in loop 5 (Rieter et al., 2013; Watanabe et al., 2012) (Figure 8 A+B). Thus, a simultaneous binding of PIP and Atg2 should be possible.

Not only the localization of Atg18 at the PAS is mediated by PI3P and a protein interaction partner. The localization at the vacuolar membrane is determined by binding to PI(3,5)P_2 and interaction with the PI3P 5-kinase Fab1 complex (Dove et al., 2004; Efe et al., 2007; Krick et al., 2008a). At endosomes the interaction

partner of Atg18 and the other homologues Atg21 and Hsv2 are still missing. PI3P and PI(3,5)P_2 are enriched at the PAS, endosomes and the vacuolar membrane (Gillooly et al., 2000; Obara and Ohsumi, 2008). Therefore, the correct temporal and spatial PROPPIN localization in the living cell seems to be mainly determined by the particular protein interaction partner (Krick et al., 2012; Rieter et al., 2013).

3 Materials and Methods

3.1 Material

3.1.1 *Saccharomyces cerevisiae* strains

Table 1: Yeast strains used in this study

***S. cerevisiae* strain**	**Genotype**	**Reference**
WCG4	WCG4a MAT α *his 2-11,15 leu 2-3,112 ura 3*	(Thumm et al., 1994)
atg1Δ	WCG4a MAT α *his 2-11,15 leu 2-3,112 ura 3 atg1Δ::KAN*	(Straub et al., 1997)
atg2Δ atg21Δ	WCG4a MAT α *his 2-11,15 leu 2-3,112 ura 3 atg2Δ::HISMX6 atg21Δ::KAN*	AG Thumm (University Göttingen)
atg3Δ	WCG4a MAT α *his 2-11,15 leu 2-3,112 ura 3 ade2Δ1 atg3Δ1::ADE2*	(Schlumpberger et al., 1997)
atg4Δ	WCG4a MAT α *his 2-11,15 leu 2-3,112 ura 3 atg4Δ::HISMX6*	T. Lang (AG Thumm, University Göttingen)
atg5Δ	WCG4a MAT α *his 2-11,15 leu 2-3,112 ura 3 atg5Δ::KAN*	AG Thumm (University Göttingen)
atg8Δ	WCG4a MAT α *his 2-11,15 leu 2-3,112 ura 3 atg8Δ::KAN*	AG Thumm (University Göttingen)
atg8Δ atg16Δ	WCG4a MAT α *his 2-11,15 leu 2-3,112 ura 3 atg8Δ::KAN atg16Δ::NatNT2*	AG Thumm (University Göttingen)
atg8Δ atg21Δ	WCG4a MAT α *his 2-11,15 leu 2-3,112 ura 3 atg8Δ::KAN atg21Δ::NatNT2*	AG Thumm (University Göttingen)
atg9Δ	WCG4a MAT α *his 2-11,15 leu 2-3,112 ura 3 atg9Δ::KAN*	AG Thumm (University Göttingen)
atg11Δ	WCG4a MAT α *his 2-11,15 leu 2-3,112 ura 3 atg11Δ::HISMX6*	AG Thumm (University Göttingen)
atg14Δ	WCG4a MAT α *his 2-11,15 leu 2-3,112 ura 3 atg14Δ::NatNT2*	this study
atg16Δ	WCG4a MAT α *his 2-11,15 leu 2-3,112 ura 3 atg16Δ::NatNT2*	AG Thumm (University Göttingen)
Atg16-HA	WCG4a MATα *his 2-11,15 leu 2-3,112 ura 3 ATG16-6xHA::NatNT2*	R. Krick (AG Thumm, University Göttingen)
Atg16$^{1-57}$-HA	WCG4a MAT α *his 2-11,15 leu 2-3,112 ura 3 ATG16$^{1-57}$-6xHA::NatNT2*	this study

Atg16$^{1-119}$-HA	WCG4a MAT α *his 2-11,15 leu 2-3,112 ura 3 ATG16$^{1-119}$-6xHA::NatNT2*	this study
Atg16-HA *atg8Δ*	WCG4a MAT α *his 2-11,15 leu 2-3,112 ura 3 ATG16-6xHA::NatNT2 atg8Δ::KAN*	this study
atg19Δ	WCG4a MAT α *his 2-11,15 leu 2-3,112 ura 3 atg19Δ::KAN*	AG Thumm (University Göttingen)
atg21Δ	WCG4a MAT α *his 2-11,15 leu 2-3,112 ura 3 atg21Δ::KAN*	(Barth et al., 2002)
atg21Δ pep4Δ	WCG4a MAT α *his 2-11,15 leu 2-3,112 ura 3 atg21Δ::KAN pep4Δ::HISMX6*	AG Thumm (University Göttingen)
atg23Δ	WCG4a MAT α *his 2-11,15 leu 2-3,112 ura 3 atg23Δ::KAN*	AG Thumm (University Göttingen)
atg27Δ	WCG4a MAT α *his 2-11,15 leu 2-3,112 ura 3 atg27Δ::HISMX6*	AG Thumm (University Göttingen)
Atg27-HA	WCG4a MAT α *his 2-11,15 leu 2-3,112 ura 3 ATG27-6xHA::NatNT2*	R. Krick (AG Thumm, University Göttingen)
Sey 6210	Sey 6210 MAT α *ura 3-52 leu 2-3,112 his 3-Δ200 lys 2-801 trp 1-Δ901 suc 2-Δ9 mel GAL*	G. Fischer von Mollard (University Bielefeld)
atg4Δ	Sey 6210 MAT α *ura 3-52 leu 2-3,112 his 3-Δ200 lys 2-801 trp 1-Δ901 suc 2-Δ9 mel GAL atg4Δ::NatNT2*	(Krick et al., 2010)
atg5Δ	Sey 6210 MAT α *ura 3-52 leu 2-3,112 his 3-Δ200 lys 2-801 trp1-Δ901 suc 2-Δ9 mel GAL atg5Δ::NatNT2*	this study
atg16Δ	Sey 6210 MAT α *ura 3-52 leu 2-3,112 his 3-Δ200 lys 2-801 trp 1-Δ901 suc2-Δ9 mel GAL atg16Δ::NatNT2*	this study
Atg27-GFP	ATTC201388 Mat a *ura 3 leu 2 his 3 ATG27*-GFP*::HIS3MX6*	Invitrogen
Atg27-GFP *atg21Δ*	ATTC201388 Mat a *ura 3 leu 2 his 3 ATG27*-GFP*::HIS3MX6 ATG21::NatNT2*	this study

3.1.2 *Escherichia coli* strains

Table 2: *E. coli* strains used in this study

E. coli strain	Genotyp	Reference
DH5α	F´(Φ *80 (ΔlacZ) M15) Δ (lacZYA-argF) U169 recA1 endA1 hsdR17* r_K-m_K + *supE44 thi-1 gyrA relA*	(Hanahan, 1983)
BL21 (DE3) pLysS	F`*dcm ompT hsdSB (rB-, mB-) gal λ (DE3); pLysS (CamR)*	Stratagene

3.1.3 Plasmids

Table 3: Plasmids used in this study

Name	Genotype	Reference
ApeI-RFP	pRS313 CEN6 HIS3 ApeI-RFP	AG Thumm (University Göttingen)
ApeI-RFP	pRS315 CEN6 LEU2 ApeI-RFP	AG Thumm (University Göttingen)
ApeI-YFP	pRS313 CEN6 HIS3 ApeI-YFP	AG Thumm (University Göttingen)
Atg4 C-YC	p426 2µ URA3 ADH Atg4 C-YC	this study
Atg5-Cub	pRS313 CEN6 HIS3 MET25 Atg5-Cub-RURA3	this study
Atg5-YFP	pRS316 CEN6 URA3 Atg5-YFP	Y. Ohsumi (Tokyo Institute of Technology)
Atg16-Cub	pRS313 CEN6 HIS3 MET25 Atg16-Cub-RURA3	this study
Atg16-GFP	pRS313 CEN6 HIS3 Atg16-GFP	AG Thumm (University Göttingen)
Atg16-GFP^{D101A}	pRS313 CEN6 HIS3 Atg16-GFP^{D101A}	this study
Atg16-GFP^{E102A}	pRS313 CEN6 HIS3 Atg16-GFP^{E102A}	this study
Atg16-GFP^{D101A_E102A}	pRS313 CEN6 HIS3 Atg16-GFP^{D101A_E102A}	this study
Atg16-GFP^{K94A}	pRS313 CEN6 HIS3 Atg16-GFP^{K94A}	this study
Atg16-HA	pRS313 CEN6 HIS3 CUP1 Atg16-HA	this study
Atg16-HA$^{1-57}$	pRS313 CEN6 HIS3 CUP1 Atg16-HA	this study
Atg16-HA$^{1-119}$	pRS313 CEN6 HIS3 CUP1 Atg16-HA$^{1-119}$	this study
Atg16-HA$^{58-150}$	pRS313 CEN6 HIS3 CUP1 Atg16-HA$^{58-150}$	this study
Atg16-HA^{D101A}	pRS313 CEN6 HIS3 CUP1 Atg16-HA^{D101A}	this study
Atg16-HA^{E102A}	pRS313 CEN6 HIS3 CUP1 Atg16-HA^{E102A}	this study
Atg16-HA^{D101A_E102A}	pRS313 CEN6 HIS3 CUP1 Atg16-HA^{D101A_E102A}	this study
Atg16-HA^{K94A}	pRS313 CEN6 HIS3 CUP1 Atg16-HA^{K94A}	this study

Atg16-HA^{E97A}	pRS313 CEN6 HIS3 *CUP1* Atg16-HA^{E97A}	this study
Atg21-Cub	pRS313 CEN6 HIS3 MET25 Atg21-Cub-RURA3	R. Krick (AG Thumm, University Göttingen)
Atg21 C-YC	p426 2µ URA3 ADH Atg21 C-YC	this study
Atg21 C-YC	p416 CEN URA3 MET25 Atg21 C-YC	this study
Atg21-TAP	pRS316 CEN6 URA3 Atg21-TAP	AG Thumm (University Göttingen)
Atg21-YFP	pRS316 CEN6 URA3 Atg21-YFP	(Meiling-Wesse et al., 2004)
Atg23-Cub	pRS313 CEN6 HIS3 MET25 Atg23-Cub-RURA3	this study
Atg27-Cub	pRS313 CEN6 HIS3 MET25 Atg27-Cub-RURA3	this study
Atg27-Cub$^{1-198}$	pRS313 CEN6 HIS3 MET25 Atg27-Cub$^{1-198}$-RURA3	R. Krick (AG Thumm, University Göttingen)
Atg27-Cub$^{1-221}$	pRS313 CEN6 HIS3 MET25 Atg27 Cub$^{1-221}$-RURA3	R. Krick (AG Thumm, University Göttingen)
C-YC	p426 2µ URA3 ADH C-YC	(Skarp et al., 2008)
C-YC	p416 CEN6 URA3 C-YC	this study
GFP-Atg8	pRS313 Cen6 HIS3 GFP-Atg8	AG Thumm (University Göttingen)
GFP	pUG36 CEN6 HIS3 GFP	AG Thumm (University Göttingen)
GFP-Atg21	pUG36 CEN6 HIS3 GFP-Atg21	(Krick et al., 2008a)
GST	pGEX-4T-3 GST	Amersham
GST-Atg16	pGEX-4T-3 GST-Atg16	this study
GST-Atg16$^{1-57}$	pGEX-4T-3 GST-Atg16$^{1-57}$	this study
GST-Atg16$^{1-119}$	pGEX-4T-3 GST-Atg16$^{1-119}$	this study
GST-Atg16$^{58-150}$	pGEX-4T-3 GST-Atg16$^{58-150}$	this study
mCherry	pUG36 CEN6 URA3 mCherry	R. Krick (AG Thumm, University Göttingen)
mCherry-Atg19	pUG34 CEN6 HIS3 mCherry-Atg19	P. Rube (AG Thumm, University Göttingen)
mCherry-Atg21	pUG36 CEN6 URA3 mCherry-Atg21	R. Krick (AG Thumm, University Göttingen)
Nui-Atg1	pRS314 CEN6 TRP1 CUP1 Nui-Atg1	F. Reggiori (University Medical Center Utrecht)
Nui-Atg5	pRS314 CEN6 TRP1 CUP1 Nui-Atg5	R. Krick (AG Thumm, University Göttingen)

Nui-Atg7	pRS314 CEN6 TRP1 CUP1 Nui-Atg7	this study
Nui-Atg8	pRS314 CEN6 TRP1 CUP1 Nui-Atg8	R. Krick (AG Thumm, University Göttingen)
Nui-Atg9	pRS314 CEN6 TRP1 CUP1 Nui-Atg9	F. Reggiori (University Medical Center Utrecht)
Nui-Atg12	pRS314 CEN6 TRP1 CUP1 Nui-Atg12	this study
Nui-Atg16	pRS314 CEN6 TRP1 CUP1 Nui-Atg16	this study
Nui-Atg18	pRS314 CEN6 TRP1 CUP1 Nui-Atg18	F. Reggiori (University Medical Center Utrecht)
Nui-Atg19	pRS314 CEN6 TRP1 CUP1 Nui-Atg19	this study
Nui-Atg21	pRS314 CEN6 TRP1 CUP1 Nui-Atg21	F. Reggiori (University Medical Center Utrecht)
Nui-Atg23	pRS314 CEN6 TRP1 CUP1 Nui-Atg23	this study
Nui-Atg27	pRS314 CEN6 TRP1 CUP1 Nui-Atg27	this study
Nui-Hsv2	pRS314 CEN6 TRP1 CUP1 Nui-Hsv2	R. Krick (AG Thumm, University Göttingen)
Nui-Ubc6	pRS314 CEN6 TRP1 CUP1 Nui-Ubc6	R. Krick (AG Thumm, University Göttingen)
Nui-Trs85	pRS314 CEN6 TRP1 CUP1 Nui-Trs85	F. Reggiori (University Medical Center Utrecht)
Nui-Vam1	pRS314 CEN6 TRP1 CUP1 Nui-Vam1	AG Thumm (University Göttingen)
N-YC	p426 2µ URA3 ADH N-YC	(Skarp et al., 2008)
N-YN	p425 2µ LEU2 *ADH* N-YN	(Skarp et al., 2008)
N-YN	p415 CEN6 LEU2 MET25 N-YN	this study
N-YN Atg8	p425 2µ LEU2 *ADH* N-YN Atg8	this study
N-YN Atg8	p415 CEN6 LEU2 MET25 N-YN Atg8	this study
N-YC Atg4	p426 2µ URA3 ADH N-YC Atg4	this study
N-YC Atg21	p426 2µ URA3 ADH N-YC Atg21	this study
pFA6-natNT2	pFA6-natNT2	Euroscarf; (Janke et al., 2004)
pRS313-*CUP1*	pRS313 CEN6 HIS3 CUP1	R. Krick (AG Thumm, University Göttingen)
pRS314	pRS314 CEN6 TRP1	AG Thumm (University Göttingen)

p415-*MET25*	p415 CEN LEU2 MET25 672	(Mumberg et al., 1995)
p416-*MET25*	p416 CEN URA3 MET25 673	(Mumberg et al., 1995)
Ste14-Cub	pRS313 CEN6 HIS3 MET25 Ste14-Cub-RURA3	F. Reggiori (University Medical Center Utrecht)
SUMO	K27 6xHIS SUMO	AG Rehling (University Göttingen)
SUMO-Atg21	K27 6xHIS SUMO-Atg21	R. Krick (AG Thumm, University Göttingen)

3.1.4 Oligonucleotides

Table 4: Oligonucleotides used in this study

Name	Sequence (5`to 3`)
ATG5::NatNT2	
Atg5::NAT_fwd	GTTCTTTTGGTTCTAGAAGAACGGAGATAGGAAACCTATGATGTAAGTAT G***CGTACGCTGCAGGTCGAC***
Atg5::NAT_rev	CTGCGATATTTGAATGACACTTTTAAATGCGTATATAACAGCTCTTA***ATC GATGAATTCGAGCTCG***
ATG14::NatNT2	
atg14_ko_fw	CGAGTAGAGAAAAAGGGAAGTAAAAGTTAAAAACTAGAATCCTAGTATG ACATG *CGTACGCT GCAGGTCGAC*
atg14_ko_rev	GACTGACTACATGCAACTTTATACACACGGCAGGAAAAAAAGTGCGCACT CTA *ATCGATGAATTCGAGCTCG*
ATG21::NatNT2	
ATG21 KO-S1:	CAAAAGACAATTCCACTCCTTTGGATTTGAAATAGACAGATAGAAAAGGA T**ATG***CGTACGCTGCAGGTCGAC*
ATG21 KO-S2:	CGTGAATACGTACAATATCTATTAAGATTATGAAAACTGCACATATGCA**T TA***ATCGATGAATTCGAGCTCG*
chromosomal Atg16$^{1-119}$-HA	
Atg16$^{1-119}$-HA-S3_fwd	GAACCATTGAAAATAATGTTTTACAACAAAAACTCTCGGAT**CGTACGCTG CAGGTCGAC**
Atg16$^{1-119}$-HA-S2_rev	TTAGCCATCTCGCAACTAGCTGGGAATGTTCTTTTTTCAG**ATCGATGAAT TCGAGCTCG**
chromosomal Atg16$^{1-57}$-HA	

Atg16$^{1-57}$-HA-S3_fwd	GTTGTTTCAAGATAATAGTGGCGCCATTGGTGGCAACATT**CGTACGCTGC AGGTCGAC**
Atg16$^{1-57}$-HA-S2_rev	GAATTGCCAGTGTATTCAATAAAGCATCGTCATGGCTGAC**ATCGATGAA TTCGAGCTCG**
Split-ubiquitin plasmids	
Nui-Atg23_BamHI_fwd	AGTAGCAAT**ggatcc**ctgggtctgggGAACTGAATCAGGTTTTAG
Nui_Atg23_KpnI_rev	ATTCCTACTT**GGTACC**GAAAGCCTAGATCATGATC
Atg23-Cub_StuI_fwd	AGTAGCAAT**aggcct**ATGGAACTGAATCAGGTTTTAG
Atg23_Cub_SalI_rev	ATTCCTACTT**gtcgac**CCTTCAACTTTTTTTGATATGGCATC
Nui-Atg12_StuI_fwd	AGTAGGAATggatc**aggcct**tctgggAGTAGGATCCTAGAGAGCG
Nui-Atg12_XhoI_rev	ATTCCTACTT**CTCGAG**gtgagtttataacgctcaagtac
Nui-Atg27_BamHI_fwd	AGTAGCAAT**ggatcc**ctgggtctgggGTATCGAAGACTTGGATATGTGG
Nui-Atg27_XhoI_rev	ATTCCTACTT**CTCGAG**gtataatgtagatataaaagcttag
Nui-Atg16_BamHI_fwd	AGTAGCAAT**ggatcc**ctgggtctgggGGCAATTTCATTATAACAGAAAGG
Nui-Atg16_XhoI_rev	ATTCCTACTT**CTCGAG**acctctttattgcaaacactttg
Nui-Atg19_BamHI_fwd	AGTAGCAAT**ggatcc**ctgggtctgggAACAACTCAAAGACTAACCAACAG
Nui-Atg19_XhoI_rev	ATTCCTACTT**CTCGAG**ggaagtaaagagtttcgaaaaggg
Nui-Atg7_BamHI_fwd	AGTAGCAAT**ggatcc**ctgggtctgggTCGTCAGAAAGGGTCTTAAG
Nui-Atg7_KpnI_rev	ATTCCTACTT**GGTACC**GTATGCAAAATAGTATAGCAAG
Atg5Cub_StuI_fwd	AGTAGCAAT**aggcct**ATGAATGACATTAAACAATTACTTTG
Atg5Cub_SalI_rev	ATTCCTACTT**gtcgac**CCGAGCTCAGAGGAAGCTTTATC
Atg16Cub_ClaI_fwd	AGTAGCAAT**atcgat**ATGGGCAATTTCATTATAACAG
Atg16Cub_SalI_rev	ATTCCTACTT**gtcgac**CCTTTCGTTCCATCTATTTCGCTG
Atg27Cub_ClaI_fwd	AGTAGCAAT**atcgat**ATGGTATCGAAGACTTGGATATG
Atg27Cub_SalI_rev	ATTCCTACTT**gtcgac**CCAACGGCGCTATAACCGCCTC
GST-Atg16 plasmid variants	
GST-Atg16_BamHI_fwd	AGTAGCAAT**ggatcc**ATGGGCAATTTCATTATAACAG
GST-Atg16_XhoI_rev	ATTCCTACTT**CTCGAG**TCATTTCGTTCCATCTATTTCG
GST-Atg16$^{1-57}$_XhoI_rev	ATTCCTACTT**CTCGAG**TCAAATGTTGCCACCAATGGCG
GST-Atg16$^{1-119}$_XhoI_rev	ATTCCTACTT**CTCGAG**TCAATCCGAGAGTTTTTGTTGTAAAAC
GST-Atg16$^{58-150}$_BamHI_fwd	AGTAGCAAT**ggatcc**GTCAGCCATGACGATGC
Atg16-HA plasmid variants	
Atg16Cub_ClaI_fwd	AGTAGCAATatcgatATGGGCAATTTCATTATAACAG

Atg16HA_XhoI_rev	AGTAGCAAT**ctcgag**GATCTCTTGAATGATCGTTCC
Atg16HA_58-150_ClaI_fwd	AGTAGCAATatcgatATGGTCAGCCATGACGATGC
Atg16 point mutants	
Atg16_K94A_fwd	GCGTTGAAAAATgcGAATACGGAAAGGTTGAATGACG
Atg16_K94A_rev	CGTCATTCAACCTTTCCGTATTCGCATTTTTCAACGC
Atg16_E97A_fwd	GAATACGGcAAGGTTGAATGACGAATTGATTAGTGGAACCATTG
Atg16_E97A_rev	CAATGGTTCCACTAATCAATTCGTCATTCAACCTTGCCGTATTC
Atg16_D101A_fwd	GAATACGGAAAGGTTGAATGcCGAATTGATTAGTGGAACC
Atg16_D101A_rev	GGTTCCACTAATCAATTCGgCATTCAACCTTTCCGTATTC
Atg16_E102A_fwd	GAATACGGAAAGGTTGAATGACGcATTGATTAGTGGAACC
Atg16_E102A_rev	GGTTCCACTAATCAATgCGTCATTCAACCTTTCCGTATTC
Atg16_DE_fwd	GAATACGGAAAGGTTGAATGcCGcATTGATTAGTGGAACCATTG
Atg16_DE_rev	CAATGGTTCCACTAATCAATgCGgCATTCAACCTTTCCGTATTC
BiFC plasmids	
Atg21_C-YC_BamHI_fwd	atcatcggatccATGAAAGTATTACAATTCAATCAAG
Atg21_C-YC_SalI_rev	gatgatgtcgacTGTAAATTTATTATTTTTAGTCAGCAC
Atg21_N-YC_BamHI_fwd	atcatcggatccCAAAGTATTACAATTCAATCAAGATG
Atg21_N-YC_SalI_rev	gatgatgtcgacTTATGTAAATTTATTATTTTTAGTCAGC
Atg8_N-YN_BamHI_fwd	atcatcggatccAAGTCTACATTTAAGTCTGAATATC
Atg8_N-YN_SalI_rev	atcatcggatccCTACCTGCCAAATGTATTTTCTC
Atg4_C-YC_EcoRI_fwd	atcatcgaattcATGCAGAGGTGGCTACAACTG
Atg4_C-YC_SalI_rev	gatgatgtcgacgcatttttcatcaataggactgtg
Atg4 N-YC_EcoRI_fwd	atcatcgaattcGCAGAGGTGGCTACAACTGTGG
Atg4 N-YC_SalI_rev	gatgatgtcgacCTAGCATTTTTCATCAATAGGACTG
Control Primer	
Atg5_K1_fwd	GAAGTAGCATGCTCAGAAGTG
NatNT2_r	cgattcgtcgtccgattcgtc
Atg5_K3_rev	CAACGTAGGATTGACTCCAGTC
atg14_K1_fw	GGGAAAGGACCAAATACAAAAGTG
atg14_K3_rev	TGAGTTGGTTCTTACCCGAATGC
Atg21_pro_f	GAGCGTGAGCTGCAGAAAG
atg21-seq1r	caacaatttcatgtgggaaaac
Sequencing primer	
pRS313-CUP1_fwd	GCAATATGGATTGTCAGAATC
pRS313-CUP1_rev	CACACAGGAAACAGCTATGACC

pGEX-4T3_fwd	gatcatgtaacccatcc
pGEX-4T3_rev	GCCACCTGACGTCTAAG
Atg16 seq 2 rev	CTTCGTATTTCTTGCTCC
Nui-Seq3_f	CTTGTCTTGTATCAATTG
Atg23_Seq1_fwd	CTTCTGCGGATCAAATGATAC
Atg23_seq1_rev	GTATCATTTGATCCGCAGAAG
Atg23_Seq2_fwd	GTAGGAGATTTGGAAAGC
ATG16_seq_6_rev	GGATAACAATTTCACACAGG
Cub-RURA3-seq f	CACCTTGTCCAATTGAAC
Cub_Seq_rev	CTAACTCCAGTAATTCCTTG
Atg12 Seq 1 fwd	CAAGAATTAAGATCATCTCC
Atg12 Seq2 fwd	CGTTTGCGCCAAGTCCGCAG
Atg12 Seq2 rev	CTGCGGACTTGGCGCAAACG
Atg27 Seq1 fwd	CAGGTGGGAAAATTTAGCTC
Atg27 Seq2 fwd	GGACTTCGTGGTTCACTTGG
Atg27 Seq2 rev	CCAAGTGAACCACGAAGTCC
ATG16 seq 2 for	GGAGCAAGAAATACGAAG
Atg16 seq 3 fwd	GCCATGAACAGCGAAATAG
Atg16 seq3 rev	CTATTTCGCTGTTCATGGC
Atg19 Seq1 fwd	GCTTGGATAACTTCATGAAAC
Atg19 Seq1 rev	GTTTCATGAAGTTATCCAAGC
Atg19 Seq2 fwd	CCAACCACGCAAATTATTGAC
Atg19 Seq2 rev	GTCAATAATTTGCGTGGTTGG
Atg7_Seq1_fwd	GGCTGTTCTCAAAGTGTC
Atg7_Seq1_rev	GACACTTTGAGAACAGCC
Atg7_Seq2_fwd	GTAAACGAGGAGGCTCAG
Atg7_Seq2_rev	CTGAGCCTCCTCGTTTAC
Atg7_Seq3_fwd	GACTTCCTTACTACAGACC
Atg5_Seq1_fwd	CCCCTCATTTGGAACAAG
Atg5_Seq1_rev	CTTGTTCCAAATGAGGGG
Atg5_Seq2_fwd	GTTCATCAAGACCGCGAC
Atg5_Seq2_rev	GTCGCGGTCTTGATGAAC
pADH 1 for	CGGTATACGGCCTTCCTTCC
C-YC Seq rev	CTCGTCCATGCCGAGAGTG
N-YC Seq fwd	GTGCAGCTCGCCGACCAC
Atg4 C-YC Seq1 f	CAGAGGTGGCTACAACTGTG
Atg4 C-YC Seq1 r	CTATAGGAACAAATCTTGTCCG
Atg4 C-YC Seq2 f	CCGATCAGTACAATAGAGGAC

Atg4 C-YC Seq2 r	GATGCCACATTCGGGGAAGC
Atg4 C-YC Seq3 f	GTTCTTGTTGGGCGTGAAGC
Atg4 C-YC Seq3 r	GTTGCCAGTCTTTTTCGCCC
Atg4 C-YC Seq4 f	GGATGACGTGGAAAGTGTAAG
Atg4 C-YC Seq4 r	CATCAATAGGACTGTGAATACC

3.1.5 Media

All media listed in this chapter were prepared with deionized water (ddH_2O). The respective pH was adjusted using NaOH or HCl. The media were autoclaved at 121°C for 20 min for sterilization. The listed percent values indicate weight per volume (w/v). For the preparation of solid media to generate plates, 2% of preheated, sterile agar was added.

3.1.5.1 YPD-medium, pH 5.5

YPD is a rich medium for yeast cells consisting of:

1% Bacto® Yeast Extract

2% Bacto® Pepton

2% D-glucose

3.1.5.2 CM-medium, pH 5.6

CM-medium is a synthetic medium for yeast cells and was used as selective medium.

0.67% Yeast Nitrogen Base w/o amino acids

2% D-glucose

0.0117% L-alanine

0.0117% L-arginine

0.0117% L-asparagine

0.0117% L-aspartic acid

0.0117% L-cysteine

0.0117% L-glutamine

0.0117% L-glutamic acid

0.0117% L-glycine

0.0117% L-isoleucine

0.0117% L-methionine

0.0117% L-phenylalanine

0.0117% L-proline

0.0117% L-serine

0.0117% L-threonine

0.0117% L-tyrosine

0.0117% L-valine

0.0117% myo-inositol

0.0117% p-aminobenzoic acid

For overexpression experiments using *MET25* promoter L-methionine was excluded from the drop out mix.

Following supplements were added depending on selection of genetic markers:

0.3 mM L-histidine	0.4 mM L-tryptophan
1.7 mM L-leucine	0.3 mM adenine
1 mM L-lysine	0.2 mM uracil

3.1.5.3 SD(-N)-medium

Nitrogen free SD(-N)-medium was used as starvation medium for yeast cells.

0.67% Yeast Nitrogen Base w/o amino acids and w/o ammonium sulfate

2% D-glucose

3.1.5.4 LB-medium, pH 7.5

LB-medium was used as standard growth medium for *E. coli* cultures.

1% Bacto® Trypton

0.5% Bacto® Yeast extract

0.5% sodium chloride

For plasmid selection 75 µg/ml ampicillin, 50 µg/ml kanamycin, and/or 25 µg/ml chloramphenicol was added.

3.1.5.5 SOC-medium, pH 7.5

SOC-medium was used as regeneration medium for electroporated *E. coli* cells.

2% Bacto® Trypton

0.5% Bacto® Yeast extract

0.4% D-glucose

10 mM sodium chloride	10 mM magnesium sulfate
10 mM magnesium chloride	2.5 mM potassium chloride

3.1.6 Antibodies

Table 5: Antibodies used in this study

Antibody	**Dilution** (in TBST containing 1% skim milk powder (w/v))	**Source**
anti-mouse-HRPO-conjugate	1 : 10.000	Dianova, Hamburg
anti-rabbit-HRPO-conjugate	1 : 5000	Medac, Hamburg
anti-rat-HRPO-conjugate	1 : 10.000	Jackson ImmunoResearch, UK

rabbit-anti-ApeIp	1 : 3000	Eurogentech, Belgium
rabbit-anti-Aut7	1 : 10.000 in TBST	M. Thumm
rabbit-anti-CPY	1 : 10.000	Molecular Probes, Leiden, NL
mouse-anti-GFP*	1 : 10.000	Roche, Mannheim
mouse-anti-GFP**	1 : 10.000	Abcam, Cambridge, UK
mouse-anti-PGK	1 : 10.000	Molecular Probes, Leiden, NL
rat-anti-Red	1 : 1000	Chromotek, München
mouse-anti-HA	1 : 10.000	Santa Cruz Bio-technology, Heidelberg

*In general, the GFP-antibody from Roche was used if not stated otherwise.

**The GFP-antibody from Abcam was used to detect both fragments of eYFP on immunoblots prepared for BiFC (see chapter 4.3.5.1).

3.1.7 Commercial available Kits

Kit systems listed in Table 6 were used according to the manufacturer`s recommendations.

Table 6: Commercial available Kits used in this study

Name of the Kit	Source
ECL Western Blotting Detection Reagents	Amersham Biosciences, GB
QIAquick Gel Extraction Kit	Qiagen, Hilden
QIAquick PCR Purification Kit	Qiagen, Hilden
QuikChange II Site-Directed Mutagenesis Kit	Agilent Technologies; Santa Clara, USA
Wizard Plus SV Miniprep Kit	Promega, Mannheim

3.1.8 Chemicals and consumables

Standard chemicals were used in analytical grade quality and obtained from AppliChem (Darmstadt), Sigma (Deisenhofen), Roth (Karlsruhe) or Merck (Darmstadt). Restriction enzymes were obtained from NEB (Frankfurt). Deoxyoligonucleotides were ordered from Eurofins MWG Operon (Ebersberg) and used as primers for PCR or site-directed mutagenesis. Special chemicals and enzymes are listed in Table 7.

Table 7: Special chemicals

Name	Source
Bacto® -Agar	Becton Dickinson, Heidelberg
Bacto® Peptone	Becton Dickinson, Heidelberg
Bacto® Tryptone	Becton Dickinson, Heidelberg
Bacto® Yeast Extract	Becton Dickonson, Heidelberg
Benzonase	Sigma, Deisenhofen
clon NAT (nourseotricine)	Werner BioAgents, Jena
Complete™ protease inhibitor (EDTA-free)	Roche, Mannheim
Deoxyadenosin-triphosphate (dATP)	NEB, Frankfurt
Deoxycytidin-triphosphate (dCTP)	NEB, Frankfurt
Deoxyguanosin-triphosphate (dGTP)	NEB, Frankfurt
Deoxythymidin-triphosphate (dTTP)	NEB, Frankfurt
DNA-marker (1kb DNA-ladder)	NEB, Frankfurt
ECL	USB, Santa Clara, CA
Glass beads	Schütt, Göttingen
Herring-sperm-DNA	Promega, Madison, USA
Immersion oil	Applied Precision, USA
Ligation buffer	NEB, Frankfurt
DNA polymerase (FideliTaq)	USB, Santa Clara, USA
DNA polymerase (Klenow)	NEB, Frankfurt
DNA polymerase (KOD)	Novagen, Darmstadt
DNA polymerase (Taq)	NEB, Frankfurt
DNA polymerase (Vent)	NEB, Frankfurt
Precision Plus Protein All Blue Standards	Biorad, Munich
Protease inhibitor cocktail (bacteria)	Sigma, Deisenhofen
RNAse A	Applichem, Darmstadt
Sepharose / Slurry	GE Healthcare, München
Skim milk powder	Granovita, Lüneburg
T4-Ligase	NEB, Frankfurt
Difco Yeast nitrogen base w/o amino acids	Becton Dickinson, Heidelberg
Difco Yeast nitrogen base e/o amino acids and ammonium	Becton Dickinson, Heidelberg
Zymolyase T100	Seikagaku, Japan

3.1.9 Equipment

Table 8: Equipment used in this study

Name of product	Source
Agarose gel equipment Bio RAD Mini-SUB Cell GT	Bio-Rad Laboratories GmbH, München
ÄKTApurifier 10 UPC	GE Healthcare, München
Autoclave	Adolf Wolf, SANOclav, Bad Überkingen-Hausen
Autoclave DX200	Systec, Wettenberg
Bench	BDK Luft- und Reinraumtechnik GmbH, Sonnenbühl
Blot Shaker GFL 3019	GFL, Burgwedel
Centrifuge 5804	Eppendorf, Hamburg
Centrifuge 5404R	Eppendorf, Hamburg
Centrifuge 5415D	Eppendorf, Hamburg
Centrifuge 5415R	Eppendorf, Hamburg
Chemical balance	Sartorius, Göttingen
Cuvettes no. 67.742	Sarstedt, Nümbrecht
Cuvettes for electroporation; 2mm	peqlab, Erlangen
Electroporator 2510	Eppendorf; Hamburg
Freezer (-20°C)	Liebherr, Bulle, CH
Freezer (-80°C)	Heareus, Hanau
Glassbeads	Schütt, Göttingen
Hood	BDK Luft- und Reinraumtechnik, Sonnenbrühl-Genkingen
Incubator (37°C)	Heraeus, Hanau
Incubator 4200	Innova, USA
Incubator Thermomixer comfort	Eppendorf, Hamburg
Labshaker for diverse culture sizes	A. Kühner, Birsfelden, Schweiz
LAS 3000 Intelligent Dark Box	Fuji/Raytest, Benelux
Magnetic stirrer MR 3001	Heidolph, Kelheim
Microscope DeltaVision, Olympus IX71	Applied Precision, USA
Microscope slides (76x26mm)	Menzel-Gläser, Braunschweig
Microscope cover slips	Menzel-Gläser, Braunschweig
Microwave R-939	Sharp, Hamburg
Multivortex IKA vibray VXR basic	IKA, Staufen
Over head shaker Roto-Shake Genie	Scientific Industries Inc, USA
PCR Mastercycler gradient	Eppendorf, Hamburg
pH meter pH537	WTW, Weilheim

Photometer	Eppendorf, Hamburg
Pipettes	Eppendorf, Hamburg
PowerPac Basic Power Supply	Bio-Rad Laboratories GmbH, München
PowerPac HC Power Supply	Bio-Rad Laboratories GmbH, München
PVDF membrane Hybond-P	Amersham; GE healthcare, Freiburg
Refrigerator (4°C)	Bosch, Stuttgart / Liebherr, Bulle, CH
Rotor JA 10	Beckmann, Krefeld
Rotor JA 20	Beckmann, Krefeld
Rotor TLA-100.3	Beckmann, Krefeld
Rotor TLS-55	Beckmann, Krefeld
OmniTrays Nunc	SIGMA-ALDRICH, St. Louis, USA
Superose™ 6 10/300 GL column	Amersham Pharmacia Biotech, Schweden
SDS-PAGE equipment BioRAD Mini Protean cell	Bio-Rad Laboratories GmbH, München
Pipette tips, petri dishes, …	Sarstedt, Nümbrecht / Eppendorf, Hamburg
Sterile filter	Whatman, GE healthcare, München
Thermomixer Comfort	Eppendorf, Hamburg
Transilluminator TI 1	Whatman Biometra, Göttingen
Ultracentrifuge	Beckman, Krefeld
vacuum pump	Vacuubrand, Wertheim
Water bath SWB25	Thermo Electron, Karlsruhe
Western Blot equipment Trans Blot Cell	Bio-Rad Laboratories GmbH, München

3.2 Cultivation of *S. cerevisiae*

3.2.1 Growth of liquid yeast cultures

For liquid yeast precultures, the yeast strain was inoculated with a sterile toothpick from an agar plate and incubated at 30°C with 220 rpm over night. The preculture was used to inoculate the main liquid yeast culture with a defined dilution depending on the requested OD_{600} and growth ability of the respective strain. Cultures were shaken at 220 rpm and 30°C over night (12 - 14 h) if not pointed otherwise.

3.2.2 Short-term storage

For short-term storage of yeast stocks, yeast strains were stored on agar plates up to 4 - 6 weeks at 4°C.

3.2.3 Long-term storage

For long-term storage of yeast strains, 0.65 ml of a yeast culture was supplemented with 0.65 ml of sterile 30% glycerine and stored at -80°C.

3.2.4 Cell density determination

The cell density was determined by OD_{600} measurement using a photometer in a dilution of 1:10. The empty medium was used as reference. 1 OD_{600} of yeast cells corresponds to 3 x 10^7 cells per ml.

3.2.5 Split-ubiquitin assay

1 OD_{600} of a yeast preculture was diluted 1:10, 1:100, 1:1000 and 1:10 000 with sterilized ddH_20. 4 µl was spotted on three different solid plates (Laser et al., 2000):

1) growth control plate consisting of selective medium (CM-His-Trp)
2) negative interaction control plate consisting of selective medium (CM-His-Trp) lacking uracil but containing 250 µM methionine and 100 µM $CuSO_4$
3) positive interaction control plate consisting of selective medium (CM-His-Trp) containing 250 µM methionine, 100 µM $CuSO_4$ and 1 mg/ml FOA

Plates were incubated for two to three days at 30°C and imaged using LAS-3000 (Fujifilm) for growth pattern analysis.

3.3 Cultivation of *E. coli* cultures

3.3.1 Growth of liquid *E. coli* cultures

Liquid *E. coli* cultures were inoculated with cells from an agar plate, a short-term or long-term culture using a sterile toothpick. The cells were shaken at 37°C and 220 rpm over night (12 - 14 h) or for a depicted time period in LB medium containing the appropriate antibiotic/s for selection.

3.3.2 *E. coli* short-term storing

For short-time storage, over night liquid cultures were stored at 4°C for up to 4 weeks.

3.3.3 *E. coli* long-term storing

For long-term storage, 0.65 ml of an over night liquid culture was supplemented with 0.65 ml of sterile 60% glycerine and stored at -80°C.

3.3.4 Preparation of electrocompetent *E. coli* cells

Competent *E. coli* cells were prepared from a 1 l culture of $OD_{600} \sim 0.6$. Cells were cooled down on ice for 10 min and afterwards harvested by centrifugation (8 min, 6500 rpm, 4°C). They were washed two times with ice-cold ddH_2O and once with ice-cold 10% (v/v) glycerine. Finally, cells were resuspended in 2 ml ice-cold 10% (v/v) glycerine, split into 40 µl aliquots and stored at -80°C.

3.4 Microscopy

3.4.1 Fluorescence microscopy

An essential part of this work represented the *in vivo* visualization and evaluation of proteins labeled with a fluorescent tag by direct fluorescence microscopy. Yeast cells expressing the desired fluorescent-tagged proteins were grown over night at 30°C in CM selection media to the preferred growth phase. To cells expressing pMET25-mCherry-Atg21, 0.3 mM methionine was added to induce endogenous protein expression level. 4 - 5 µl of the culture was dropped on a slide and covered with a cover slip. Pictures were taken using a DeltaVision Spectris fluorescence microscopy (Olympus IX71, Applied Precision) equipped with a CoolSNAP HQ camera and either FITC and TRITC filter or specific GFP, YFP and mCherry filter sets (see Table 9). Images were generating using a 100 x objective by collecting a stack of at least 18 pictures with focal planes 0.20 µm apart. Pictures were deconvoluted using SoftWoRx software (Applied Precision) and processed using Adobe Systems Photoshop and Illustrator. A single focal plane is shown at each time.

Table 9: Overview of the used filter sets in fluorescence microscopy

Filter Sets	Excitation wavelength (nm)	Emmision wavelength (nm)
FITC	475/28	523/36
TRITC	542/27	594/45
GFP	475/28	525/50
YFP	513/17	559/38
mCherry	575/25	632/60
POL	-50/28	-50/0

3.4.2 Bimolecular Fluorescence Complementation (BiFC)

Bimolecular Fluorescence Complementation is described as a suitable method to study protein-protein interaction in their cellular environment using direct fluorescence microscopy (Skarp et al., 2008). For this purpose, two proteins of interest were fused to one fragment of eYFP. Expression vectors allowing high-copy expression of the fusion protein tagged either at the amino- or carboxy terminus with eYFP fragments from a constitutive *ADH* promotor were kindly provided by Skarp *et al.* (2008). In addition, expression vectors enable inducible expression of the tagged target proteins from a *MET25* promotor were used. Constructs were made as described in chapter 3.5.10.2.

Cells expressing fusion proteins from the *ADH* promoter were grown to log phase and visualized using a DeltaVision Deconvolution microscope as described in chapter 3.4.1.

Cells expressing fusion proteins from the *MET25* promoter were grown to mid-log phase in CM selective medium containing an excess of methionine. Cells were subsequently diluted to an OD_{600} of 0.3 in CM selective medium containing 0.5 mM methionine to induce fusion protein expression. Cells were grown at 30°C for an indicated period of time and visualized using a DeltaVision Deconvolution microscope as described in chapter 3.4.1.

For determination of the expression level of the fusion proteins, cells were grown in selective medium containing an indicated amount of methionine at 30°C over night to mid-log phase. Cells were subsequently alkaline lysed and the samples subjected to immunoblotting and analyzed using anti-GFP antibody (Abcam).

3.4.3 Determination of colocalization rates

In this study, direct fluorescence microscopy was predominantly used for localization studies of a particular protein. For this, the localization of this protein was determined by colocalization with other proteins that served as a reference like a PAS marker.

For the PAS localization studies of Atg21-YFP, first the percentage of cells positive for both, an Atg21-YFP and ApeI-RFP signal (PAS rate), was determined by analyzing at least 130 cells from at least three independent experiments. Subsequently, the quantity of ApeI-RFP dots colocalized with Atg21-YFP was determined (Colocalization Rate).

Similarly, the PAS and colocalization rate of mCherry-Atg21 and ApeI-YFP was determined as described above by analyzing at least 190 cells from three independent experiments.

To determine the Atg5/Atg16 rate, at least 322 cells from three independent experiments were observed for a perivacuolar Atg5-YFP respectively Atg16-GFP puncta.

For colocalization studies of mCherry-Atg21 and Atg16-GFP respectively Atg5-YFP, the quantity of Atg16-GFP respectively Atg5-YFP dots colocalized with mCherry-Atg21 was determined by analyzing at least 350 cells from at least four independent experiments.

For colocalization studies of mCherry-Atg21 and cAtg27-GFP, first the quantity of mCherry-Atg21 dots colocalized with cAtg27-GFP per cell was determined by analyzing 76 cells from two independent experiments. These cells were aligned into four categories:

1) no mCherry-Atg21 dot colocalized with cAtg27-GFP
2) 1 – 49% of the mCherry-Atg21 dots colocalized with cAtg27-GFP
3) 49 – 99% of the mCherry-Atg21 dots colocalized with cAtg27-GFP
4) all of the mCherry-Atg21 dots colocalized with cAtg27-GFP

3.5 Molecular biology methods

3.5.1 Isolation of chromosomal DNA

For the isolation of chromosomal DNA, 1.5 ml of an over night liquid yeast culture was harvested by centrifugation (13200 rpm, 1 min), washed once with

ddH_2O and resuspended in 200 µl breaking buffer (10 mM Tris/HCl pH 8.0, 100 mM NaCl, 1 mM EDTA, 1% SDS, 2% Triton X-100). After addition of 200 µl phenol/chloroform solution (50% (v/v) phenol, 50% (v/v) chloroform) and 200 µl glass beads, the cells were lysed by harsh mixing for 20 min at 4°C. 200 µl ddH_2O was added and the sample was centrifuged for 10 min at 13200 rpm. The upper phase was transferred into a new reaction tube, mixed with 1 ml ice-cold ethanol and incubated for 10 min at -20°C for precipitation of DNA. After centrifugation for 10 min at 13200 rpm and 4°C the supernatant was removed. The pellet was resuspended in 400 µl ddH2O and 3 µl RNase A (10 mg/ml) and incubated for 5 min at 37°C to digest the RNA. For further precipitation of the remaining DNA, 1 ml of ice-cold ethanol and 10 µl 5 M ammonium acetate were added. After incubation of 15 min at -20°C, the DNA was harvested by centrifugation for 10 min at 13200 rpm and 4°C. The supernatant was removed, the DNA pellet was dried at 37°C and finally resolved in 35 µl ddH_2O.

3.5.2 High efficiency transformation of DNA in yeast

A 50 ml liquid yeast culture was inoculated from a log phase yeast culture with a dilution of 1:10. The cells were grown for 2 - 6 h at 30°C to an OD_{600} of 0.5 - 0.8 and subsequently harvested by centrifugation (5 min, 2000 rpm, RT). After two washing steps with ddH_2O and one with LiOAC-Sorb (100 mM lithiumacetate, 10 mM Tris/acetate pH 8.0, 1 mM EDTA, 1 M sorbitol) the cells were resuspended in 100 – 500 µl LiOAC-Sorb and incubated for 15 min at 30°C for recovery. 50 µl cells were used for one transformation reaction. For this, 300 µl PEG in Li-TE buffer (100 mM lithiumacetate, 10 mM Tris/acetate pH 8.0, 1 mM EDTA, 40% PEG 3350), 5 µl herring sperm DNA and 3 – 10 µl of the respective DNA were added. The reaction was first incubated for 30 min at 30°C and then shifted to 42°C for 15 min. For recovery, the cells were transferred into 2 ml YPD-medium and shaken for 2 h at 30°C. Finally, the cells were harvested by centrifugation (5 min, 2000 rpm, RT) and spread on the respective selection medium.

3.5.3 "Quick and Dirty" transformation of plasmid-DNA in yeast

For the fast transformation of plasmid-DNA, yeast cells were taken from an agar plate and resuspended in 300 µl PEG in Li-TE buffer (100 mM lithiumacetate,

10 mM Tris/acetate pH 8.0, 1 mM EDTA, 40% PEG 3350). 5 µl of herring sperm DNA and 3 – 5 µl of the plasmid/s were added. After gently mixing, the cells were incubated for 30 min at 30°C and then shifted to 42°C. Afterwards, cells were harvested by centrifugation (5 min, 2000 rpm, RT), resuspended in 70 µl ddH_2O and directly spread on the respective selection medium.

3.5.4 Transformation of plasmid-DNA into *E. coli*

In this study, transformation of plasmid-DNA in *E. coli* was achieved by electroporation. Here, the permeability of the cell membrane is increased by an applied electric impulse resulting in the uptake of external DNA (Sheng et al., 2005). For transformation, electrocompetent *E. coli* cells (see 3.3.4) were thawed on ice, mixed with 1 - 2 µl of the appropriate DNA and transferred to a pre-chilled electroporation tube. The electroporation occurred at 2500 V. The cells were resuspended in 900 µl SOC-medium and shaken for 1 h at 37°C for recovery. After harvesting by centrifugation (5 min, 3000 rpm, RT), the cells were spread on LB-plates containing the appropriate antibiotics for plasmid selection.

3.5.5 Plasmid-DNA isolation from *E. coli*

Liquid *E. coli* cultures were inoculated with cells from either an agar plate using a sterile toothpick, from a short-term culture or from a long-term culture. The cells were shaken at 37°C over night (12 - 14 h) at 220 rpm. Plasmid-DNA was isolated using the Wizard Plus SV Kit from Promega according to the manufacturer´s instructions.

3.5.6 DNA agarose gel electrophoresis

The DNA agarose gel electrophoresis was used as a standard method to separate DNA fragments according to their size in an electric field. Depending on the size of the DNA fragments, 1 – 2% agarose gels supplemented with 1 µg/ml ethidiumbromide in TAE buffer (40 mM Tris/acetate pH 8.1, 2 mM EDTA, 0.114% acetic acid) were used. The DNA samples were mixed with DNA sample buffer (1 M Tris/HCl pH 8.0, 50% (v/v) glycerol, 0.1% (w/v) bromphenolblue) and separated for 20 – 30 min at 120 V. To determine the DNA fragment size, the

DNA Ladder Mix TriDye (1 kb, NEB) was used. DNA bands were documented by an UV-transilluminator.

3.5.7 DNA gel extraction (Gel Extraction Kit)

For purification of DNA fragments from agarose gels, the Qiagen Gel Extraction Kit from Qiagen (Hilden) was used according to the manufacturer´s instructions.

3.5.8 Polymerase chain reaction

DNA fragments used for molecular cloning or for homologous recombination in yeast were amplified by PCR using the Taq DNA polymerase (NEB) or for longer DNA fragments the KOD Hot Start DNA Polymerase (Novagen) according to the recommendations of the manufacturer. Therefore, standard PCR reactions in a 50 µl scale were performed. Plasmid DNA or yeast genomic DNA were used as templates. The respective program was adapted for each PCR reaction depending on oligonucleotides and product size. The amplified DNA was purified using the Qiagen PCR Purification Kit from Qiagen according to the manufacturer´s instructions.

3.5.9 Molecular cloning

In this study, several plasmids were constructed for the expression of a desired fusion protein (see Table 3). Therefore, the insert DNA sequence was amplified by PCR using chromosomal DNA or another plasmid as template. Here, flanking restriction sites for cloning were introduced by the designed primers (see Table 4). The DNA fragment was analyzed by agarose gel electrophoresis and purified using the Qiagen Gel Extraction Kit (see chapter 3.5.6 + 3.5.7).

The insert DNA fragment and the plasmid backbone were digested with the respective restriction enzymes (NEB) according to the manufacturer´s instructions in a scale of 30 µl. The reaction was incubated for 90 min at the enzyme optimal temperature. Afterwards the fragments were again purified and used for ligation. For determination of the optimal DNA ratio the following equation was used:

Equation 1: Equation to calculate optimal plasmid-insert ratio in ligation mix

$$\text{mass insert (ng)} = \frac{5 \times \text{mass plasmid (ng)} \times \text{length insert (bp)}}{\text{length plasmid (bp)}}$$ [1]

To the appropriate volumes of plasmid and insert DNA, 1 µl of ligation buffer and 2.5 U T4-DNA-ligase (NEB) were added and the reaction was filled up to 10 µl with ddH_2O. The ligation reaction was incubated for 2 h at room temperature or over night at 16°C. The ligated constructs were transformed in *E. coli* Dh5α by electroporation (see chapter 3.5.4). Potential clones were analyzed by restriction analysis and finally verified by sequencing.

3.5.10 Plasmid construction

3.5.10.1 Plasmid constructs used in split-ubiquitin assay

For the construction of all split-ubiquitin plasmids, the plasmids pRS313-MET25-STE14-Cub-RURA3 (provided by F. Reggiori (University Medical Centre Utrecht, Utrecht, The Netherlands) and N. Johnsson (Universität Ulm, Ulm, Germany)) and pRS314-CUP1-Nui-UBC6 (provided by N. Johnsson; (Wittke et al., 1999)) were used as initial plasmid backbone. The gene sequence of *STE14* was cut out with ClaI and SalI (if not stated otherwise) and replaced with the respective gene sequence. Similarly, the sequence of *UBC6* was cut out with BamHI and XhoI, if not stated otherwise.

For MET25-ATG16-Cub-RURA3, *ATG16* was amplified with Atg16Cub_ClaI_fwd and Atg16Cub_SalI-rev, cut with ClaI and SalI and ligated in MET25-Cub-RURA3.

For MET25-ATG27-Cub-RURA3, *ATG27* was amplified with Atg27Cub_ClaI_fwd and Atg27Cub_SalI_rev, cut with ClaI and SalI and ligated in MET25-Cub-RURA3.

For MET25-ATG23-Cub-RURA3, *ATG23* was amplified with Atg23Cub_StuI_fwd and Atg23Cub_SalI_rev. For MET25-ATG5-Cub-RURA3, *ATG5* was amplified with Atg5Cub_StuI_fwd and Atg5Cub_SalI_rev. Both fragment were cut with StuI and SalI and ligated in MET25-Cub-RURA3. Before, pRS313-MET25-STE14-Cub-RURA3 was cut with ClaI, treated with the DNA-polymerase Klenow to generate a blunt side and finally cut with SalI to remove *STE14*.

[1] Mülhardt, Cornel: Der Experimentator Molekularbiologie/Genomics; 5. Auflage, München 2006, Seite 136

For CUP1-Nui-ATG16, *ATG16* was amplified with Nui-Atg16_BamHI_fwd and Nui-Atg16_XhoI_rev. For CUP1-Nui-ATG27, *ATG27* was amplified with Nui-Atg27_BamHI_fwd and Nui-Atg27_XhoI_rev. All DNA fragments were cut with BamHI and XhoI and ligated into pRS314-CUP1-Nui.
For CUP1-Nui-ATG23, *ATG23* was amplified with Nui-Atg23_BamHI_fwd and Nui-Atg23_KpnI_rev, cut with BamHI and KpnI and ligated in pRS314-CUP1-Nui. Before, pRS314-CUP1-Nui-UBC6 was cut with BamHI and KpnI to remove *UBC6*.
For CUP1-Nui-ATG12, *ATG12* was amplified with Nui-Atg12_StuI_fwd and Nui-Atg12_XhoI_rev, cut with StuI and ligated in pRS314-CUP1-Nui. Before, pRS314-CUP1-Nui-UBC6 was cut with BamHI, treated with the DNA-polymerase Klenow to generate a blunt side and finally cut with XhoI to remove *UBC6*.

3.5.10.2 Plasmid constructs for BiFC

Plasmids for expression of proteins fused to one half of eYFP were kindly provided by Skarp *et al.* (2008). p426-ADH-C-YC and p426-ADH-N-YC allowed fusion of the C-terminal fragment of eYFP (amino acids 173 to 238) to the C- respectively N-terminus of a target protein. p425-ADH-N-YN allowed fusion of the N-terminal fragment of eYFP (amino acids 1 to 172) to the N-terminus of a target protein (Skarp et al., 2008).
For ADH-ATG21-C-YC, *ATG21* was amplified with Atg21_C-YC_BamHI_fwd and Atg21_C-YC_SalI_rev, cut with BamHI and SalI and ligated in p426-ADH-C-YC. For ADH-N-YC-ATG21, *ATG21* was amplified with Atg21_N-YC_BamHI_fwd and Atg21_N-YC_SalI_rev, cut with BamHI and SalI and ligated in p426-ADH-N-YC.
For ADH-ATG4-C-YC, *ATG4* was amplified with Atg4_C-YC_EcoRI_fwd and Atg4_C-YC_SalI_rev, cut with EcoRI and SalI and ligated in p426-ADH-C-YC. For ADH-N-YC-ATG4, *ATG4* was amplified with Atg4_N-YC_EcoRI_fwd and Atg4_N-YC_SalI_rev, cut with EcoRI and SalI and ligated in p426-ADH-N-YC.
For ADH-N-YN-ATG8, *ATG8* was amplified with Atg8_N-YN_BamHI_fwd and Atg8_N-YN_SalI_rev, cut with BamHI and SalI and ligated in p425-ADH-N-YN.
p416-MET25-C-YC was constructed by ligating a SalI and XhoI *C-YC* fragment from p426-ADH-C-YC into p416-MET25. Similarly, p415-MET25-N-YN was constructed by ligating a SpeI and BamHI *N-YN* fragment from p425-ADH-N-YN into p415-MET25.

p416-MET25-ATG21-C-YC was constructed by ligating a BamHI and XhoI *ATG21-C-YC* fragment from p426-ADH-ATG21-C-YC into p416-MET25. Similarly, p415-MET25-N-YN-ATG8 was constructed by ligating a SpeI and HindIII *N-YN ATG8* fragment from p425-ADH-N-YN-ATG8 into p415-MET25.

3.5.10.3 Atg16 plasmid constructs

For pRS313-CUP1-Atg16-HA, *ATG16-HA* was amplified with Atg16Cub_ClaI_fwd and Atg16HA_XhoI_rev using genomic DNA prepared from cAtg16-HA yeast cells. Similarly, for pRS313-CUP1-ATG16$^{1-57}$-HA and pRS313-CUP1-ATG16$^{1-119}$-HA, *ATG16$^{1-57}$-HA* and *ATG16$^{1-119}$-HA* were amplified with the same primer using genomic DNA prepared from cAtg16$^{1-57}$-HA respectively cAtg16$^{1-119}$-HA yeast cells. For pRS313-CUP1-ATG16$^{58-150}$-HA, *ATG16$^{58-150}$-HA* was amplified with Atg16HA_58-150_ClaI_fwd and Atg16HA_XhoI_rev using genomic DNA prepared from cAtg16-HA yeast cells. The DNA fragments were cut with ClaI and XhoI and ligated into pRS313-CUP1.

pRS313-CUP1-Atg16^{D101A}-HA, pRS313-CUP1-Atg16^{E102A}-HA, pRS313-CUP1-Atg16^{D101A_E102A}-HA, pRS313-CUP1-Atg16^{E97A}-HA and pRS313-CUP1-Atg16^{K94A}-HA were constructed using the QuikChange II Site-Directed Mutagenesis Kit (Agilent) as described in the manufacturer´s manual (see chapter 3.5.11). Point mutations were introduced using the respective primers: Atg16_D101A_fwd+_rev; Atg16_E102A_fwd+_rev; Atg16_DE_fwd+_rev; Atg16_E97A_fwd+_rev; Atg16_K94A_fwd+_rev.

For pGEX-4T3-GST-Atg16, *ATG16* was amplified with GST-Atg16_BamHI_fwd and GST-Atg16_XhoI_rev using genomic yeast DNA. Similarly, *ATG16$^{1-57}$* was amplified with GST-Atg16_BamHI_fwd and GST-Atg16$^{1-57}$_XhoI_rev, *ATG16$^{1-119}$* was amplified with GST-Atg16_BamHI_fwd and GST-Atg16$^{1-119}$_XhoI_rev and *ATG16$^{58-150}$* was amplified with GST-Atg16$^{58-150}$_BamHI_fwd and GST-Atg16_XhoI_rev. DNA fragments were digested with BamHI and XhoI and ligated into pGEX-4T3. Point mutations were introduced as described above.

pRS313-Atg16^{D101A}-GFP, pRS313-Atg16^{E102A}-GFP, pRS313-Atg16^{D101A_E102A}-GFP, pRS313-Atg16^{K97A}-GFP were generated as described above using pRS313-Atg16-GFP as template.

3.5.11 Site-directed mutagenesis of plasmids

To introduce point mutations in previously cloned genes, the QuikChange Site-Directed Mutagenesis Kit (Agilent) was used as described in the manufacturer´s manual. For this, complementary primers containing the respective nucleotide exchange were generated. The successful introduction of the point mutation was verified by sequencing.

3.5.12 Sequencing of DNA

All new designed constructs were verified by sequencing using the Sanger method. For this purpose, 1 µl of template plasmid DNA was mixed with 1 µl sequencing mix (polymerase, dNTP mix with fluorescent dyes, 30 mM magnesium chloride and buffer substances), 8 pmol oligonucleotides and 6 µl ddH_2O. After the sequencing reaction (25 cycles: 96°C 10 sec; 55°C 15 sec; 60°C 4 min), the DNA was precipitated by adding 1 µl 3 M sodium acetate (pH 5.2), 1 µl 125 mM EDTA and 50 µl ethanol. The DNA was harvested by centrifugation (13200 rpm, 10 min, RT), washed with 70% ethanol and dried. Finally, the DNA was resuspended in 15 µl HiDye (formamide) and analyzed by the Department of Developmental Biology of the Georg-August-Universität Göttingen using the Genetic Analyzer 3100 (Applied Biosystems).

At the end of this study, sequencing was performed by GATC Biotech (Konstanz) as described in the manufacturer´s instructions.

3.5.13 Gene deletion using homologous recombination

In this study, several deletion strains were performed using homologous recombination as described in Longtine *et al.* (1998). For this approach, a DNA fragment was amplified by PCR with special designed primers built up of a 45 bp homologous sequence to the flanking region of the target gene followed by a 20 bp homologous sequence of the selection gene (NatNT2 cassette). For amplification of the DNA fragment, the respective primers listed in Table 4 and pFA6a-NatNT2 (see Table 3) as plasmid template were used. The resulting DNA fragment, comprised of the selection gene, flanked by the homologous sequence to the up- and downstream region of the target gene, was transformed into the respective yeast strain using the high efficiency transformation protocol for yeast (see chapter 3.5.2). In principle, the similar sequence to the flanking

regions of the target gene results in the exchange with the selection gene by homologous recombination. Potential clones were selected on medium containing NatNT2. The successful deletion of the target gene was verified by control PCR analysis using chromosomal DNA as template and primers binding to a region upstream of the target gene and within the selection gene respectively.

3.6 Biochemical methods

3.6.1 SDS-Polyacrylamide-Gel-Electrophorese (SDS-PAGE)

Discontinuous SDS-PAGE was performed as a standard method to separate proteins according to their electrophoretic mobility as described in Laemmli *et al.* (1970). For this purpose 5% acrylamide stacking gels and, depending on the molecular size of the relevant proteins, 10 - 15% acrylamide separating gels were used.

Table 10: Contents of the separating gel

Separating Gel	2 x 10%	2 x 12%	2 x 15%
ddH_2O	3.9 ml	3.4 ml	2.4 ml
1.5M Tris (pH 8.8)	2.5 ml	2.5 ml	2.5 ml
Protogel	3.5 ml	4 ml	5 ml
10% SDS	100 µl	100 µl	100 µl
10% APS	100 µl	100 µl	100 µl
TEMED	5 µl	5 µl	5 µl

Table 11: Contents of the stacking gel

Stacking Gel	2 x
ddH_2O	6.1 ml
0.5M Tris (pH 6.8)	2.5 ml
Protogel	1.3 ml
10% SDS	100 µl
10% APS	100 µl
TEMED	10 µl

By default, 10 µl of the protein sample and as a marker the Precision Plus Protein All Blue Standard (Bio-Rad) were loaded (molecular weights: 250 kDa, 150 kDa,

100 kDa, 75 kDa, 50 kDa, 37.5 kDa, 25 kDa, 15 kDa 10 kDa). Electrophoresis was performed in a Mini-PROTEAN III electrophoresis chamber from Bio-Rad at a voltage of 150 V until the bromphenolblue front reached the end of the gel. The separating gel was subsequently stained with colloidale Coomassie or used for Western Blot analysis (see chapter 3.6.2 and 3.6.3).

SDS-sample-buffer:	116 mM Tris/HCl pH 6.8, 12% (w/v) glycerol, 3.42% (w/v) SDS, 0.004% bromphenolblue, 2% β-mercaptoethanol
SDS-running-buffer:	200 mM glycerol, 25 mM Tris, 0.1% SDS

3.6.2 Western Blot analysis

Proteins separated by SDS-PAGE were transferred onto a PDVF membrane using custom-made semi dry blotting chambers or a wet blot Mini Trans-Blot Cell from Bio-Rad. For the semi dry blotting, the SDS-gel, a PVDF membrane and six thin Whatman filter papers were soaked with semi dry blotting buffer (25 mM Tris, 192 mM glycine) and built up as shown in Figure 9. The transfer took place with 70 mA per gel for 90 min at room temperature.

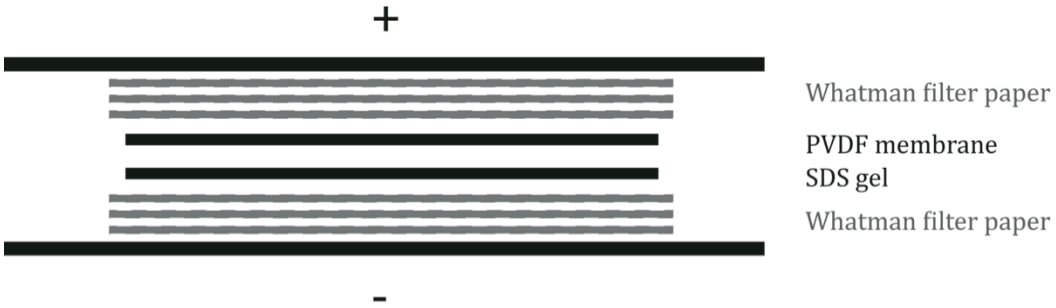

Figure 9: Scheme of semi dry Western Blot setting

For the wet blotting, the SDS-gel, a PDVF membrane, four thick Whatman filter papers and two filter pads were soaked with wet blotting buffer (192 mM glycin, 25 mM Tris and 20% methanol), assembled and inserted into the gel holder cassette as shown in Figure 10. The gel holder cassette was injected into the buffer tank filled with cold wet blotting buffer and an ice pack. The transfer was performed with 70 mA per gel for at least four hours up to over night at 4°C.

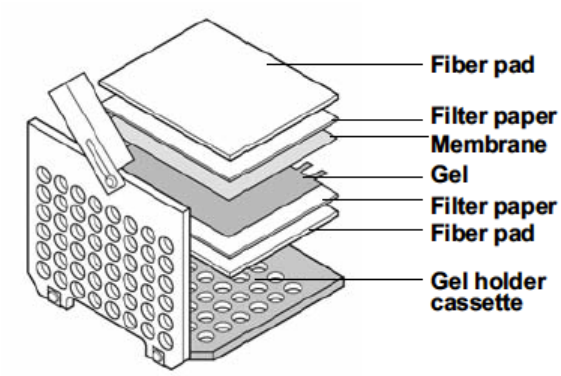

Figure 10: Scheme of Wet Western Blot settings (adapted from Mini Trans-Blot® Electrophoretic Transfer Cell Instruction Manual)

After successful blotting, the membrane was incubated in blocking buffer (TBST (20 mM Tris/HCl pH 7.6, 137 mM $NaCl_2$, 0.1% (w/v) Tween20) containing 10% (w/v) skim milk powder) for at least one hour at room temperature or over night at 4°C to mask all unspecific binding sites on the membrane. After washing three times with 25 ml TBST for 5 min, the membrane was incubated with the primary antibody (see Table 5) for at least 2 h at room temperature or over night at 4°C. After that, the membrane was washed again three times with 25 ml TBST for 10 min and incubated for one hour at room temperature with the HRP coupled secondary antibody in 25 ml TBST containing 1% (w/v) skim milk powder (see Table 5). The membrane was washed again three times with TBST for 10 min and the signals were analyzed using the ECL™ system (USB) and LAS-3000 (Fujifilm) according to the manufacturer´s instructions. Quantitative statistics were performed using the AIDA Software, Version 4.06.116 (Raytest, 2005).

It is possible to strip off the antibodies of once immunodetected membranes and to incubate the membrane with another primary antibody. For this purpose, the membrane was first activated by methanol and after washing with TBST incubated in 10% (v/v) acetic acid for 10 min at room temperature. After washing three times with TBST the membrane was incubated in 25 ml blocking buffer and the cycle started again (see above).

3.6.3 Colloidal Coomassie staining

Unselective protein staining of SDS-gels was performed by colloidal Coomassie. The SDS-gel was first incubated for 1 h in 25 ml fixating solution (40% (v/v) ethanol, 10% (v/v) acetic acid). After three washing steps with ddH_2O, proteins

were incubated in staining solution (20% (v/v) methanol, 0.1% (w/v) Coomassie Brilliant Blue G250, 2% (w/v) ortho-phosphoric acid, 10% (w/v) ammonium sulfate) over night at room temperature. Background staining was removed by incubating in 1% acetic acid until satisfaction. The Coomassie-stained gels were stored in 1% acetic acid or ddH_2O at 4°C.

3.6.4 Determination of protein concentrations

Protein concentrations were determined using a Bradford DC™ protein assay (Bio-Rad) according to the manufacturer´s instructions.

3.6.5 Alkaline lysis of yeast cells

For a quick and harsh lysis of yeast cells the alkaline lysis procedure was used. For this purpose, 1 - 2 OD_{600} of yeast cells was harvested by centrifugation (13200 rpm, 1 min, RT) and resuspended in 1 ml ice-cold ddH_2O and 150 µl lysis solution (1.85 M NaOH, 7.5% (v/v) β-mercaptoethanol). After 10 min incubation on ice and repeated harsh mixing, 150 µl 50% TCA solution was added and thoroughly mixed. After incubation on ice for 10 min, the sample was centrifuged for 10 min at 13200 rpm (4°C). The supernatant was removed and the pellet was washed twice with 200 µl ice-cold acetone. Finally, the pellet was resuspended in 50 - 100 µl 2 x SDS-sample buffer (116 mM Tris/HCl pH 6.8, 12% (w/v) glycerol, 3.42% (w/v) SDS, 0.004% bromphenolblue, 2% β-mercaptoethanol) and analyzed by SDS-PAGE and Western Blotting.

3.6.6 Cell lysis for detection of Atg8-PE

For detection of Atg8-PE, cells were lysed as described in Suzuki *et al.* (2001). In detail, 60 OD_{600} of growing yeast cells was harvested by centrifugation at 2000 rpm for 5 min and resuspended in 500 µl lysis buffer (50 mM Tris/HCl pH 7.5, 150 mM NaCl, 5 mM EDTA, 5 mM EGTA, 1 mM PMSF, Complete™ (Roche), protease inhibitor). After addition of 200 µl glass beads, the cells were lysed by harsh mixing for 10 min at 4°C. Afterwards, the cell lysate was cleared by centrifugating for 5 min at 3000 rpm and 4°C. 200 µl of the supernatant was transferred into a new reaction tube and, after addition of 40 µl 6 x Laemmli, boiled at 95°C for 5 min. For separating Atg8 and Atg8-PE, the samples were

separated on a 15% SDS-PAGE containing 6 M urea, subjected to immunoblotting and analyzed using an anti-Atg8 antibody (see Table 5).

3.6.7 Preparation of whole cell extracts – the mild cell lysis procedure

For gelfiltration chromatography, sorbitol density gradient centrifugation and GFP-TRAP® analysis, it was needed to prepare crude yeast cell lysate in a special mild cell lysis procedure. For this purpose, the cells were first converted into spheroblasts and subsequently mechanically lysed using a glass/ceramic homogenizer. In detail, 500 OD_{600} yeast cells was harvested by centrifugation at 2000 rpm for 5 min. The cells were once washed with 30 ml 10 mM NaN_3, resuspended in 5 ml SP-buffer (1.4 M sorbitol, 50 mM KH_2PO_4 pH 7.5, 10 mM NaN_3, 40 mM β-mercaptoethanol) containing 1.5 mg zymolyase T100 (the zymolyase has been shaken in SP-buffer for 30 min at 30°C before) and incubated for 40 min at 30 min in a water bath under weak shaking. The generated spheroblasts were harvested by centrifugation at 1000 x g for 10 min at 4°C and washed with 5 ml SP-buffer. SP-buffer was added in 1 ml steps and the spheroblasts were carefully resuspended using a rounded glass stick. After centrifugation at 2000 x g for 10 min at 4°C, the spheroblasts were resuspended in 500 µl of the particular lysis buffer (see below) and transferred into an ice-cooled glass/ceramic homogenizer. The cells were lysed with 30 pushes and the cell lysate was transferred into a new reaction cup. The homogenizer was rinsed with 500 µl lysis buffer, which was added to the cell lysate. If not stated otherwise, 0.5% Triton X-100 was added and the mix was incubated for 5 min at 4°C. Cell debris was removed by centrifugation at 3000 x g for 10 min at 4°C and the remaining crude cell lysate was used for the particular application mentioned above. The volume of the SP- and lysis buffer was adapted to the particular yeast amount if the approach was scaled up or down.

3.6.8 GFP-TRAP®

For the GFP-TRAP®, 350 OD_{600} yeast cells was harvested, treated and lysed in 350 µl TRAP lysis buffer (1 x PBS pH 7.4, 0.2 M sorbitol, 5 mM $MgCl_2$, 1 mM PMSF, Complete™ (Roche), protease inhibitors) as described in chapter 3.6.7. For immunoblot analysis, 25 µl of the cell lysate was diluted with 25 µl 6 x Laemmli buffer containing 6% β-mercaptoethanol and boiled for 10 min at

95°C (refer to as input). The remaining crude cell lysate was supplemented with 10 µl GFP-TRAP® bead slurry, which was washed twice with 100 µl PBS before (2700 x g, 2 min, 4°C). After incubation for 2 – 4 h at 4°C under constant inverting, the beads were harvested by centrifugation at 2000 x g for 2 min at 4°C. 25 µl of the supernatant was diluted with 25 µl 6 x Laemmli buffer containing 6% β-mercaptoethanol and boiled for 10 min at 95°C (refer to as supernatant). The beads were washed once with 1 ml and afterwards 3 times with 0.5 ml lysis buffer (2000 x g, 2 min, 4°C) and finally eluted in 50 µl 2 x Laemmli buffer containing 2% β-mercaptoethanol by boiling for 10 min at 95°C (refer to as bound). The samples were subjected to Wet Western Blot analysis as described in chapter 3.6.2.

3.6.9 Gelfiltration chromatography

For analysis of the high molecular weight Atg21 complex, yeast cells were grown in selection medium to mid-log phase. 1000 OD_{600} log cells were prepared and lysed in 1 ml GF lysis buffer (0.8 M sorbitol, 10 mM MOPS pH 7.2, 1 mM EDTA, 2 mM PMSF, Complete™ (Roche), protease inhibitors) as described in chapter 3.6.7. After preclearing for 10 min at 500 x g and 4°C, the cell lysate was centrifuged at 49 000 rpm for 30 min at 4°C (Beckman ultracentrifuge, Rotor TLA-100.3). The resultant supernatant was separated by size exclusion chromatography on a Superose™ 6 10/300 GL column (Amersham Pharmacia Biotech, Schweden), which was equilibrated with lysis buffer before. The elution from the column was carried out at a flow rate of 0.5 ml/min and 0.8 ml fractions were collected. The fractionated cell lysate was precipitated by adding 80 µl 100% TCA and 10 min storage on ice. After centrifugation for 10 min at 13 200 rpm at 4°C, the pellet was washed twice with 200 µl acetone. The pellet was dried at 37°C for 10 min and finally resuspended in 50 µl Laemmli buffer containing 2% β-ME and analyzed by SDS-PAGE and Wet Western Blotting as described in chapter 3.6.2. To determine the size of potential high molecular weight complexes, marker proteins (ApeI, PGK1 and CPY1) with well known molecular masses were detected by immunoblot analysis using anti-ApeI, -PGK1 and –CPY1 antibodies (see Table 5).

3.6.10 Density gradient centrifugation

Density gradient centrifugation was used to further analyze the high molecular weight Atg21 complex. Cells expressing pMET25-mCherry or pMET25-mCherry-Atg21 were grown in the absence of methionine to mid-log phase. 500 OD_{600} of cells was harvested, treated and lysed in 500 µl lysis buffer (10 mM MOPS pH 7.2, 0.2 M sorbitol, 1 mM EDTA, 2 mM PMSF, Complete™, protease inhibitor) as described in chapter 3.6.7. After preclearing of the crude cell extract (10 min, 500 x g, 4°C), the supernatant was ultracentrifuged for 30 min at 100 000 x g and 4°C (Beckman ultracentrifuge, Rotor TLA-100.3). The resulting supernatant was loaded on the top of a glycerol density gradient (per step 450 µl 50%, 40%, 30%, 20% glycerol) or sorbitol density gradient (per step 450 µl 2.5 M, 2 M, 1.5 M, 0.9 M sorbitol). After 4 h of ultracentrifugation at 259 000 x g and 4°C (Beckman ultracentrifugation, Rotor TLS-55), ten fractions each 200 µl were collected and precipitated with 20 µl 100% TCA. The sediments were washed two times with 200 µl acetone, resuspended in 100 µl 2 x Laemmli buffer and subjected to immunoblotting.

Table 12: Densities of the glycerol or sorbitol solutions used in density gradient centrifugation

density [g/ml]	Glycerol	Sorbitol
1.145	50%	2.5 M
1.111	40%	2 M
1.085	30%	1.5 M
1.049	20%	0.9 M

3.6.11 Pull down of His-SUMO-Atg21

3.6.11.1 Purification of recombinant 6xHis-SUMO-Atg21 and 6xHis-SUMO

Liquid precultures were inoculated with *E. coli* BL21 (DE3) pLysS cells expressing 6xHis-SUMO-Atg21 or 6xHis-SUMO alone from either an agar plate using a sterile toothpick or from a short-term culture. The cells were shaken at 37°C over night (12 – 14 h) at 220 rpm. At the next morning the cells were diluted to an OD_{600} of 0.2 and shaken for 90 min at 30°C and 220 rpm. To induct the expression of 6xHis-SUMO-Atg21 or 6xHis-SUMO, 0.2 mM IPTG and 1 mM PMSF were added. The cells were grown at 30°C for 4.5 - 5 h, harvested by centrifugation (5 min, 5000 rpm, RT), washed with 10 ml 1 x PBS (pH 7.4) and

finally frozen in liquid nitrogen. The cell pellets were stored at -80°C until use. The frozen cell pellets were resuspended in ice-cold lysis buffer (1 x PBS pH 7.4, 2 mM $MgCl_2$, protease inhibitors (Sigma), 1 µl benzonase) and stored on ice for 10 min. For immunoblot analysis, 15 µl of the cell lysate was diluted with 15 µl 6 x Laemmli buffer containing 50 mM DTT and boiled for 10 min at 72°C (refer to as *E. coli* L). After addition of 1% (v/v) Triton X-100, the unsoluble parts were spun out for 10 min at 10 000 rpm and 4°C. For immunoblot analysis, 15 µl of the supernatant was diluted with 15 µl 6 x Laemmli buffer containing 50 mM DTT and boiled for 10 min at 72°C (refer to as *E. coli* T). To couple 6xHis-SUMO-Atg21 to an agarose matrix via its His-tag, the remaining supernatant was added to 100 µl 50% Ni-NTA beads slurry (Qiagen, Hilden), which was washed twice with 1 ml ddH_2O and once with 1 ml 1 x PBS (pH 7.4) before. After addition of 20 mM imidazole (fresh prepared) to reduce unspecific background binding, the mix was incubated for 45 min at 4°C under constant shaking. The beads were harvested by centrifugation (5 min, 500 x g, 4°C), washed four times with 500 µl wash buffer (1 x PBS pH 7.4, 20 mM imidazole) and finally stored in 500 µl 1 x PBS (pH 7.4) on ice until use.

3.6.11.2 6xHis-SUMO-Atg21 pull down with crude yeast cell extract

50 OD_{600} yeast cells was harvested by centrifugation (2000 rpm, 5 min, 4°C), washed with 5 ml 1 x PBS (pH 7.4) and subsequently resuspended in 1 ml lysis buffer (1 x PBS pH 7.4, 5 mM EDTA, 0.5% (v/v) Triton X-100, 1 mM PMSF, Complete™ (Roche), protease inhibitors). After addition of 0.2 ml glass beads, the cells were mixed harsh for 20 min at 4°C followed by a preclearing centrifugation step at 3000 rpm and 4°C for 5 min. For immunoblot analysis, 50 µl of the supernatant was diluted with 10 µl 6 x Laemmli buffer containing 50 mM DTT and boiled for 10 min at 72°C (refer to as yeast input). The remaining supernatant was given to the prepared Ni-NTA-6xHis-SUMO-Atg21 or –SUMO beads (see chapter 3.6.11.1). The mix was incubated 2 – 4 h at 4°C under constant shaking. After extensive washing with lysis buffer, bound proteins were eluted with 50 µl Laemmli buffer containing 50 mM DTT, boiled for 10 min at 72°C (refer to as bound) and analyzed by 12% SDS-PAGE and following Wet Western Blot analysis (see chapter 3.6.2).

3.6.11.3 Purification of GST-Atg16

To test, if Atg21 and Atg16 interact directly with each other, recombinant expressed GST-Atg16 was incubated with recombinant 6xHis-SUMO-Atg21. For this purpose, GST-Atg16 was expressed and purified analogous to 6xHis-SUMO-Atg21 (see chapter 3.6.11.1) without imidazole. Furthermore, 100 µl of a 50% Glutathione Sepharose™ 4B (GE healthcare) was used for coupling. The bound GST-Atg16 constructs were eluted with 300 µl glutathione elution buffer (10 mM reduced glutathione, 50 mM Tris/HCl pH 8.0) in a three-step procedure. For this purpose, 100 µl of the elution buffer was added to the GST column and incubated for 10 min at room temperature under constant mixing. After sedimentation of the beads (3 min, 500 x g, RT), the supernatant containing eluted GST-Atg16 was collected and the elution procedure was repeated two times. The protein concentration of the eluted GST-Atg16 constructs was determined using Bradford assay (see chapter 3.6.4). The purified GST-Atg16 variants were used for the direct SUMO-Atg21 pull down (see chapter 3.6.11.4).

3.6.11.4 6xHis-SUMO-Atg21 pull down with recombinant proteins

To determine a direct interaction of Atg21 and Atg16, purified recombinant 6xHis-SUMO-Atg21 was incubated with purified recombinant GST-Atg16. For this purpose, purified GST-Atg16 variants (see chapter 3.6.11.3) were diluted with binding buffer (20 mM Na-P-buffer pH 7.4, 150 mM NaCl, 1 mM EDTA, 0.2% (v/v) Triton X-100, 1 mM PMSF, 1 x Complete (Roche), protease inhibitors) to a concentration of 10 µM in 500 µl. For immunoblot analysis, 20 µl of the preparation was diluted with 10 µl 6 x Laemmli buffer containing 50 mM DTT and boiled for 10 min at 72°C (refer to as input). The remaining GST-Atg16 was added to the purified and immobilized 6xHis-SUMO-Atg21 (see chapter 3.6.11.1), which was equilibrated with binding buffer before. After incubation for 2 h at 4°C under constant mixing, the beads were sedimented (5 min, 500 x g, 4°C) and washed twice with 500 µl binding buffer and once with 500 µl wash buffer (20 mM Na-P-buffer pH 7.4, 150 mM NaCl, 1.5 mM EDTA, 0.2% (v/v) Triton X-100, 1 mM PMSF, Complete™ (Roche), protease inhibitors). The bound proteins were eluted with 50 µl Laemmli buffer containing 50 mM DTT, boiled for 10 min

at 72°C (refer to as bound) and analyzed by 12% SDS-PAGE and following Wet Western Blot analysis (see chapter 3.6.2).

3.6.12 Mass spectrometry analysis

Mass spectrometry analysis was performed by the Bioanalytical Mass Spectrometry Group of Prof. Henning Urlaub (Bioanalytics, Department of Clinical Chemistry, University Göttingen).

3.6.12.1 Materials

Chemicals used were from Sigma-Aldrich, Taufkirchen. Solvents were obtained from Merck KgaA (Darmstadt) in Lichrosolv quality. Porcine trypsin was obtained from Serva Electrophoresis (Heidelberg). Chromatography materials were obtained from Dr. Maisch (Ammerbuch-Entringen).

3.6.12.2 In-gel digestion

Gel spots were washed with water, reduced with DTT (10 mM in 100 mM NH_4HCO_3, 50 min, 56°C) and alkylated with iodoacetamide (55 mM in 100 mM NH_4HCO_3, 20 min, room temperature, dark). In between sample handling steps, the gel spots were washed with acetonitrile for 15 min and taken to dryness in a Speedvac at 35°C (Savant Model SPD111V, Thermo Scientific, Dreieich) to remove excess solvent and improve uptake of reagent solution. Gel spots were rehydrated with porcine trypsin (12.5 ng/µl in 50 mM NH_4HCO_3, 5 mM $CaCl_2$), 50 mM NH_4HCO_3 added as supernatant and digested over night at 37°C.

3.6.12.3 Peptide extraction

Following digestion, 10 µl of water was added and the gel pieces were incubated at 37°C for 15 min. After a short centrifugation step, 80 µl acetonitrile was added and the samples again incubated at 37°C for 15 min. The supernatant was removed and transferred to an Eppendorf vial.

65 µl of 5% formic acid was added to the gel pieces, vortexed and incubated at 37°C for 15 min. 65 µl of acetonitrile was added and again incubated at 37°C for 15 min. After a short centrifuge step, excess solvent was removed and pooled with the supernatant from the first extraction step. The combined supernatants were taken to dryness in a Speedvac at 35°C and stored at -20°C until analysis.

3.6.12.4 Mass spectrometric analysis

The resulting peptide mixtures were concentrated on a Reversed Phase-C18 precolumn (0.15 mm ID x 20 mm self-packed with Reprosil-Pur 120 C18-AQ 3 µm material) and separated by Reversed Phase-C18 nanoflow chromatography (0.075 mm ID x 200 mm Picofrit column (New Objective, Woburn, MA/USA) self-packed with Reprosil-Pur 120 C18-AQ 3 µm material) using a 22 min linear gradient (5 - 35% acetronitrile vs. 0.1% formic acid, 240 nl/min) on an EASY nLC-1000 system (Thermo Scientific, Dreieich). The eluent was analyzed using a Top10 method in Data Dependent Acquisition mode on a Q Exactive high resolution mass spectrometry system (Thermo Scientific, Dreieich) operated under Tune 2.2 using HCD fragmentation, with a Normalized Collision Energy of 25%. Peak lists were generated using Raw2MSM v1.10 software (MPI for Biochemistry, Martinsried).

3.6.12.5 Database Searching

Tandem mass spectra were extracted by Raw2MSM software version 1.7 including charge state deconvolution and deisotoping. All MS/MS samples were analyzed using Mascot (Matrix Science, London, UK; version 2.4.1). Mascot was set up to search the SwissProt 2012_11x database (selected for Saccharomyces cerevisiae, 538585 sequences, 191240774 residues) assuming the digestion enzyme trypsin. Mascot was searched with a fragment ion mass tolerance of 0.020 Da and a parent ion tolerance of 10.0 PPM. Carbamidomethylation of cysteine was specified in Mascot as a fixed modification. Oxidation of methionine was specified in Mascot as a variable modification.

4 Results

4.1 Aim of the study

Atg21 and its homologues Atg18 and Hsv2, belong to a family of PI3P effectors involved in autophagy. They contain seven WD40 repeats, which form a seven bladed β-propeller scaffold (Baskaran et al., 2012; Krick et al., 2012; Watanabe et al., 2012). These proteins are known to serve as protein interaction platforms (Xu and Min, 2011). Atg21 has two lipid-binding pockets, which preferentially bind to PtdIns(3)P and PtdIns(3,5)P_2 and mediate its peripheral membrane association (Baskaran et al., 2012; Krick et al., 2012; Watanabe et al., 2012). While macroautophagy is only significantly reduced in the absence of Atg21, Atg21 is required for selective types of autophagy like the Cvt-pathway. Atg21 is involved in the biogenesis of the Cvt vesicles (Meiling-Wesse et al., 2004). In detail, Atg21 is required for the efficient lipidation of Atg8 and the recruitment of Atg8 and Atg5 to the pre-autophagosomal structure (PAS) (Meiling-Wesse et al., 2004; Stromhaug et al., 2004). Atg21 has been detected at endosomal compartments and at vertices of vacuolar junctions (Krick et al., 2008a; Meiling-Wesse et al., 2004). Despite its fundamental role in Cvt vesicle formation and the PAS recruitment of other autophagy-related proteins, up to now Atg21 has not been detected at the PAS itself (Stromhaug et al., 2004). Detection of its localization at the PAS and the identification of potential interaction partner of Atg21 will elucidate its molecular function and its role in the autophagic process.

4.2 Localization studies of Atg21

4.2.1 Part of Atg21-YFP was detected at the PAS

The PAS is defined as the site within a cell, where almost all of the autophagy related proteins colocalize and where the formation of the autophagosome is initiated. Although *atg21Δ* cells fail to form Cvt vesicles, Atg21 has not been detected at the PAS so far. To get a closer look, Atg21-YFP, expressed from its own promoter (Meiling-Wesse et al., 2004), was coexpressed with the PAS marker aminopeptidase I-RFP (ApeI-RFP) in *atg21Δ* cells and analyzed by direct fluorescence microscopy. Since Atg21 is required for the Cvt-pathway, that acts

under growing conditions, cells were imaged under these conditions. In growing *atg21Δ* cells, Atg21-YFP formed one to six perivacuolar puncta per cell (Figure 11). Some of them have been reported to colocalize with the late endosomal marker mRFP-FYVE (Krick et al., 2008a). For further localization analysis, the percentage of cells was determined, that exhibit an Atg21-YFP signal and an additional perivacuolar ApeI-RFP dot (PAS rate). Furthermore, the percentage of ApeI-RFP dots was determined that colocalized with Atg21-YFP (colocalization rate). Interestingly, 49% of the ApeI-RFP dots colocalized with Atg21-YFP suggesting that part of Atg21-YFP was indeed localized at the PAS. As a negative control, *atg14Δ* cells were utilized. Atg14 directs the Vps34 kinase complex I to the PAS, where it is required to generate the PAS-specific PI3P pool (Obara et al., 2006). Atg21 is peripherally membrane associated by binding to PI3P and PI(3,5)P_2 (Krick et al., 2006). In the absence of Atg14, and thus PI3P from the PAS, Atg21 should be absent from the PAS as it was shown earlier for its homologue Atg18 (Suzuki et al., 2007). Indeed, the colocalization of Atg21-YFP with the PAS marker ApeI-RFP was significantly reduced to only 22% in *atg14Δ* log cells.

For the homologue Atg18 an additional interaction with Atg2 is needed for proper membrane association at the PAS (Obara et al., 2008b; Rieter et al., 2013). To determine, which protein partner is responsible for proper PAS localization of Atg21, the colocalization rate of Atg21-YFP and the PAS marker ApeI-RFP was analyzed in several deletion strains by fluorescence microscopy as described above (Figure 11 + Figure 12).

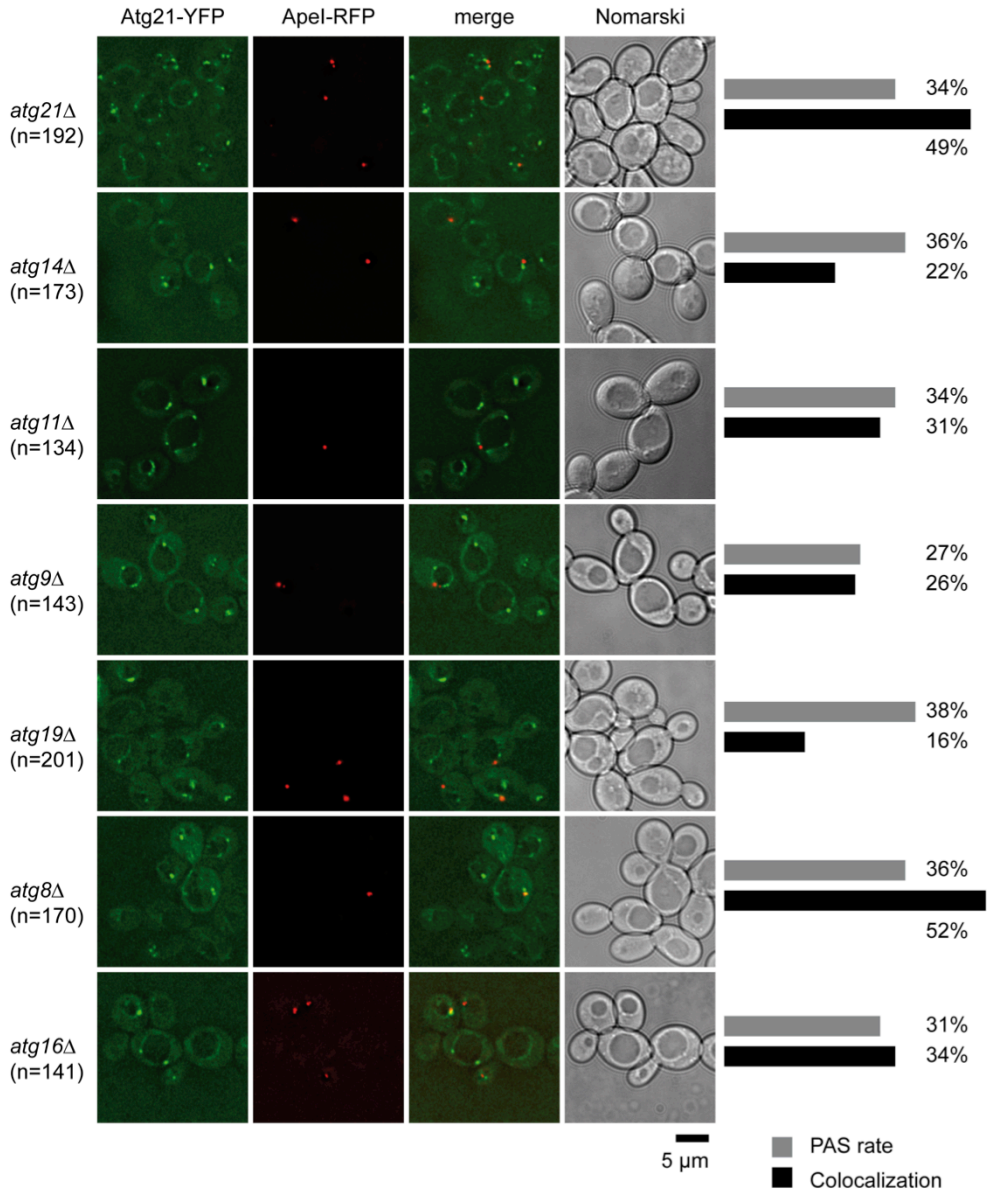

Figure 11: Part of Atg21 is localized at the PAS

The indicated strains expressing Atg21-YFP and the PAS marker ApeI-RFP were grown to log phase in selective medium at 30°C and visualized by direct fluorescence microscopy using a DeltaVision Deconvolution fluorescence microscope equipped with FITC and TRITC filter sets. Pictures were deconvoluted using SoftWoRx (Applied Precision) software. For each strain, the PAS rate and the Colocalization rate of Atg21-YFP and ApeI-RFP were determined. The PAS rate indicated, how many of the cells with an Atg21-YFP signal showed a perivacuolar ApeI-RFP dot. The Colocalization rate indicated, how many of those dots overlapped with Atg21-YFP. The number of evaluated cells (n) is indicated.

In the absence of Atg11, a scaffold protein crucial for PAS formation under growing condition, the colocalization rate of Atg21-YFP and ApeI-RFP was

slightly reduced to 34% compared to the wildtype (*atg21Δ* = 49%). The loss of the transmembrane protein Atg9, which delivers at least part of the membrane to the forming autophagosome or the loss of the Cvt cargo receptor Atg19, led to a more significant reduction of the colocalization rate to 26% and 16%, respectively. In the absence of Atg16, member of the E3 enzyme complex required for Atg8 lipidation, the Atg18-interacting protein Atg2, or the membrane protein Atg27, the colocalization rate was slightly reduced to 34% or 38%, respectively (Figure 11+Figure 12). In contrast, neither Atg8 nor Atg23 showed an influence on the PAS localization of Atg21-YFP (52% respectively 48%).

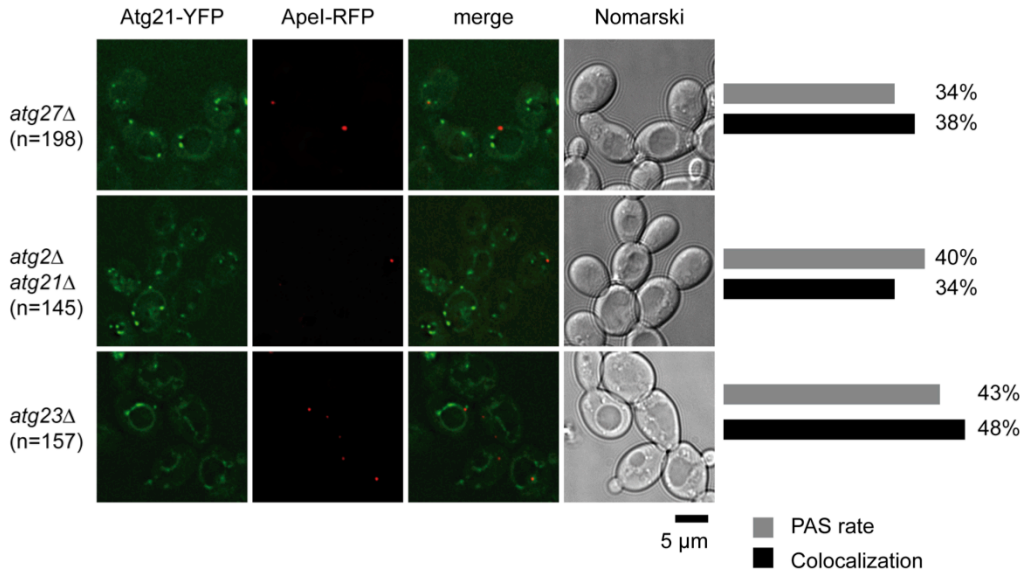

Figure 12: Additional analysis of the PAS localization of Atg21-YFP

The indicated strains expressing Atg21-YFP and the PAS marker ApeI-RFP were grown to log phase in selective medium at 30°C and visualized by direct fluorescence microscopy using a DeltaVision Deconvolution fluorescence microscope equipped with FITC and TRITC filter sets. Pictures were deconvoluted using SoftWoRx (Applied Precision) software. For each strain, the PAS rate and the colocalization of Atg21-YFP and ApeI-RFP were determined. PAS rate indicated, how many of the cells with an Atg21-YFP signal showed a perivacuolar ApeI-RFP dot. Colocalization indicated, how many of these dots overlapped with Atg21-YFP. The number of evaluated cells (n) is indicated.

Furthermore, none of the tested proteins had an influence on the overall punctate appearance of Atg21-YFP.

In further approaches, a pMET25-mCherry-Atg21 construct was used. To exclude overexpression artefacts caused by the expression from the inducible *MET25* promoter, the localization of mCherry-Atg21 was analyzed by direct fluorescence

microscopy as described above. 0.3 mM methionine was added to the selective medium to induce endogenous expression level (Krick et al., 2008a). In growing *atg21Δ* cells expressing mCherry-Atg21 and the PAS marker ApeI-YFP, 46% of the ApeI-YFP dots colocalized with mCherry-Atg21, whereas the colocalization rate was significantly reduced to only 23% in growing *atg14Δ* cells (Figure 13 A). Both colocalization rates correlated with the respective rates from *atg21Δ* and *atg14Δ* cells expressing Atg21-YFP from its endogenous promoter and ApeI-RFP, indicating that mCherry-Atg21 behaves like Atg21-YFP in living cells.

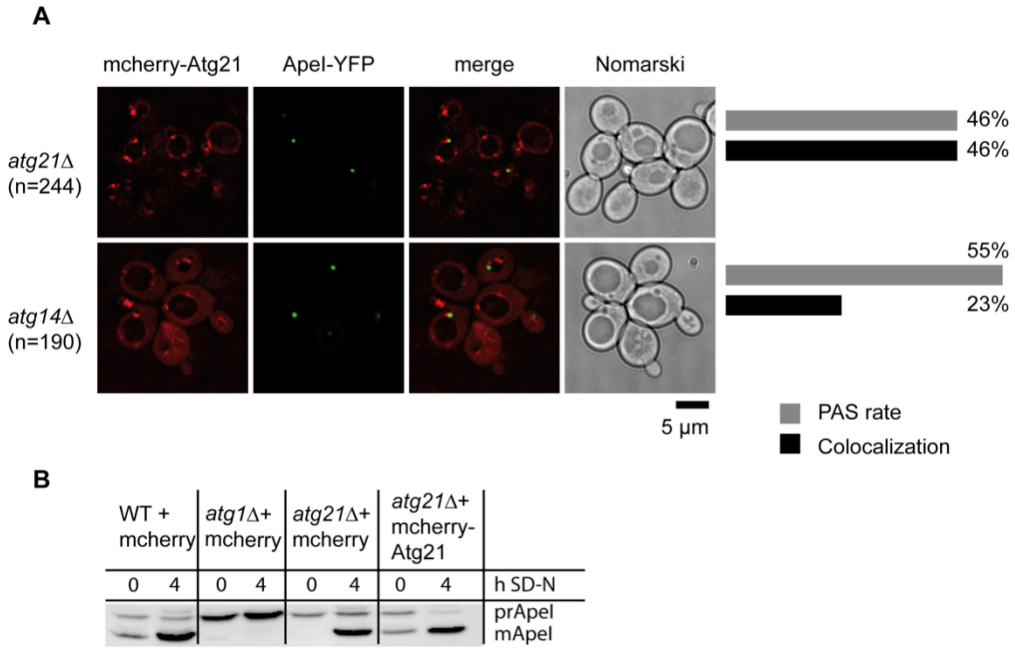

Figure 13: Complementation study of mCherry-Atg21 by monitoring ApeI maturation and determination of its PAS rate.

(A) Growing *atg21Δ* and *atg14Δ* cells expressing mCherry-Atg21 and ApeI-YFP in selective medium containing 0.3 mM methionine were visualized by direct fluorescence microscopy (DeltaVision Deconvolution microscope). Pictures were deconvoluted using SoftWoRX (Applied Precision) software. PAS rate and Colocalization rate were determined as described before (**Figure 11**). The number of counted cells (n) is indicated respectively. **(B)** Indicated strains expressing mCherry-Atg21 or mCherry alone were grown in selective medium containing 0.3 mM methionine. Mid-log cells (0 h) or cells starved for 4 h in SD-N (4 h) were alkaline lysed and immunoblotted. Using an anti-ApeI antibody, precursor ApeI (prApeI) and matured ApeI (mApeI) were detected.

To further prove the functionality of the mCherry-Atg21 construct, its ability to rescue the ApeI maturation defect of *atg21Δ* cells was tested (Figure 13 B). ApeI is expressed as a preform (prApeI) in the cytosol, where it forms large

dodecamers. These complexes are transported under growing conditions via the selective Cvt pathway, or under starvation via macroautophagy to the vacuole, where precursor ApeI is matured (mApeI). For the ApeI maturation analysis, WT, *atg1Δ* and *atg21Δ* cells expressing the empty vector and *atg21Δ* cells expressing mCherry-Atg21 were grown to mid-log phase (0 h SD-N) and subsequently starved for four hours in SD-N (4 h SD-N). Samples were taken at the indicated time points, alkaline lysed and subjected to immunoblotting. prApeI and mApeI were detected using an anti-ApeI antibody (Figure 13 B). In growing WT cells, about half of ApeI was matured, whereas after 4h of nitrogen starvation most of ApeI was found in its matured form. Atg1 is a core autophagy protein, therefore the maturation of ApeI was blocked under both growing and starvation conditions in *atg1Δ* cells. Since Atg21 is required under growing conditions, ApeI maturation was completely blocked under those conditions and severely impaired in starved *atg21Δ* cells. mCherry-Atg21 was able to fully rescue the ApeI maturation defect of *atg21Δ* cells under both, growing and starvation conditions, implicating that the mCherry-Atg21 construct was functional (Figure 13 B).

4.2.2 Atg21 is not transported into the vacuole

Within the autophagic process, the outer membrane of the completed, double-membrane layered autophagosome fuses with the vacuolar membrane to release the still one membrane layered autophagic body into the vacuole. In the vacuole the autophagic body is lysed and its contents are degraded. From the autophagy related proteins only those on the inside of the autophagosome are transported into the vacuole. Atg8 is evenly distributed across the outer and inner membrane of the autophagosome. The part, located on the inner membrane, is trapped inside the autophagosome and transported into the vacuole, whereas the Atg12-Atg5/Atg16 complex is only associated to the outer membrane and therefore not transported into the vacuole (Kirisako et al., 2000; Mizushima et al., 2001; Suzuki et al., 2001). Part of Atg21 was successfully detected at the PAS (see chapter 4.2.1). The PAS localization was dependent on Atg14 and therefore on the presence of PI3P on the forming autophagosome, suggesting that Atg21 is at least peripherally membrane associated there. To analyze, if Atg21 is evenly

distributed on the inner and outer membrane of the forming autophagosome or if it is only associated to the outer membrane, the transport of Atg21 into the vacuole was tested. *atg21Δ pep4Δ* cells were transformed with pMET25-mCherry-Atg21 and pRS313-GFP-Atg8, grown to an OD_{600} of 2 to 3 and analyzed by direct fluorescence microscopy (Figure 14). Again, 0.3 mM methionine was added to the media to induce endogenous mCherry-Atg21 expression level.

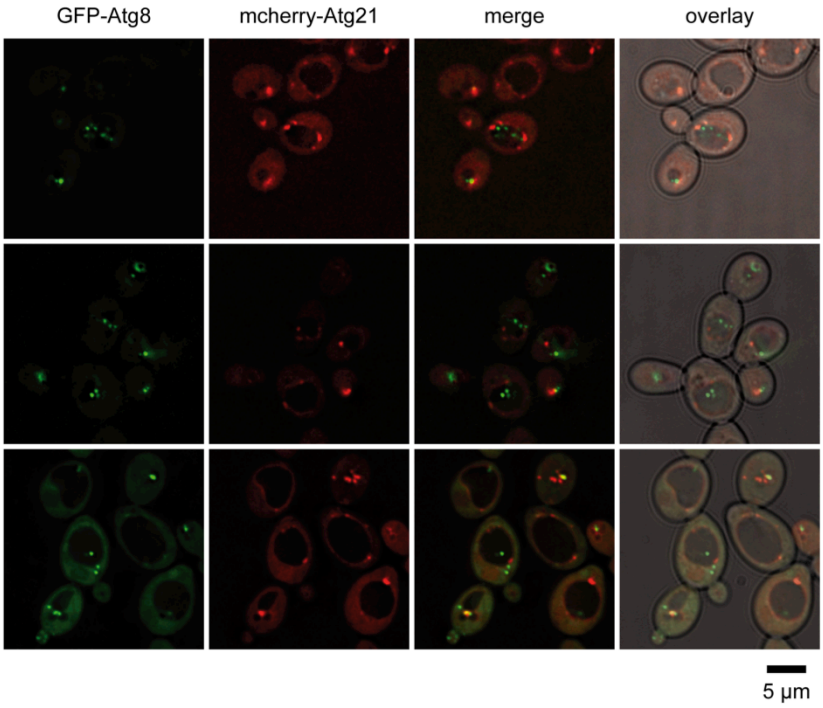

Figure 14: mCherry-Atg21 is not transported into the vacuole

atg21Δ pep4Δ cells expressing GFP-Atg8 and mCherry-Atg21 were grown in selective medium containing 0.3 mM methionine to an OD_{600} of 2 to 3. Pictures were taken using a DeltaVision fluorescence microscope equipped with a mCherry and GFP filter set and deconvoluted using SoftWoRX (Applied Precision) software.

In cells lacking the vacuolar aspartyl protease (Pep4), the autophagic bodies are not lysed within the vacuole and accumulate over the time. In this approach, they were visible as green dots within the vacuole by labeling with GFP-tagged Atg8. But none of those dots showed an additional red fluorescence for mCherry-Atg21. Furthermore, no red fluorescent dots were visible within the vacuole at all. Taken together, mCherry-Atg21 is most probably not transported into the vacuole and therefore not evenly distributed across the autophagosomal membranes.

4.3 Identification of interaction partner of Atg21

Atg21 is a WD40 repeat β-propeller. WD-repeat propeller proteins commonly create a stable platform for coordinating and mediating assembly of protein complexes (Xu and Min, 2011). Therefore, they often interact reversibly with several protein interaction partners. Identification of potential interaction partner of Atg21 will elucidate its molecular function and its role in the autophagic process.

4.3.1 Atg21 is part of a high molecular weight complex

4.3.1.1 Gelfiltration analysis of Atg21

The PAS localization of the Atg21 homologue Atg18 is specifically mediated by interaction with both, PI3P and Atg2 (Obara et al., 2008b; Rieter et al., 2013) . Obara *et al.* (2008) detected a large Atg18-Atg2 complex in gelfiltration (GF). Intriguingly, this large complex disappeared in the absence of Atg2. The gelfiltration approach was used to clarify, if Atg21 can also be found in a high molecular weight complex. Finding suitable conditions for purification of the Atg21 complex might lead to the identification of potential Atg21 interaction partner. For this purpose, pRS316-Atg21-TAP was transformed into *atg21Δ pep4Δ* cells. First, the cells were resuspended in Obara's GF-buffer (20 mM Tris/HCl pH 8.0, 150 mM KCL, 5 mM $MgCl_2$, 1 mM PMSF, 1% Triton X-100, protease inhibitors) and pneumatically lysed with a pressure of about 1500 bar in three cycles using the homogenizer EmulsiFlex C3 (Avestin). The cell lysate was cleared by ultracentrifugation at 100 000 x g for 30 min and subjected to size exclusion chromatography on a Superose 6 column. The cell lysate was eluted from the column at a flow rate of 0.5 ml/ml and 0.8 ml fractions were collected as it was described by Obara *et al.* (2008). The fractions were precipitated, dissolved in Laemmli buffer and processed for immunoblots (Figure 15). For molecular weight determination the immunoblot was decorated with antibodies against commonly used proteins with known size as ApeI and the phosphoglycerate kinase (PGK). ApeI is known to form dodecamers with a predicted molecular weight of about 670 kDa (Morales Quinones et al., 2012) and was present in fractions 16 to 17. PGK is a housekeeping protein and is,

independent from most conditions, randomly distributed in the cytosol. PGK has a molecular weight of about 45 kDa and was eluted in fractions 22 to 24.

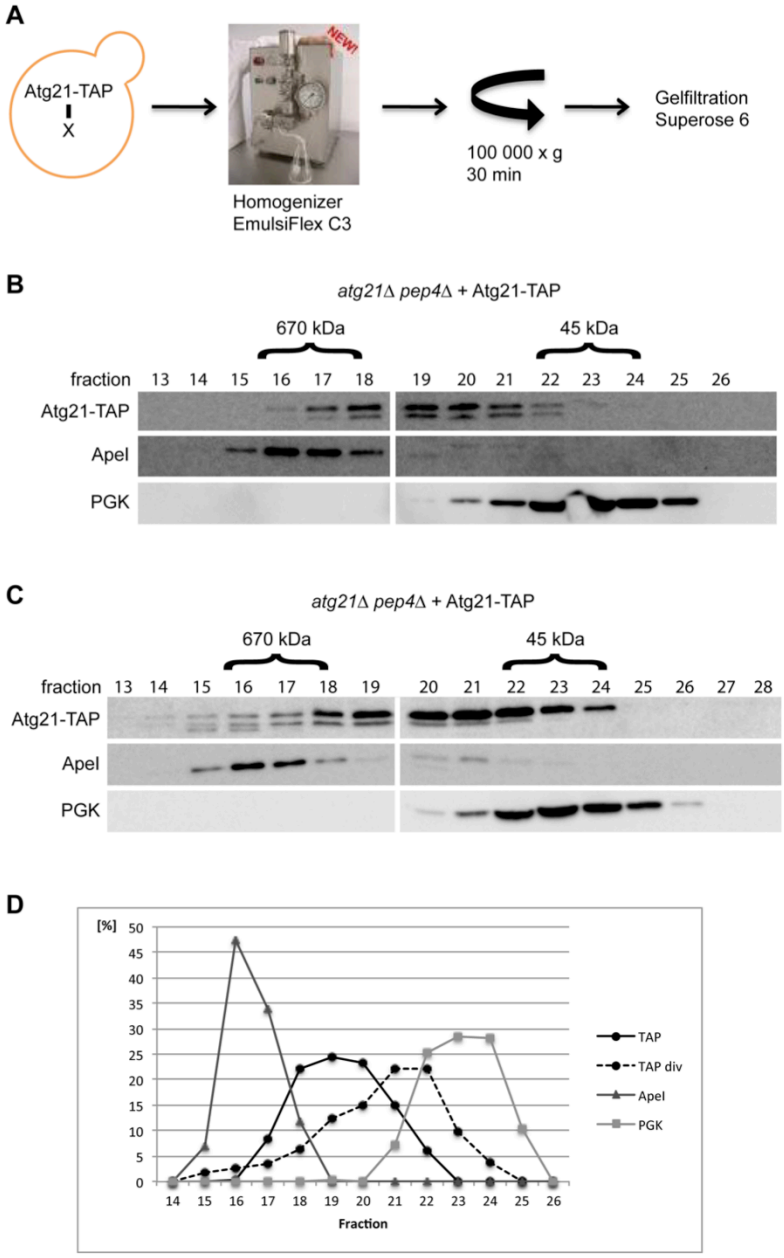

Figure 15: Atg21-TAP was present in a sensitive high molecular weight complex in gelfiltration

(A) Scheme of cell lysis and sample preparation for gelfiltration using the Homogenizer EmulsiFlex C3 (Avestin) (picture adapted from: http://www.avestin.com/ German/c3page.html). **(B)** *atg21Δ pep4Δ* cells expressing Atg21-TAP were treated as shown in (A) and subjected to size exclusion chromatography on a Superose 6 column. The cell lysate was eluted from the column at a flow rate of 0.5 ml/ml and 0.8 ml fractions were collected as it was described in Obara *et al.* (2008). Fractions were precipitated and analyzed by immunoblotting using anti-TAP, -ApeI and -PGK antibodies. **(C)** Part of Atg21-TAP is also present in its monomeric form. **(D)** Quantification of the distribution of the individual proteins in the respective fractions using AIDA software.

Atg21-TAP, with a predicted molecular weight of about 76 kDa, was eluted in fractions 18 to 20. Since fraction 18 corresponded to a molecular weight of about 670 kDa, a part of Atg21-TAP was present in a large complex (Figure 15 B+D). Unfortunately, these data were not reproducible. In further experiments, the main part of Atg21-TAP was present in fractions 21 to 22. These fractions corresponded to the predicted molecular weight of Atg21-TAP and are therefore likely to represent its monomeric form (Figure 15 C+D). To keep the apparent sensible large Atg21 complex intact, the cells were lysed in a very mild and preservative way. The cells were first converted to spheroblasts, solubilized in lysis buffer (0.8 M sorbitol, 10 mM MOPS pH 7.2, 1 mM EDTA, 2 mM PMSF, protease inhibitors) and then mechanically lysed with 30 beats of a cell homogenizer. The cell lysate was cleared and subjected to a Superose 6 column as described above (Figure 16 A). Again the immunoblot was decorated with antibodies against marker proteins as the ApeI complex (670 kDa) and the carboxypeptidase Y (CPY; 65 kDa). Under these conditions, the ApeI complex eluted in fractions 12 to 13, whereas CPY was present in fractions 16 to 17. Atg21-TAP was almost completely eluted in fractions 9 to 11, which corresponded to a molecular weight of 670 kDa and more. So Atg21-TAP seemed to be present in a high molecular weight complex (Figure 16 B). If the same cell lysis procedure was carried out by adding 0.5% Triton X-100 to the lysate after cell homogenization, a small amount of Atg21-TAP was present in additional fractions corresponding to lower molecular weights (Figure 16 C).

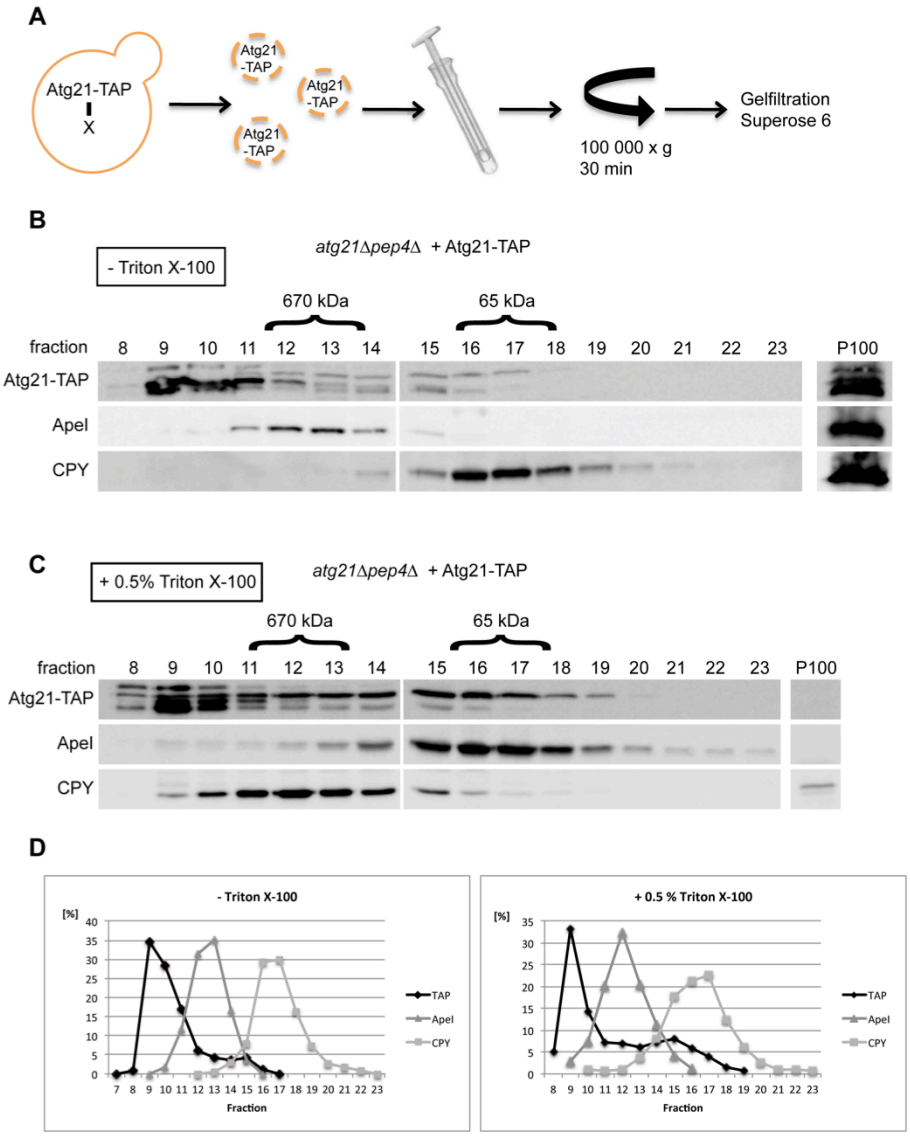

Figure 16: Alternative mild cell lysis procedure keeps the sensitive high molecular weight Atg21 complex intact

(A) Scheme of mild cell lysis procedure and sample preparation for gelfiltration using a mechanical cell homogenizer **(B)** *atg21Δ pep4Δ* cells expressing Atg21-TAP were treated as shown in (A) without detergence and analyzed by gelfiltration as described above. Distribution pattern of the respective proteins were analyzed by immunoblotting using anti-TAP, anti-ApeI and anti-CPY antibodies. **(C)** *atg21Δ pep4Δ* cells expressing Atg21-TAP were treated as shown in (A) with addition of Triton X-100 to the cell lysate after cell homogenization. Cell lysate was analyzed by gelfiltration as described in (B). **(D)** Quantification of the distribution of the individual proteins in the respective fractions using AIDA software.

In conclusion, a mild cell lysis procedure was established that keeps the sensitive high molecular weight Atg21 complex intact. Therefore, this cell lysis procedure

was used in the following experiments to further analyze the high molecular weight complex and to identify potential interaction partners of Atg21.

4.3.1.2 Sorbitol density gradient centrifugation

Density gradient centrifugation was used to further analyze the Atg21 high molecular weight complex. In this approach, proteins and protein complexes can be separated by their mass but also density and shape. In principle, a density gradient is created in a centrifugation tube. The cell lysate is placed on the top. Applied to a strong centrifugal field, proteins migrate along the gradient until they reach the point that corresponds to their density.

atg21Δ pep4Δ cells were transformed with pMET25-mCherry-Atg21 or with pMET25-mCherry as a negative control. Cells were harvested in growing phase and mildly lysed in the presence of Triton X-100 as described before (chapter 4.3.1.1). The cell lysate was placed on the top of a 20% to 50% glycerol density gradient and subsequently centrifuged for four hours at 259 000 x g (Figure 17 A). Afterwards ten fractions were collected beginning from the top of the gradient and precipitated with TCA. The pellets were dissolved in Laemmli buffer and processed for immunoblots (Figure 17 B).

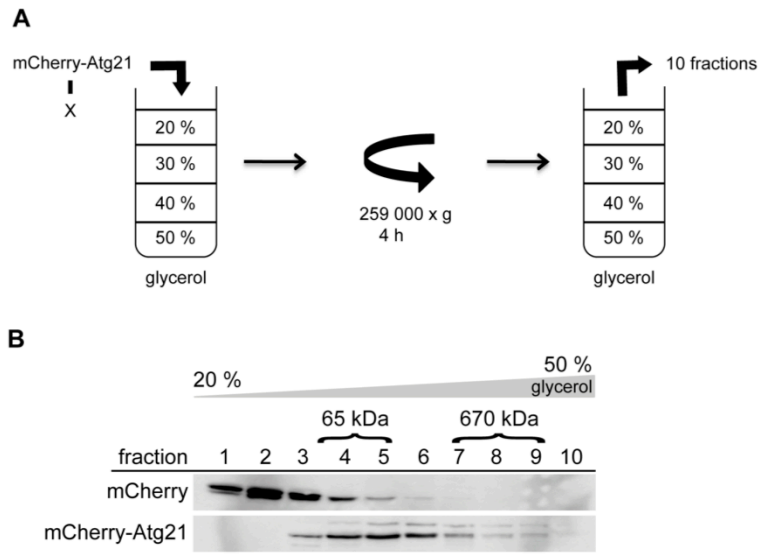

Figure 17: The high molecular weight Atg21 complex could not be detected after glycerol density gradient centrifugation

(A) Scheme of glycerol density gradient centrifugation procedure **(B)** *atg21Δ pep4Δ* cells expressing mCherry-Atg21 or mCherry alone were grown in selective medium in the absence of methionine to induce protein expression, converted to spheroblasts and mechanically lysed

using a cell homogenizer. Cell lysate was subjected to a 20% to 50% glycerol density gradient centrifugation as described in (A). Ten fractions were collected beginning from the top of the gradient and analyzed by immunoblot using an anti-ApeI, -CPY and –Red (specifically recognizes mCherry) antibody.

As a molecular weight marker monomeric CPY (65 kDa) and the ApeI complex (670 kDa) were used (data not shown). CPY was found in fractions 4 to 5, the ApeI complex in fractions 7 to 8. As expected, mCherry with a molecular weight of about 30 kDa was present in the first fractions corresponding to low density (fractions 1 to 3). mCherry-Atg21 (82.5 kDa) was detected in fraction 4 to 6, corresponding to the fractions where CPY was present. So mCherry-Atg21 was rather present in its monomeric form than in a complex. As seen in the gelfiltration analysis, the Atg21 high molecular weight complex was extremely sensitive (chapter 4.3.1.1). One possibility for the instability of the complex could be intolerance for glycerol. Sorbitol was present in the cell lysis buffer, where the Atg21 high molecular weight complex was stable as seen in gelfiltration (chapter 4.3.1.1). Therefore, the glycerol in the gradient was exchanged with sorbitol solutions with the same density, respectively (Figure 18 A). Cell lysate of *atg21Δ pep4Δ* cells expressing pMET25-mCherry-Atg21 or pMET25-mCherry as a control were loaded on a 0.9 M to 2.5 M sorbitol density gradient and centrifuged for four hours at 259 000 x g (Figure 18 A). Again, ten fractions beginning from the top of the gradient were taken and analyzed using anti-Red, anti-ApeI and anti-CPY antibodies in immunoblotting (Figure 18 B). The ApeI complex (670 kDa) was detected in fractions 7 to 9, whereas CPY (67 kDa) was mainly present in fractions 3 to 4. As expected, mCherry was again present in the first fractions (fractions 2 to 3) corresponding to low density and molecular weight. In contrast, mCherry-Atg21 was found in fractions 4 to 8 and was therefore at least partly present in fractions corresponding to high molecular weight and density.

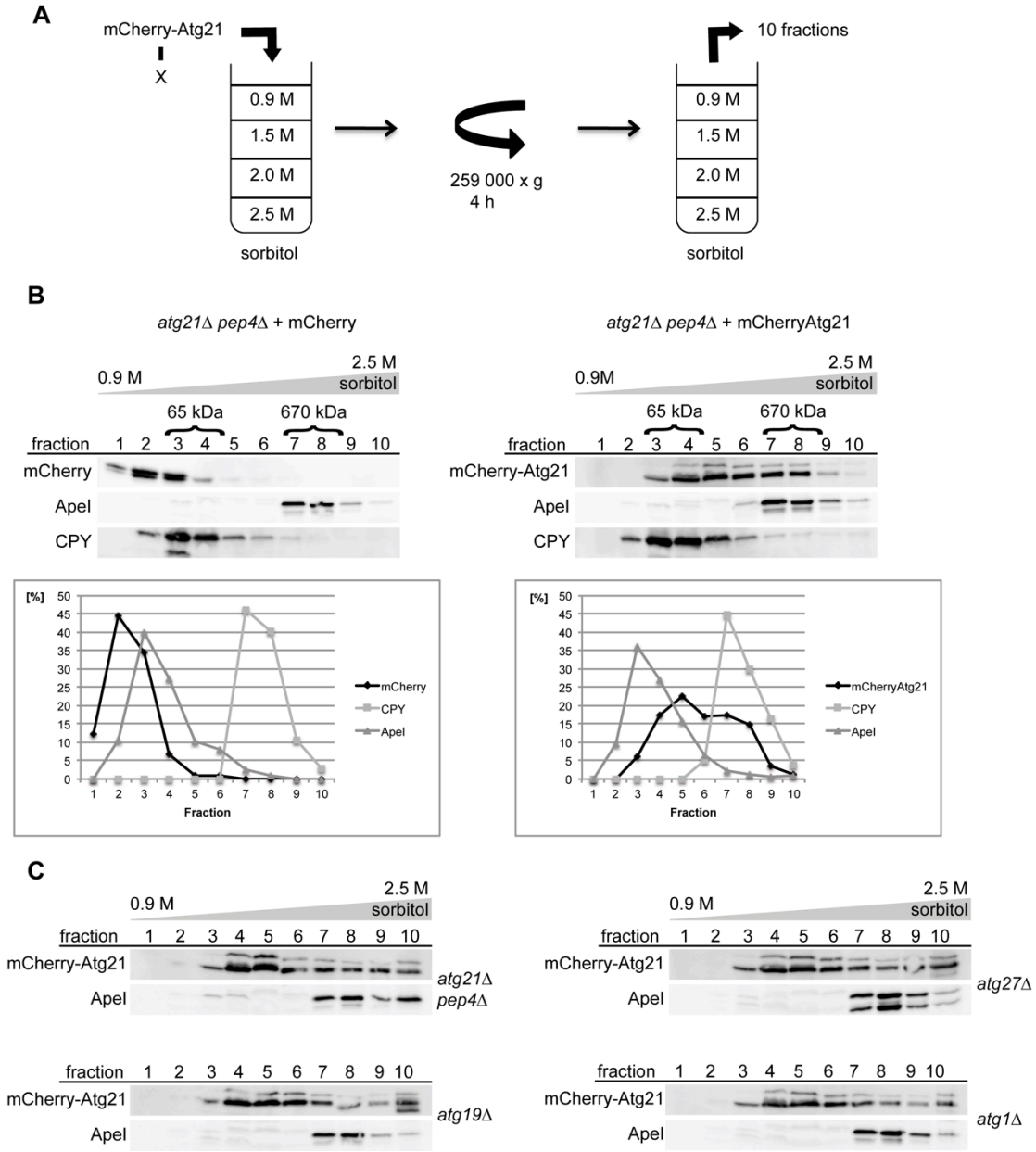

Figure 18: mCherry-Atg21 is present as a high molecular weight complex in sorbitol density gradient centrifugation

(A) Scheme of sorbitol gradient centrifugation procedure **(B)** *atg21Δ pep4Δ* cells expressing mCherry-Atg21 or mCherry were grown in selective medium without methionine to induce protein expression. Cell lysates were prepared with 0.5% Triton X-100 as described before and subjected to sorbitol density gradient centrifugation as described in (A). Ten fractions beginning from the top of the gradient were taken, TCA precipitated and analyzed by immunoblot using anti-Red, anti-ApeI and anti-CPY antibody. The distribution pattern of the respective proteins within the gradient was quantified using AIDA software. **(C)** Cell lysate of *atg21Δ pep4Δ, atg19Δ, atg27Δ* and *atg1Δ* cells expressing mCherry-Atg21 were prepared in the absence of detergence as described before and subjected to sorbitol gradient centrifugation as described in (A) and (B).

Gelfiltration revealed that detergence influenced the stability of the Atg21 high molecular weight complex (chapter 4.3.1.1). To determine, if this could also be true for sorbitol density gradient centrifugation, cells expressing pMET25-mCherry-Atg21 were lysed in the absence of detergence and cell lysate were again loaded on the top of a 0.9 M to 2.5 M sorbitol gradient. Indeed, a part of mCherry-Atg21 could be detected in fractions corresponding to high molecular weight and density (fraction 9 and 10;Figure 18 C).

Sorbitol gradient centrifugation was performed with different knock out strains expressing pUG36-mCherry-Atg21 to determine if any of these proteins had an influence on the formation of the Atg21 high molecular weight complex or might even be a component of it. To preserve the complex, cell lysates were prepared in the absence of detergence. Surprisingly, nor Atg19, Atg27 or Atg1 changed the distribution of mCherry-Atg21 in the sorbitol gradient compared to *atg21Δ pep4Δ* cells (Figure 18 C). So none of the tested proteins was involved in the formation of the high molecular weight Atg21 complex or was a stoichiometric component of it.

4.3.2 Pull down und mass spectrometry analysis to identify potential Atg21 interaction partner

Pull down experiments were used as one method to identify potential Atg21 interaction partner. Therefore, recombinant 6xHis-SUMO-Atg21 was incubated with crude yeast cell extract and the co-precipitated proteins were identified by mass spectrometry analysis. Atg21 was N-terminally fused to SUMO and an additional six histidine tag for purification (6xHis-SUMO-Atg21) (Figure 19 A). To exclude those proteins, which bound to SUMO, SUMO alone, N-terminally tagged with six histidines, was used as a negative control (6xHis-SUMO). Recombinant 6xHis-SUMO-Atg21 and 6xHis-SUMO was purified via Ni-NTA-beads (see chapter 3.6.11). Samples were taken after *E. coli* cell lysis (*E. coli* L) and after cell lysate clearance by centrifugation (*E. coli* S) to prove efficient expression and the solubility of 6xHis-SUMO-Atg21. 6xHis-SUMO-Atg21 and 6xHis-SUMO coupled to Ni-NTA beads were subsequently incubated with crude cell extract of *atg21Δ* cells expressing mCherry-Atg19 and GFP-Atg8 (yeast L). Afterwards the supernatant containing the unbound proteins (yeast S) was

removed. After extended washing, 6xHis-SUMO, 6xHis-SUMO-Atg21 and all associated proteins (E) were eluted from the beads by adding NuPAGE® sample buffer (Life Technologies) and boiling at 72°C for 10 min. The samples were also loaded on a SDS-PAGE and processed for immunoblotting. (Figure 19 B).

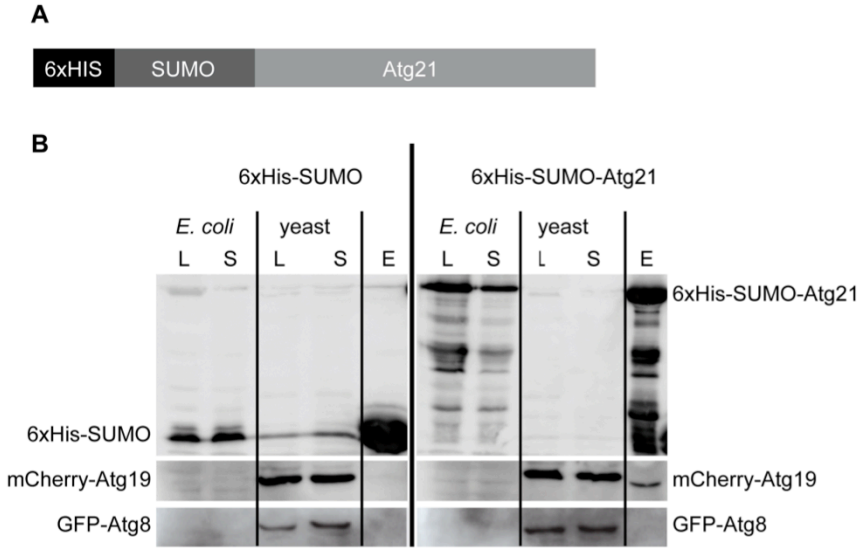

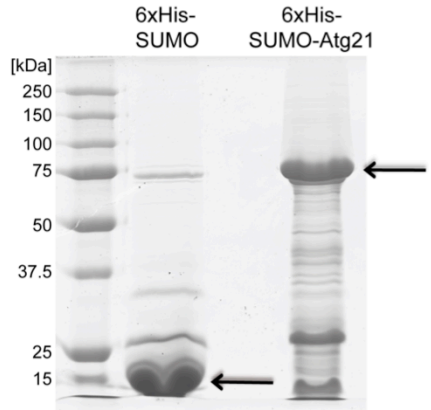

D

identified proteins	6xHis-SUMO peptide number	6xHis-SUMO peptide coverage [%]	6xHis-SUMO quantitative values	6xHis-SUMO-Atg21 peptide number	6xHis-SUMO-Atg21 peptide coverage [%]	6xHis-SUMO-Atg21 quantitative values
Tor1	0	0	0	78	40	65
Tor2	0	0	0	51	29	43
Tco89	2	2.4	3	27	45	20
Kog1	0	0	0	42	33	30
Lst8	1	2.3	6	4	19	4

Probability Legend: over 95% 50% to 79% 0% to 19%

Figure 19: Pull down analysis of SUMO-Atg21

(A) Scheme of the 6xHis-SUMO-Atg21 construct **(B)** Recombinant 6xHis-SUMO and 6xHis-SUMO-Atg21 were purified using Ni-NTA beads and incubated with crude extract of growing *atg21Δ*

cells expressing mCherry-Atg19 and GFP-Atg8. The respective yeast and *E.* coli lysates (L), cleared lysate (*E. coli* S), unbound fraction (yeast S) and the purified proteins (E) were subjected to SDS-PAGE analyzed by immunoblotting using anti-His, anti-Red and anti-GFP antibodies. **(C)** Isolated proteins (E) were further analyzed by Coomassie staining and subjected to mass spectrometry (MS) analysis for identification. **(D)** Identified members of the TORC1 complex are listed. The respective peptide number, coverage and quantitative values determined by the Scaffold3 software are shown.

6xHis-SUMO-Atg21 was present in both the *E. coli* lysate and supernatant after centrifugation in comparable amounts, suggesting that recombinant 6xHis-SUMO-Atg21 was soluble. Furthermore, 6xHis-SUMO-Atg21 could be successfully purified in sufficient amounts (see E in Figure 19 B and C). Though the potential Atg21 interaction partner GFP-Atg8 did not co-precipitate with 6xHis-SUMO-Atg21 (see below), the Cvt receptor mCherry-Atg19 could be specifically co-precipitated. Since Atg21 is required for the Cvt pathway, this indicates that 6xHis-SUMO-Atg21 was functional.

In addition, the eluates of the 6xHis-SUMO-Atg21 and 6xHis-SUMO pull down were loaded on a SDS-PAGE and analyzed by colloidal Coomassie staining. Only three additional bands to 6xHis-SUMO were visible in the 6xHis-SUMO eluate, whereas several additional bands representing potential interaction partner were prominent in the eluate of the 6xHis-SUMO-Atg21 pull down. For identification of the potential interaction partner, the eluate samples were subjected to mass spectrometry analysis (performed by Bioanalytical Mass Spectrometry Group of Prof. Henning Urlaub, Universität Göttingen). In total, 912 proteins were identified. Based on quantitative values, those proteins were excluded that were present in the negative control (6xHis-SUMO) in an equivalent or higher amount compared to the 6xHis-SUMO-Atg21 sample. Regardless of the low quantitative values of some of the proteins, 728 proteins were specifically identified that bind to 6xHis-SUMO-Atg21. Curiously, none of them represented an Atg protein. However, all components of the target of rapamycin complex 1 (TORC1) were identified (Figure 19 D). Among other functions, TORC1 is a key actor in autophagy regulation. TORC1 consists of Tco89, Kog1, Lst8 and either Tor1 or Tor2 (Loewith and Hall, 2011). Tor1, Tor2, Tco89 and Kog1 were present in high quantitative values in the 6xHis-SUMO-

Atg21 sample. The negative control 6xHis-SUMO showed no binding to the subunits of TORC1 other than Lst8. Though the quantitative value was slightly higher in the negative control, only one peptide was detected leading to a peptide coverage of only 2.3%. In contrast, in the 6xHis-SUMO-Atg21 pull down four peptides of Lst8 were identified leading to a peptide coverage of 19%. Based on this, the probability in the 6xHis-SUMO pull down was limited to only 50% compared to 100% in the 6xHis-SUMO-Atg21 sample (Figure 19 D). However, these data supported an interaction of 6xHis-SUMO-Atg21 with TORC1.

4.3.3 Split-ubiquitin analysis of Atg21

The split-ubiquitin assay represents an analytic tool for measurement of protein interaction in living yeast cells (Müller and Johnsson, 2008) and was used for a large-scale search for potential interaction partners of Atg21.

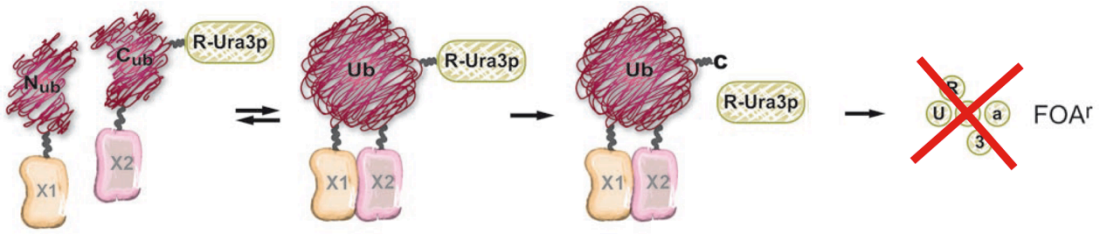

Figure 20: Scheme of the principle of the split-ubiquitin assay (adapted from (Müller and Johnsson, 2008))

For this purpose, ubiquitin is split into two halves and fused to two proteins of interests (Figure 20). In detail, the N-terminal half of ubiquitin (Nui) was fused to the N-terminus of one of the proteins (prey) and the C-terminal half of ubiquitin (Cub) was fused to the C-terminus of the other protein (bait). In addition, the Cub fragment was attached to the reporter protein R-Ura3. Ura3 represents the orotidine 5-phosphate decarboxylase and plays a crucial role in the synthesis of uracil. Furthermore, it is able to convert 5-Fluoroorotic acid (5-FOA) into the toxic compound 5-fluorouracil, so that it can be used as both a positive and negative reporter protein. If both proteins of interest interact with each other, the two halves of ubiquitin reassemble into native-like ubiquitin. Ubiquitin can now be recognized by ubiquitin specific proteases, which in turn cleave off the reporter protein R-Ura3. Because an arginine residue was introduced at the Cub-Ura3 junction, the free R-Ura3 protein exposes an N-terminally arginine residue,

which is according to the N-end-rule a destabilizing amino acid and leads to the rapid degradation of R-Ura3 and therefore to uracil auxotrophy (Müller and Johnsson, 2008). Consequently, cells expressing interacting proteins are able to grow on plates containing 5-FOA but not on plates lacking uracil. The other way round, if the two proteins do not interact with each other, the two halves of ubiquitin do not reassemble to native ubiquitin. Therefore, the reporter protein R-Ura3 is not cleaved off and degraded. Thus, cells expressing non-interacting proteins are able to grow on plates lacking uracil but not on plates containing 5-FOA.

Atg21 was tested for an interaction with several autophagy related proteins. 1 OD_{600} cells expressing Atg21-Cub and the respective Nui-Atg protein were diluted in 10-fold steps and spotted on CM-Trp-His (growth control), on CM-Trp-His +FOA (growth indicated interaction of the proteins) and on CM-Trp-His-Ura (growth indicated no interaction of the proteins). The expression of the proteins of interest was induced by the addition of either 100 µM $CuSO_4$ (Nui) or 250 µM methionine (Cub) to the selective medium (Laser et al., 2000). After two to three days the growth pattern was analyzed. Cells expressing the interacting proteins Ste14-Cub and Nui-Ubc6 served as a positive control, cells expressing Ste14-Cub and the empty vector (pRS314) as a negative control (Krick et al., 2010). Atg21-Cub was tested for an interaction with Nui-Atg1, -Atg5, -Atg7, -Atg8, -Atg9, -Atg12, -Atg16, -Atg18, -Atg19, -Atg21, -Atg23, -Atg27, -Hsv2, -Trs85 and -Vam1. Three of them, Atg27, Atg8 and Atg16 showed a potential interaction and have been analyzed in more detail.

4.3.4 Interaction studies of Atg21 und At27

Atg27 is a type I membrane protein. It directly interacts with the second autophagy related membrane protein Atg9, which in turn interacts with the cytosolic protein Atg23 to form a trimeric complex. All three proteins cycle between the PAS and a peripheral pool and are dependent on each other for efficient cycling (Legakis et al., 2007; Yen et al., 2007). Comparable to Atg21, Atg27 is absolutely required for the Cvt pathway, whereas macroautophagy is only significantly reduced in *atg27Δ* cells (Yen et al., 2007). Both, PI3P binding and interaction with its interacting partner Atg2, are crucial for proper PAS

localization of the Atg21 homologue Atg18 (Rieter et al., 2013). As a membrane protein required for the Cvt pathway, Atg27 would be a good candidate for the missing interaction partner of Atg21 at the PAS.

4.3.4.1 Atg27 and Atg21 interact with each other in split-ubiquitin assay

In the split-ubiquitin assay, Atg21-Cub showed neither an interaction with Nui-Atg9 nor Nui-Atg27 (Figure 21 A). Furthermore, there was no interaction detectable between Atg23-Cub and Nui-Atg21 or its indirect binding partner Nui-Atg27 (Figure 21 B). In contrast, an interaction of Atg23-Cub and its direct interaction partner Nui-Atg9 was detected, serving as a positive control.

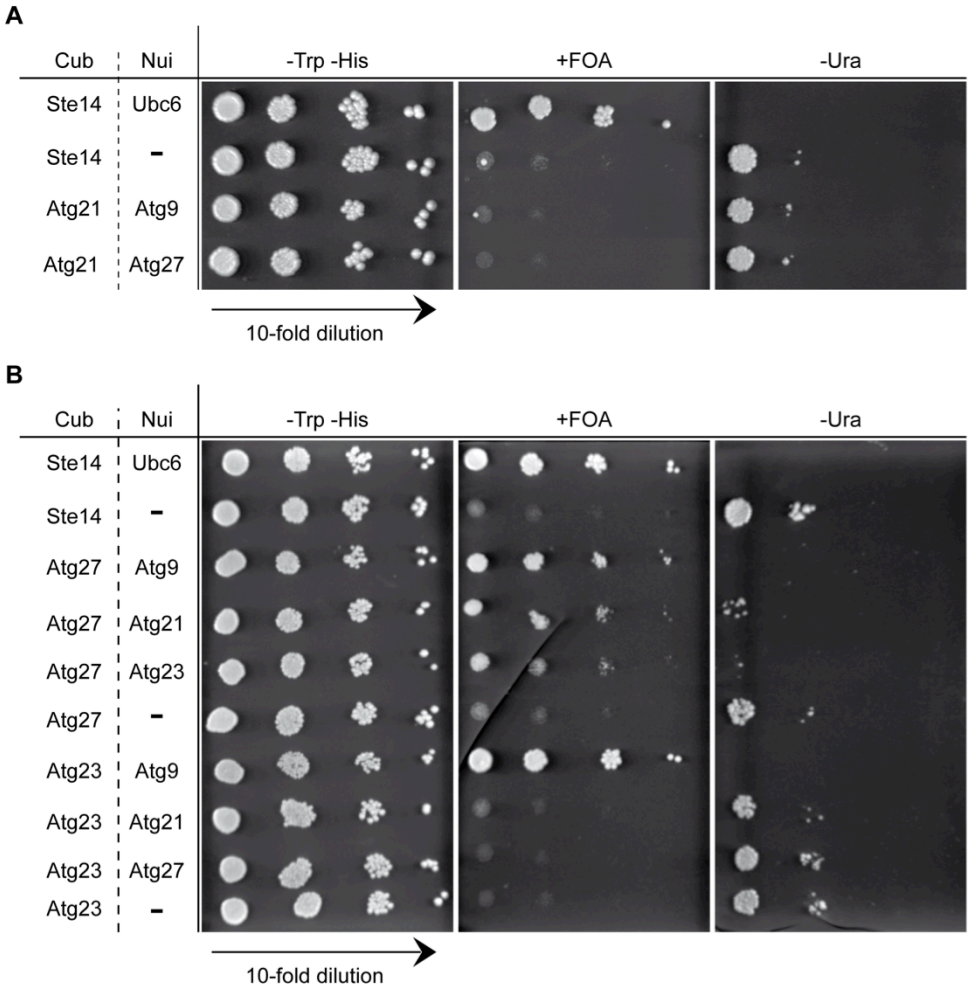

Figure 21: An interaction of Atg27 and Atg21 in split-ubiquitin assay was detected

(A)+(B) 1 OD_{600} WT cells expressing the indicated Cub (bait) and Nui (prey) constructs were diluted in 10-fold steps and spotted on CM-Trp-His (growth control), on CM-Trp-His +FOA (growth implies interaction of the respective proteins) and CM-Trp-His-Ura (growth implies no interaction of the respective proteins). Pictures were taken after three days of growth at 30°C. Ste14-Cub/Nui-Ubc6: positive control; Ste14-Cub/pRS314: negative control

Using Atg27-Cub as bait, an interaction with Nui-Atg9, Nui-Atg21 and Nui-Atg23, but not with the empty vector was detected. Atg27 and Atg9 interact directly with each other, resulting in a strong growth on selective medium containing FOA. The interaction with Atg23 was mediated by Atg9 and represented therefore an indirect interaction, resulting in a significantly weaker growth on selective medium containing FOA. Cells expressing Atg27-Cub and Nui-Atg21 showed a medium growth (Figure 21 B).

Atg27 consists of 271 amino acids and is a membrane protein type I. Therefore its C-terminal region faces towards the cytosol. Additionally, Atg27 contains a N-terminal signal sequence. Amino acids 199 to 221 represent the transmembrane domain (see Figure 22 A). Amino acid 1 to 198 or amino acid 1 to 221 of Atg27 were fused to the C-terminal half of ubiquitin ($Atg27^{1-198}$-Cub and $Atg27^{1-221}$-Cub) and tested for an interaction with its known interacting partner Nui-Atg9 or –Atg21 (Figure 22 A+B).

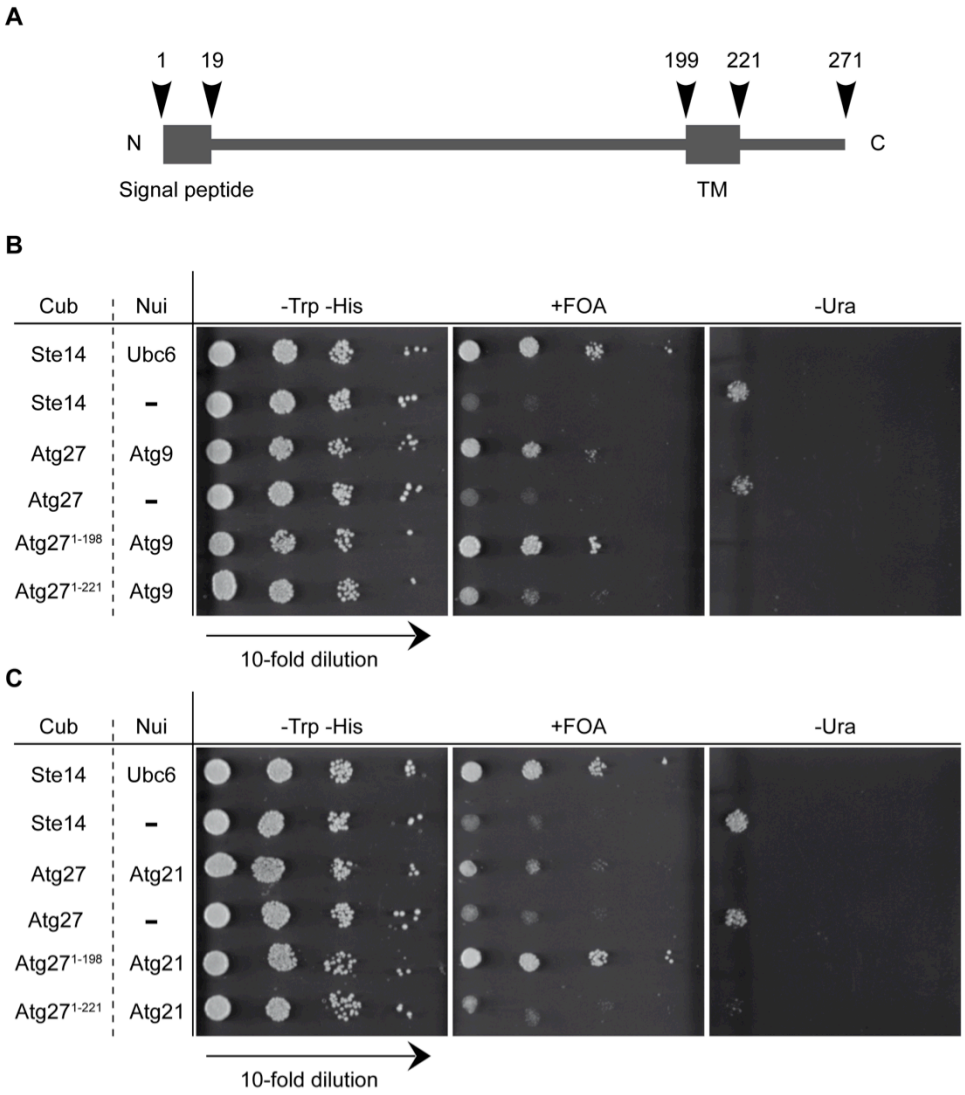

Figure 22: Interaction analysis of truncated Atg27 in split-ubiquitin assay

(A) Predicted domain structure of Atg27 (Yen et al., 2007) **(B)+(C)** 1 OD_{600} WT cells expressing the indicated Cub (bait) and Nui (prey) constructs were diluted in 10-fold steps and spotted on CM-Trp-His (growth control), on CM-Trp-His +FOA (growth implies interaction of the respective proteins) and CM-Trp-His-Ura (growth implies no interaction of the respective proteins). Pictures were taken after three days of growth at 30°C. Ste14-Cub/Nui-Ubc6: positive control; Ste14-Cub/pRS314: negative control

The control combination Atg27-Cub and Nui-Atg9 interacted with each other, resulting in a growth on selective medium containing FOA, whereas Atg27-Cub and the empty vector did not. A strong interaction between Atg27$^{1-198}$-Cub, representing only the lumenal part of Atg27, and Nui-Atg9 was detected, as the growth on selective medium containing FOA was improved. In contrast,

Atg27$^{1-221}$-Cub, additionally containing the transmembrane domain, only weakly interacted with Nui-Atg9 (Figure 22 A).

Nearly the same result was obtained for an interaction with Nui-Atg21. Atg27-Cub interacted with Nui-Atg21, but not with the empty vector alone, as seen before. An enhanced interaction of Atg27$^{1-198}$-Cub and Nui-Atg21 was detected, whereas Atg27$^{1-221}$-Cub interacted only very weakly with Nui-Atg21 (Figure 22 B).

4.3.4.2 Atg21 and Atg27 colocalized in direct fluorescence microscopy

Legakis *et al.* (2007) analyzed the Atg23-Atg9-Atg27 complex by direct fluorescence microscopy analysis and showed that approximately 50% of the Atg9-RFP dots per cell were colocalized with both Atg23-GFP and Atg27-GFP. The same situation was obtained for Atg23-RFP and Atg27-GFP (Legakis et al., 2007). To support a potential interaction of Atg27 and Atg21, both proteins were also analyzed by direct fluorescence microscopy. For this purpose, *ATG21* was deleted in a strain, chromosomally expressing Atg27-GFP (cAtg27-GFP). cAtg27-GFP was fully functional as it showed wild type ApeI maturation under both growing and starvation conditions (Figure 23 A). In cAtg27-GFP *atg21Δ* cells the maturation of ApeI was completely blocked under growing conditions and severely impaired under starvation, confirming a successful deletion of *ATG21*. Wild type and *atg1Δ* cells served as a respective positive and negative control (Figure 23 A).

cAtg27-GFP *atg21Δ* cells were transformed with mCherry-Atg21 expressed from the *MET25* promoter, grown to log phase in the presence of 0.3 mM methionine to induce endogenous mCherry-Atg21 expression level, and visualized by direct fluorescence microscopy (Figure 23 B). cAtg27-GFP was visible as several green dots within the cell. As shown before, mCherry-Atg21 formed perivacuolar puncta.

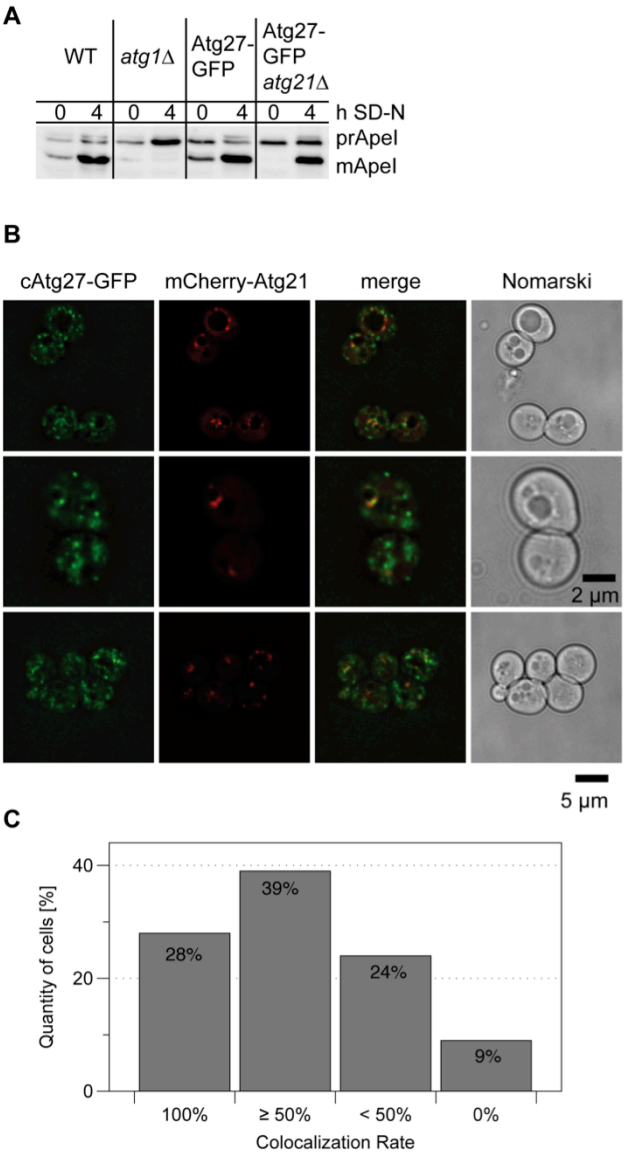

Figure 23: mCherry-Atg21 and Atg27-GFP colocalized in direct fluorescence microscopy

(A) Complementation analysis of chromosomally tagged Atg27-GFP (cAtg27-GFP) in WT and *atg21Δ* cells by monitoring ApeI maturation. Wild type and *atg1Δ* cells served as a control. Samples were taken from growing cells (0 h) and cells starved in SD-N for four hours (4 h), alkaline lysed and immunoblotted. Precursor (prApeI) and matured ApeI (mApeI) were detected using an anti-ApeI antibody. **(B)** Growing cAtg27-GFP *atg21Δ* cells expressing mCherry-Atg21 from the *MET25* promoter were grown to log phase and visualized using a DeltaVision Deconvolution microscope equipped with a TRITC and FITC filter set. Pictures were deconvoluted using SoftWoRx (Applied precision) software. **(C)** Colocalization rate was quantified by counting the number of mCherry-Atg21 dots that colocalized with cAtg27-GFP per cell (n = 76). The cells were sorted into the four indicated categories.

The number of mCherry-Atg21 dots that colocalized with cAtg27-GFP per cell (Colocalization rate) was determined to correlate their expression pattern

(Figure 23 C). In 28% of the cells, all mCherry-Atg21 dots were colocalized with Atg27-GFP. At least 50% colocalization was obtained in 39% of the counted cells. In 24% of the cells, less than 50% of the mCherry-Atg21 dots showed a colocalization with cAtg27-GFP, whereas in only 9% of the cells, no colocalization of both proteins was detected. Taken together, in more than 50% of the cells, at least 50% of mCherry-Atg21 colocalized with cAtg27-GFP, supporting an interaction of both proteins.

4.3.4.3 Analysis of the potential interaction of Atg21 and Atg27 by pull down and GFP-TRAP®

To further investigate a potential interaction of Atg21 and Atg27, the binding of Atg27 to Atg21 was examined in pull down experiments and GFP-TRAP®s. For this purpose a chromosomally tagged Atg27-HA (cAtg27-HA) strain was used. As mentioned before, Atg27 has a specific Cvt phenotype (Yen et al., 2007). cAtg27-HA showed no defect in ApeI maturation in mid-log phase, suggesting that it was functional (Figure 24 A).

For pull down experiments, recombinant 6xHis-SUMO-Atg21 was purified using Nickel-NTA beads. Immobilized 6xHis-SUMO-Atg21 was subsequently incubated with crude extract of log cAtg27-HA yeast cells. After extensive washing, all bound proteins were eluted from the beads, subjected to SDS-PAGE and analyzed by immunoblotting (Figure 24 B). A small part of cAtg27-HA bound specifically to 6xHis-SUMO-Atg21, but not to 6xHis-SUMO alone, supporting an interaction. Surprisingly, this was not reproducible, as a binding of Atg27-HA to 6xHis-SUMO-Atg21 could no longer be obtained in further pull down experiments (data not shown).

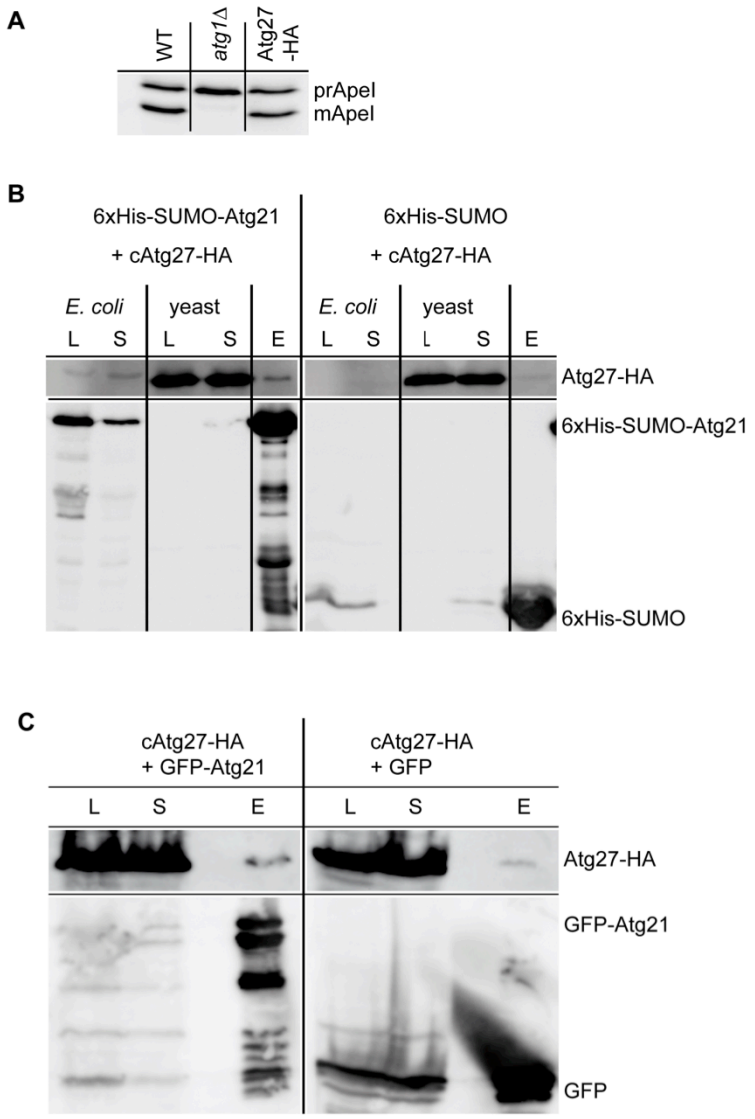

Figure 24: Atg27 does not specifically interact with Atg21 in pull down and GFP-TRAP® experiments

(A) Complementation study of cAtg27-HA by monitoring ApeI maturation. WT, *atg1Δ* and cells chromosomally expressing Atg27-HA (cAtg27-HA) were alkaline lysed in growing phase and immunoblotted. Precursor (prApeI) and matured (mApeI) ApeI were detected using an anti-ApeI antibody. **(B)** Recombinant 6xHis-SUMO-Atg21 and 6xHis-SUMO alone as negative control were purified using Ni-NTA beads and incubated with crude extract of growing cAtg27-HA cells. Samples from the respective *E. coli* and yeast lysates (L), cleared lysate (*E. coli* S), unbound fractions (yeast S) and the purified proteins (E) were analyzed by immunoblotting using anti-HA and anti-His antibodies. **(C)** Growing cAtg27-HA cells expressing GFP-Atg21 or GFP alone as negative control were lysed using the mild cell lysis procedure and subjected to GFP-TRAP® analysis. Samples from the cell lysate (L), the unbound fraction (S) and from the purified proteins were analyzed by immunoblotting using anti-HA and anti-GFP antibodies.

In addition, GFP-TRAP® analysis with growing cAtg27-HA cells expressing GFP-Atg21 or GFP alone as control were performed. Here, a part of cAtg27-HA bound to GFP-Atg21, but also to GFP alone (see Figure 24 C). Although the GFP-bound part was apparently smaller than the GFP-Atg21-bound part, an unspecific binding of cAtg27-HA to GFP-Atg21 could not be excluded.

4.3.5 Interaction studies of Atg21 und Atg8

Atg8 is one of the core autophagy related proteins. It plays dual roles in autophagy. It is critical for the elongation of the forming autophagosome and it also links the cargo to the autophagosome by direct binding to the cargo receptor during selective types of autophagy. To fulfill its function, Atg8 has to be covalently coupled to PE in a ubiquitin-like manner. Atg8 is synthesized with an additional arginine at its C-terminal end, which is cleaved off by Atg4. Shortened Atg8 is subsequently activated by the E1 enzyme Atg7, transferred to the E2 enzyme Atg3 and finally covalently conjugated to PE by the help of the E3 complex Atg12-Atg5/Atg16 (see chapter 2.2.4.4). Atg21 was shown to be involved in efficient lipidation and in the PAS recruitment of Atg8 (Meiling-Wesse et al., 2004; Stromhaug et al., 2004).

For the split-ubiquitin assay, Atg8 was only N-terminally fused to the N-terminal half of ubiquitin (Nui-Atg8) because of its C-terminal processing and was tested for an interaction with Atg21-Cub (Figure 25).

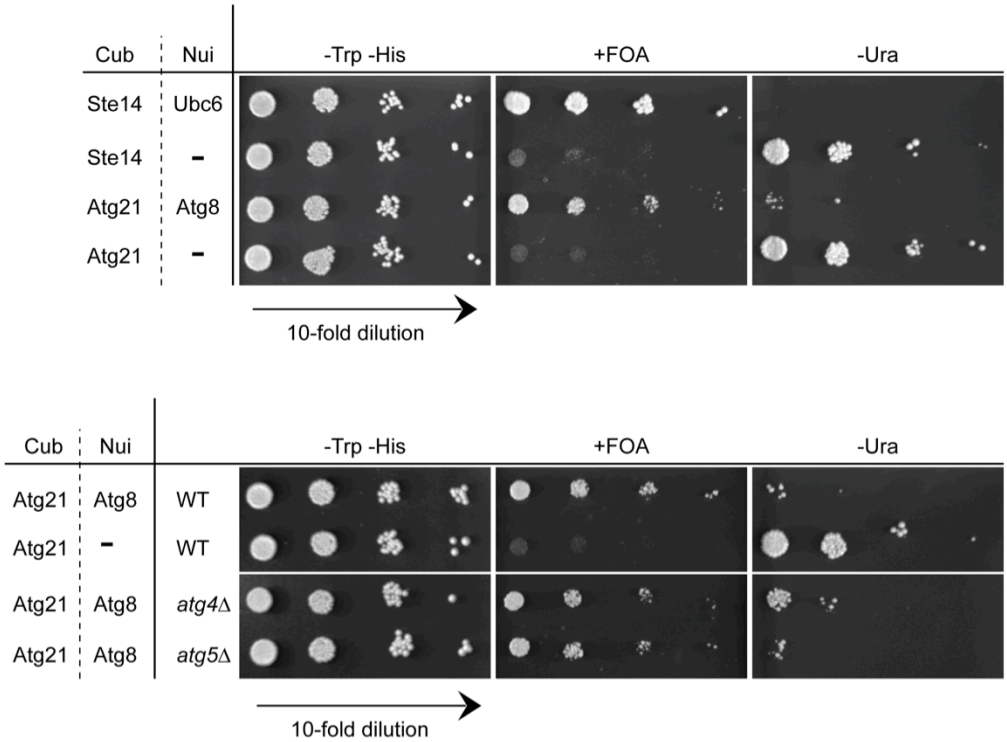

Figure 25: Atg21 and Atg8 interact with each other in split-ubiquitin assay

1 OD_{600} WT, *atg4Δ* and *atg5Δ* cells expressing the indicated Cub (bait) and Nui (prey) constructs were diluted in 10-fold steps and spotted on CM-Trp-His (growth control), on CM-Trp-His +FOA (growth implies interaction of the respective proteins) and CM-Trp-His-Ura (growth implies no interaction of the respective proteins). Pictures were taken after three days at growth at 30°C. Ste14-Cub/Nui-Ubc6: positive control; Ste14-Cub/pRS314: negative control

Cells expressing both constructs were able to grow on plates containing FOA, but not on plates lacking uracil. In contrast, cells expressing Atg21-Cub and the empty vector (pRS314) showed the opposite growth phenotype and served as an additional negative control (Figure 25). Taken together, this strongly pointed to an interaction of Atg21 and Atg8.

Atg8 exists in two forms within a cell, either unlipidated or covalently conjugated to PE. To test which form interacts with Atg21, the interaction of Atg8 and Atg21 was tested in strains lacking Atg4 or Atg5, where Atg8 lipidation is impaired. In both strains, a clear interaction of Atg21 and Atg8 was detected (Figure 25).

4.3.5.1 Bimolecular Fluorescence Complementation (BiFC) analysis

To further evaluate a possible interaction of Atg8 and Atg21, Bimolecular Fluorescence Complementation (BiFC) analysis was used. For this purpose, two proteins of interest are fused to either the nonfluorescent N-terminal (YN) or C-

terminal (YC) part of enhanced YFP (eYFP). Both fragments are brought together and are able to reassemble into fluorescent eYFP, if the target proteins interact with each other ((Skarp et al., 2008);Figure 26 A). The interaction of two proteins within the living cell can be easily visualized by fluorescence microscopy. Therefore, it is also possible to determine the interacting site within the cell.

Atg8 was only N-terminally tagged, because it is processed at its C-terminal end. To exclude sterical hindrance, Atg8 was, concerning the split-ubiquitin assay, N-terminally fused to the N-terminal fragment of eYFP (N-YN Atg8) according to the instructions of Skarp *et al.* (Skarp et al., 2008). Atg21 and Atg4 as a positive control were fused to the corresponding C-terminal fragment (YC) either at the N- or C-terminus. All constructs were tested for functionality by monitoring ApeI maturation. Wild type and *atg1Δ* cells expressing the empty vector were used as a positive and negative control respectively. N-terminally tagged Atg4 (N-YC Atg4) was able to restore ApeI maturation in both growing and nitrogen starved *atg4Δ* cells, whereas C-terminally tagged Atg4 (Atg4 C-YC) was not (Figure 26 B). In contrast, C-terminally tagged Atg21 (Atg21 C-YC) complemented the ApeI maturation defect in growing and nitrogen starved *atg21Δ* cells, whereas N-terminal tagged Atg21 (N-YC Atg21) did not (Figure 26 B). For this reason N-YC Atg4 and Atg21 C-YC were chosen for further analysis. Interestingly, N-YN Atg8 was able to nearly fully restore ApeI maturation in growing *atg8Δ* cells coexpressing C-YC alone (Figure 26 D). But in growing *atg8Δ* cells expressing both N-YN Atg8 and Atg21 C-YC, the ApeI maturation was slightly delayed.

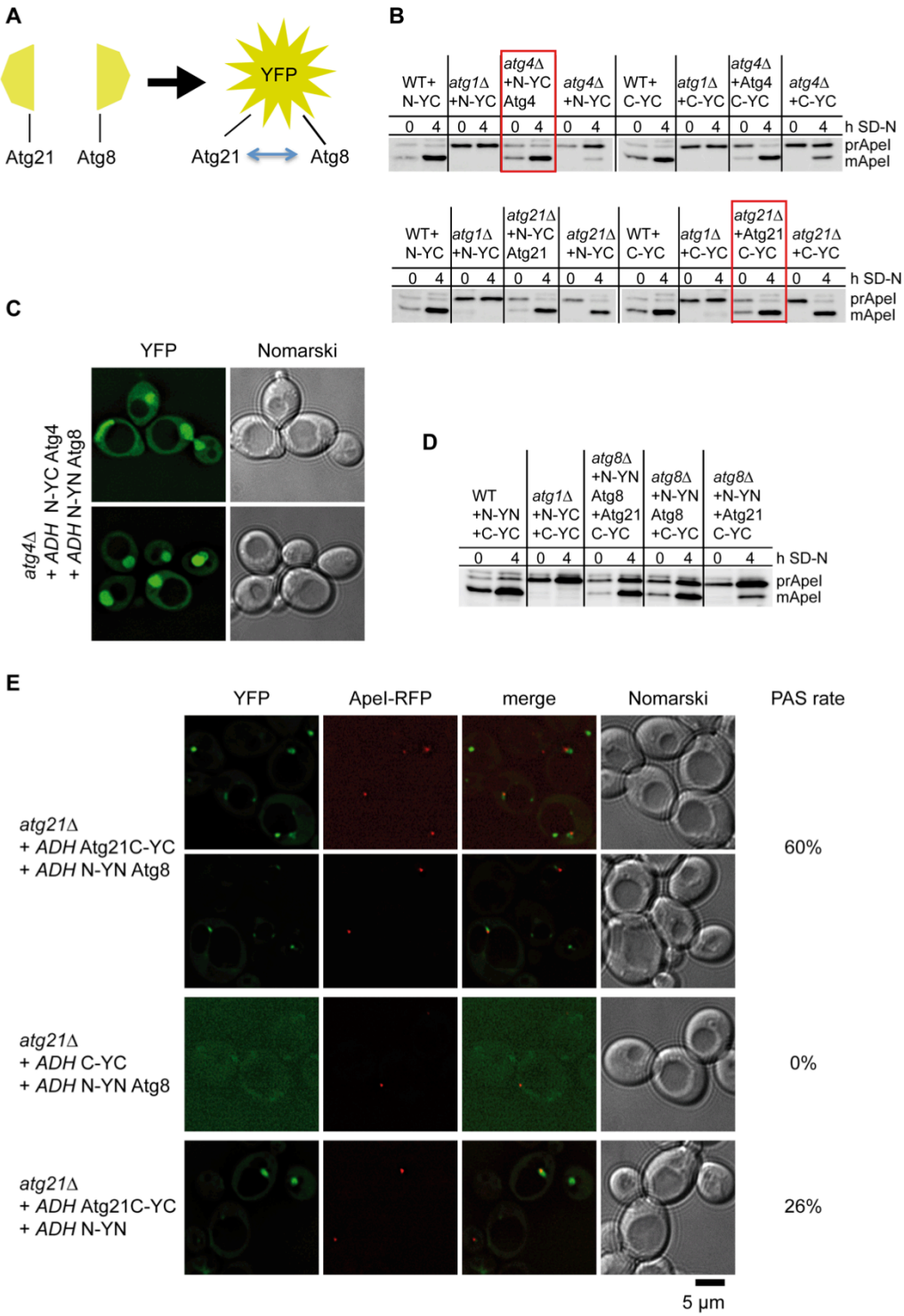

Figure 26: Bimolecular Fluorescence Complementation (BiFC) analysis of Atg8 and Atg21

(A) Scheme of the BiFC analysis. **(B)** Complementation studies of N-YC Atg4, Atg4 C-YC, N-YC Atg21 and Atg21 C-YC by monitoring ApeI maturation. WT, *atg1Δ*, *atg4Δ*, *atg21Δ* cells expressing the indicated Atg4 or Atg21 constructs or the respective empty vector were grown to mid-log phase (0 h) and further starved for four hours in SD-N (4 h). Samples, taken at the indicated time points, were alkaline lysed and immunoblotted. Precursor (prApeI) and matured ApeI (mApeI) were detected using an anti-ApeI antibody. **(C)** Growing *atg4Δ* cells expressing N-YC Atg4 and N-YN Atg8 from an *ADH* promoter were visualized using a DeltaVision Deconvolution microscope equipped with a TRITC and FITC filter set. Pictures were

deconvoluted using SoftWoRx (Applied Precision) software. **(D)** Complementation studies of N-YN Atg8. ApeI maturation was analyzed as described in (B) **(E)** Growing *atg21Δ* cells expressing Atg21 C-YC and N-YN Atg8 from a *ADH* promoter were visualized as described in (C). Both, *atg21Δ* cells expressing N-YN Atg8 and C-YC alone or Atg21 C-YC and N-YN alone from an *ADH* promoter served as negative controls. The PAS rate indicates the number of ApeI-RFP dots that colocalized with an eYFP dot.

First, growing *atg4Δ* cells coexpressing N-YC Atg4 and N-YN Atg8 from the strong and constitutive *ADH* promoter were analyzed by direct fluorescence microscopy. Since Atg4 and Atg8 interact directly with each other for C-terminal procession of Atg8 (Kirisako et al., 2000; Lang et al., 1998), a clear eYFP signal representing the Atg4-Atg8-eYFP complex, was detected. But unexpectedly, it was exclusively present in the nucleus (Figure 26 C). A localization of Atg8 and/or Atg4 in the nucleus has not been reported before, suggesting that N-YC Atg4 and N-YN Atg8 were mislocalized.

Next, growing *atg21Δ* cells expressing N-YN Atg8 and Atg21 C-YC from the *ADH* promoter were analyzed by direct fluorescence microscopy. One to five, but intensive green fluorescent dots per cell were detected, strongly suggesting an interaction of Atg8 and Atg21. Since these dots localized at the perivacuolar site, the PAS marker ApeI-RFP was coexpressed to determine if the interaction occurred at the PAS. Indeed, 60% of the ApeI-RFP dots colocalized with the Atg21-Atg8-eYFP complexes, suggesting that Atg21 and Atg8 interacted with each other at the PAS.

As expected, in the negative control, *atg21Δ* cells expressing N-YN Atg8 and C-YC alone from the *ADH* promoter, no eYFP fluorescence signal could be obtained (Figure 26 E). Surprisingly, in the second negative control, *atg21Δ* cells expressing Atg21 C-YC and N-YN alone, green fluorescent, perivacuolar dots were detectable, comparable to the signal obtained in cells expressing the respective Atg21 and Atg8 constructs (Figure 26 E). In contrast, the PAS rate of these dots was significantly reduced to only 26%.

The fusion proteins tested so far were highly overexpressed from the constitutive *ADH* promoter. To avoid overexpression artefacts, a plasmid was constructed, where Atg21 C-YC was expressed from an inducible *MET25* promoter. In addition to the regulation of the expression strength, it is possible to induce the expression at a specific time point and therefore to limit the

expression period of the target protein. To define the appropriate expression level of Atg21 C-YC, that corresponds to the N-YN Atg8 level, *atg21Δ* cells carrying the pRS425-ADH-N-YN Atg8 and pUG36-MET25-Atg21 C-YC plasmids were grown in media with different concentrations of methionine. Samples were taken in mid-log phase, alkaline lysed and analyzed by immunoblotting using an anti-GFP antibody (Figure 27 A).

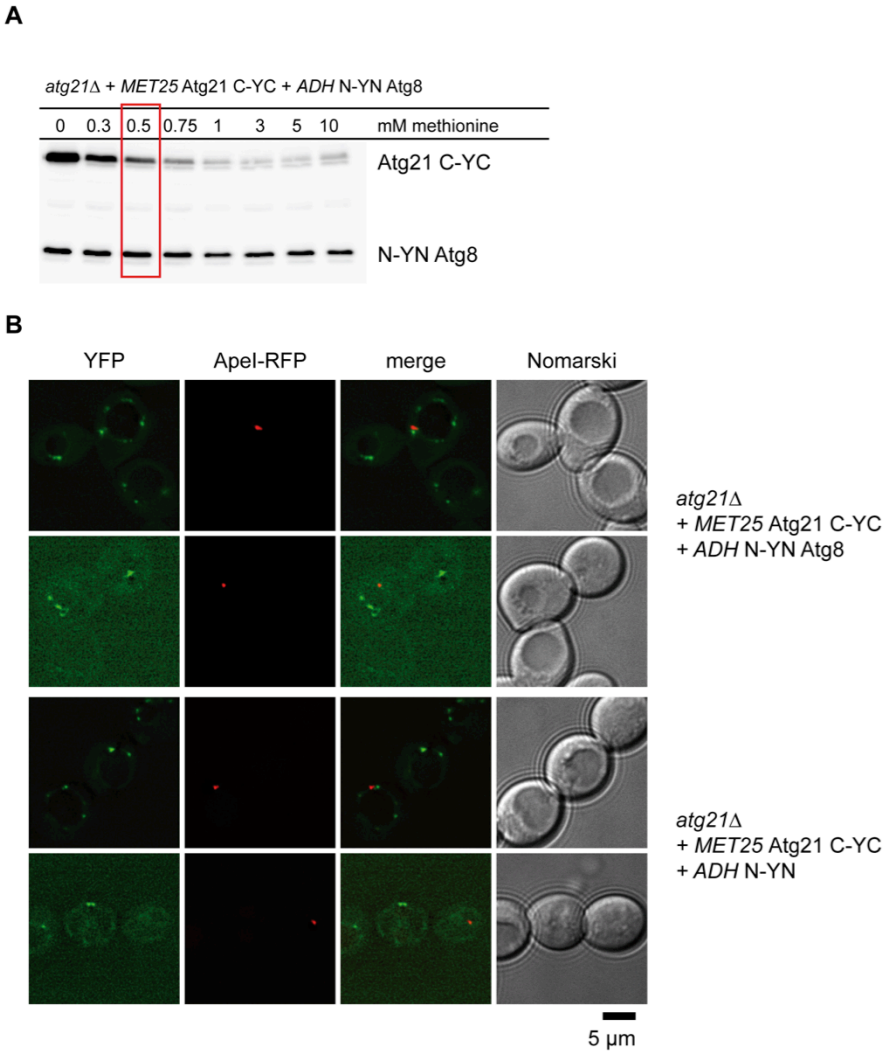

Figure 27: BiFC study of MET25-Atg21 C-YC and ADH-N-YN Atg8

(A) Expression test of MET25-Atg21 C-YC and ADH-N-YN Atg8. Cells were grown in medium containing the indicated methionine concentration to mid-log phase. Samples were alkaline lysed, subjected to immunoblotting and analyzed using an anti-GFP (abcam) antibody. For further studies a concentration of 0.5 mM methionine was chosen. **(B)** *atg21Δ* cells expressing MET25-Atg21 C-YC and ADH-N-YN Atg8 or ADH-N-YN alone were grown in the presence of 0.5 mM methionine to log phase and subsequently visualized using a DeltaVision Deconvolution microscope equipped with a TRITC and FITC filter set. Pictures were deconvoluted using SoftWoRx (Applied Precision) software.

Since N-YN Atg8 was still expressed from the constitutive *ADH* promoter, its concentration remained the same independent of the methionine concentration. In contrast, the amount of Atg21 C-YC decreased with increasing methionine concentration. For further approaches, a concentration of 0.5 mM methionine was chosen.

atg21Δ cells expressing MET25-Atg21 C-YC and ADH-N-YN Atg8 or ADH-N-YN alone were first grown in selective medium containing an excess of methionine to inhibit the expression of Atg21 C-YC. Cells were diluted to an OD_{600} of approximately 0.3 in medium containing 0.5 mM methionine to induce the Atg21 C-YC expression. After cells reached mid-log phase (after three to four hours at 30°C), they were analyzed by direct fluorescence microscopy. Again, in growing *atg21Δ* cells expressing MET25-Atg21 C-YC and ADH-N-YN Atg8 one to few perivacuolar, green fluorescent dots per cell were detectable (Figure 27 B). In contrast to the conditions used before, the intensity of the dots was much fainter, leading to a greater background noise. Unfortunately, the *atg21Δ* cells expressing MET25-Atg21 C-YC and ADH-N-YN alone showed the same fluorescence signals, pointing again to false positive signals.

As a next step, the amount of N-YN Atg8 was additionally reduced by constructing a plasmid, where N-YN Atg8 was expressed from the *MET25* promoter. As before, the expression level of both fusion proteins at different methionine concentrations was tested via immunoblot analysis (Figure 28 A). Again, the amount of MET25-Atg21 C-YC decreased with increasing methionine concentration. MET25-N-YN Atg8 was only detectable in the full absence of methionine and therefore at the strongest expression level. This amount was comparable to N-YN Atg8 expressed from the *ADH* promoter. To avoid overexpression artefacts, a methionine concentration of 0.5 mM was chosen.

As before, *atg21Δ* cells expressing Atg21 C-YC and N-YN Atg8 or N-YN alone from the *MET25* promoter were grown in the presence of 0.5 mM methionine until log phase and analyzed by direct fluorescence microscopy (Figure 28 B).

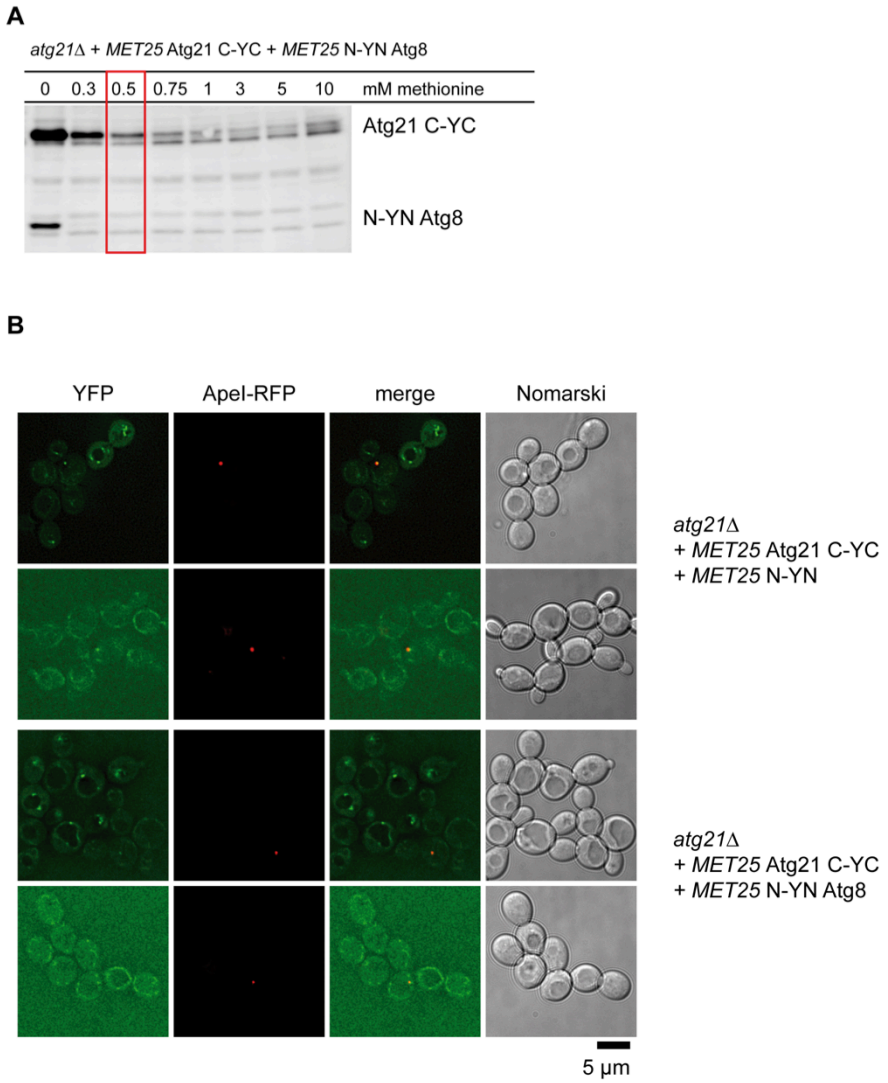

Figure 28: BiFC study of MET25 Atg21 C-YC and MET25 N-YN Atg8

(A) Expression test of *MET25* Atg21 C-YC and *MET25* N-YN Atg8. Cells were grown in medium containing the indicated methionine concentration to mid-log phase. Samples were alkaline lysed, subjected to immunoblotting and analyzed using an anti-GFP (abcam) antibody. For further studies a concentration of 0.5 mM methionine was chosen. **(B)** *atg21Δ* cells expressing MET25 Atg21 C-YC and MET25 N-YN Atg8 or MET25 N-YN alone were grown in the presence of 0.5 mM methionine to log phase and subsequently visualized using a DeltaVision Deconvolution microscope equipped with a TRITC and FITC filter set. Pictures were deconvoluted using SoftWoRx (Applied Precision) software.

Again, there was no difference in the fluorescence signal in cells expressing both protein constructs or in the negative control expressing only Atg21 C-YC. In further efforts, the methionine concentration, the expression duration and strain background was varied diversely (data not shown). But taken together, all cells

expressing Atg21 C-YC exhibited a false-positive signal, independent of expression partner, expression level and duration.

4.3.5.2 Is Atg8 part of the Atg21 high molecular weight complex detected in gelfiltration?

Part of Atg21 was detected as a high molecular weight complex in gelfiltration (Figure 16 B+C). To examine if Atg8 was part of this complex, *atg21Δ pep4Δ* cells were transformed with pRS313-GFP-Atg8 and pMET25-mCherry-Atg21 or pMET25-mCherry as negative control. 0.3 mM methionine was added to the media to induce endogenous expression level of mCherry-Atg21. The cells were harvested in late growing phase and resuspended in lysis buffer (10 mM MOPS pH 7.2, 0.2 M sorbitol, 1 mM EDTA, 2 mM PMSF, protease inhibitors). Cells were lysed using the mild cell lysis procedure and subjected to gelfiltration analysis as described before (chapter 4.3.1.1).

The main part of mCherry-Atg21 was eluted in fraction 10 and fractions 14 to 15 corresponding to ≥ 670 kDa (Figure 29 A). The main part of GFP-Atg8 was eluted in fractions 15 to 17, and was therefore partly overlapping with the mCherry-Atg21 fractions (Figure 29 B). However, the distribution of GFP-Atg8 was not changed in the absence of mCherry-Atg21, indicating, that GFP-Atg8 was not part of the Atg21 high molecular weight complex. Furthermore, GFP-Atg8 has a molecular weight of about 40 kDa. The fractions, where GFP-Atg8 was present corresponded to ≥ 65 kDa, indicating that GFP-Atg8 was not present in its monomeric form but as an oligomer or in a complex. Nevertheless, since the distribution of GFP-Atg8 was not changed in the absence of mCherry-Atg21, this was independent of Atg21.

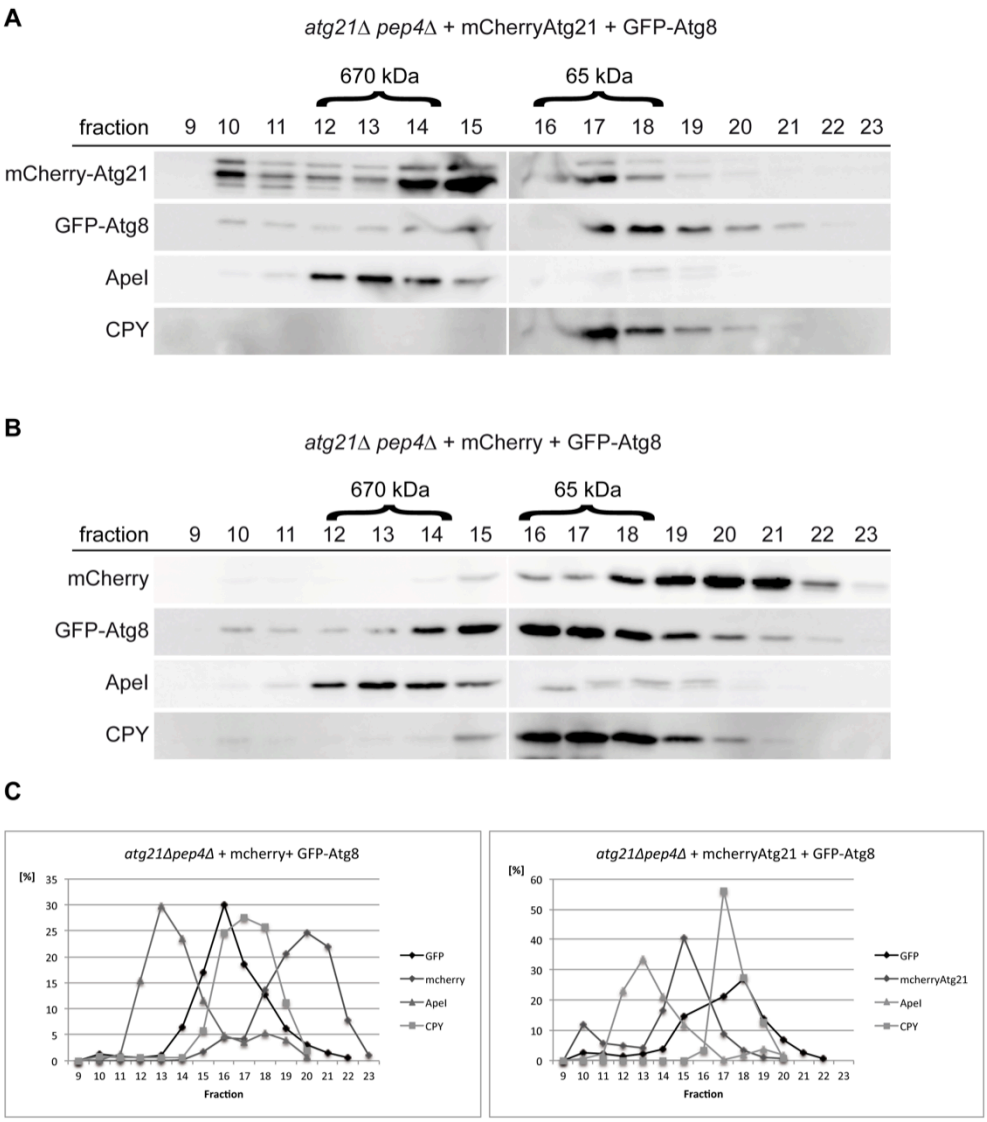

Figure 29: Atg8 distribution in gelfiltration was not changed in the absence of Atg21

Growing *atg21Δ pep4Δ* cells expressing GFP-Atg8 and mCherry-Atg21 **(A)** or mCherry alone **(B)** were lysed using the mild cell lysis procedure and subjected to size exclusion chromatography on a Superose 6 column. The cell lysate was eluted from the column at a flow rate of 0.5 ml/ml and 0.8 ml fractions were collected as it was described in (Obara et al., 2008b). Fractions were precipitated and analyzed by immunoblotting using anti-RED, anti-GFP, anti-ApeI and anti-CPY antibodies. **(C)** Quantification of the distribution of the individual proteins in the respective fractions using AIDA software.

4.3.6 Interaction studies of Atg21 und Atg16

Atg16 is part of the Atg12-Atg5/Atg16 complex, which acts as an E3-like enzyme in the ubiquitin-like conjugation of Atg8 to PE (Fujita et al., 2008; Hanada et al., 2007).

4.3.6.1 Atg21 and Atg16 interact with each other in the split-ubiquitin assay

In the split-ubiquitin assay, Atg21-Cub was tested for an interaction with all members of the Atg12-Atg5/Atg16 complex. Only cells expressing Atg21-Cub and Nui-Atg16 showed a weak growth in the presence of FOA, indicating a weak interaction (Figure 30 A). The interaction could be disturbed by steric hindrance and/or interference with endogenous Atg16. To improve the interaction of Atg21 and Atg16, *atg16Δ* cells expressing Atg16-Cub and Nui-Atg21 were tested in the split-ubiquitin assay (Figure 30 B).

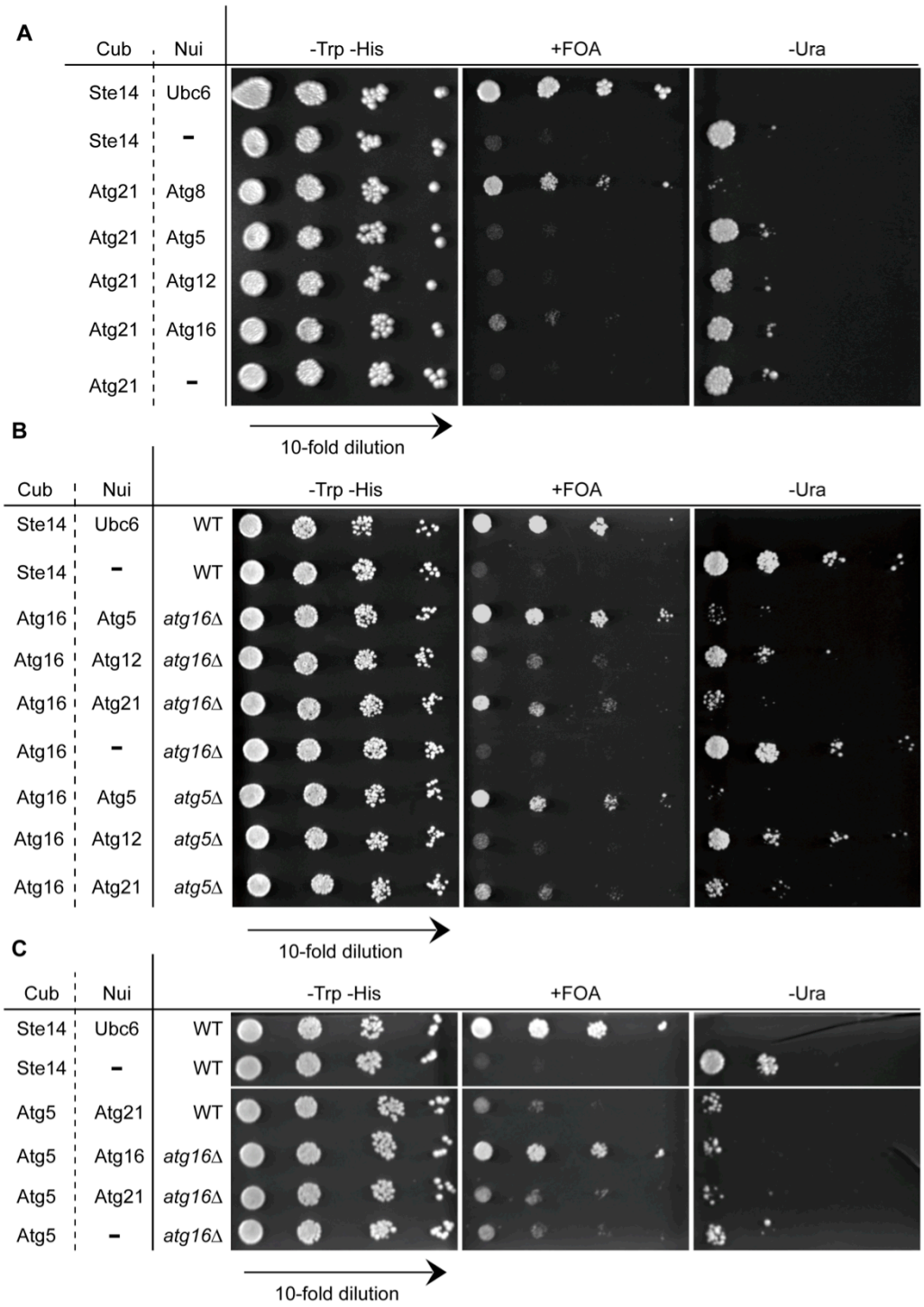

Figure 30: Atg16 and Atg21 interact in the split-ubiquitin assay

(A)+(B)+(C) 1 OD_{600} WT, *atg5Δ* and *atg16Δ* cells expressing the indicated Cub (bait) and Nui (prey) constructs were diluted in 10-fold dilution steps and spotted on CM-Trp-His (growth control), CM-Trp-His+FOA (growth indicated interaction of the respective proteins) and CM-Trp-His-Ura (growth indicated no interaction of the respective proteins). Ste14-Cub/Nui-Ubc6: positive, Ste14-Cub/pRS314: negative control

In the E3 complex Atg16 and Atg5 interact directly. Therefore, the Atg16-Atg5 interaction was used as a reference for direct interaction in this analysis. *atg16Δ* cells expressing Atg16-Cub and Nui-Atg5 showed a strong growth phenotype in the presence of FOA, whereas the same cells were not able to grow in the absence of uracil. Atg12 and Atg16 interact indirectly via Atg5. Therefore, the combination of Atg16-Cub and Nui-Atg12 resulted in a reduced but still detectable growth on FOA medium. Furthermore, the interaction of Atg16-Cub and Nui-Atg12 could no longer be obtained in *atg5Δ* cells. Indeed, a clear interaction of Atg16-Cub and Nui-Atg21 was detected. The growth strength of *atg16Δ* cells expressing Atg16-Cub and Nui-Atg21 on FOA medium was significantly improved compared to wild type cells and ranged between the observed direct and indirect control interactions. Furthermore, this interaction was independent of Atg5, as shown in *atg5Δ* cells.

To support further that Atg21 interacts specifically with Atg16 and not with another member of the Atg12-Atg5/Atg16 complex, Atg5 and Atg21 were further tested using the split-ubiquitin assay (Figure 30 C). No interaction of Atg5-Cub and Nui-Atg21 was observed, either in WT or in *atg16Δ* cells. In contrast, Atg5-Cub and Nui-Atg16 interacted with each other as expected, confirming the functionality of Atg5-Cub.

In conclusion, the split-ubiquitin assay pointed to an interaction of Atg21 with Atg16, but with no other member of the Atg12-Atg5/Atg16 complex.

4.3.6.2 Fluorescence microscopy analysis of Atg5 and Atg16

Atg5 and Atg16 are only transiently located at the PAS and therefore hardly detectable in fluorescence microscopy. Stromhaug *et al.* (2004) showed, that the PAS localization of Atg5-GFP can be enhanced in mutants defective in the progression of the Cvt / autophagy pathways as *atg8Δ* cells. Furthermore, the PAS localization of Atg5-GFP observed in *atg8Δ* cells was prevented in the additional absence of Atg21 (Stromhaug et al., 2004). Regarding Atg16, Nair *et al*. (2010) showed that the perivacuolar puncta formation of chromosomally tagged Atg16-GFP was significantly decreased in starved *atg18Δ atg21Δ* cells. Since Atg21 is required for the Cvt pathway, which takes place under growing conditions, the PAS localization of Atg16 was observed in growing cells. As a

prerequisite for further successful colocalization studies of Atg5 and Atg16, the observations reported by Stromhaug *et al.* (2004) should be reproduced. For this purpose, *atg8Δ* and *atg8Δ atg21Δ* cells expressing Atg5-YFP and the PAS marker ApeI-RFP were grown to mid-log phase and visualized using a DeltaVision fluorescence microscope (Figure 31 A).

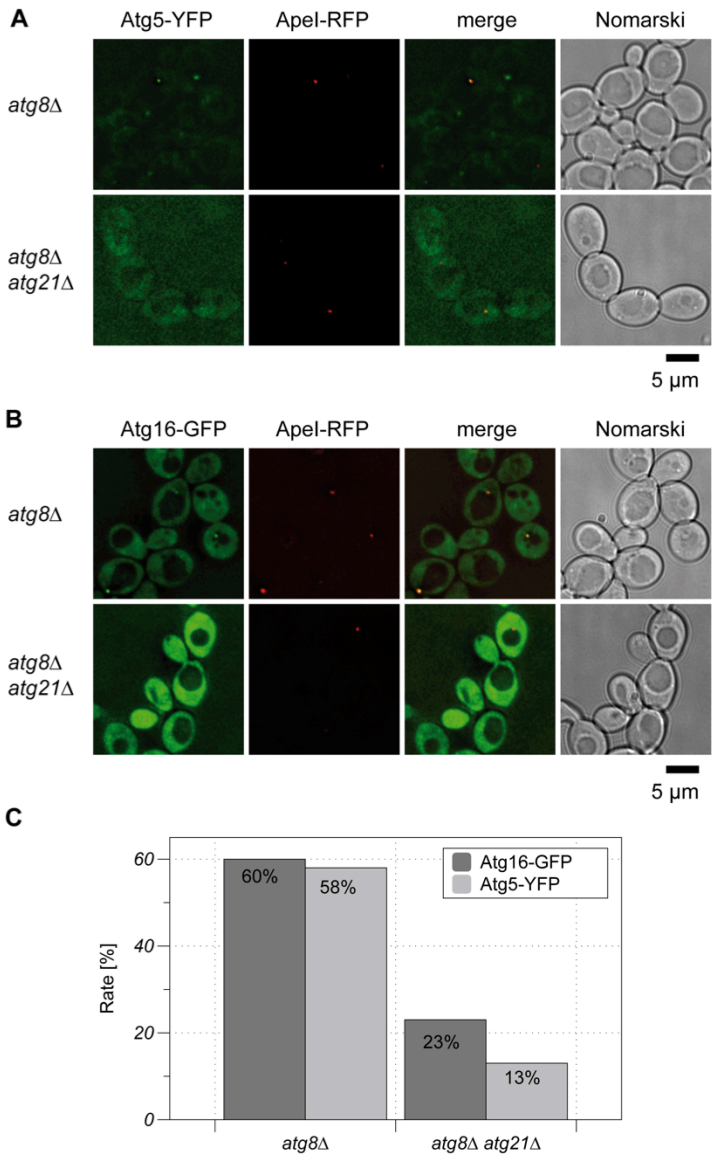

Figure 31: Atg5 and Atg16 are absent from the PAS in growing *atg8Δ atg21Δ* cells

(A) Growing *atg8Δ* and *atg8Δ atg21Δ* cells expressing Atg5-YFP and the PAS marker ApeI-RFP were visualized using a DeltaVision Deconvolution microscope equipped with YFP and RFP filter sets. Pictures were deconvoluted using SoftWoRx (Applied Precision) software. **(B)** Growing *atg8Δ* and *atg8Δ atg21Δ* cells expressing Atg16-GFP and the PAS marker ApeI-RFP were visualized as described in (A). **(C)** The percentage of cells showing a perivacuolar Atg5-YFP respective Atg16-GFP puncta was determined for each strain.

A clear perivacuolar Atg5-YFP punctum was observed in 58% of the *atg8Δ* cells. Nearly each of these puncta was colocalized with the PAS marker ApeI-RFP. In contrast, only 13% of the *atg8Δ atg21Δ* cells showed a much fainter perivacuolar Atg5-YFP punctum (Figure 31 A+C). These observations correlated perfectly with the data obtained by Stromhaug *et al.* (2004), confirming the functionality of this assay. Next, *atg8Δ* and *atg8Δ atg21Δ* cells expressing Atg16-GFP and the PAS marker ApeI-RFP were grown to log phase and visualized by direct fluorescence microscopy. In 60% of the *atg8Δ* cells, a clear perivacuolar Atg16-GFP punctum was observed (Figure 31 B+C). All these puncta colocalized with the PAS marker ApeI-RFP. The PAS localization of Atg16-GFP could therefore also be enhanced in mutants defective in the progression of the Cvt / autophagy pathways as published for Atg5. Furthermore, the PAS localization of Atg16-GFP observed in *atg8Δ* cells was significantly reduced by additional deletion of *ATG21*, since only 23% of *atg8Δ atg21Δ* cells showed a perivacuolar Atg16-GFP punctum (Figure 31 B+C). Again, these puncta were much fainter, compared to those observed in *atg8Δ* cells. In conclusion, both Atg5-YFP and Atg16-GFP were absent from the PAS in growing *atg8Δ atg21Δ* cells.

Additionally, the colocalization of Atg5-YFP and Atg16-GFP with mCherry-Atg21 was determined in different mutant strains (Figure 32 A+B). 0.3 mM methionine was added to the selective medium to induce endogenous expression of mCherry-Atg21.

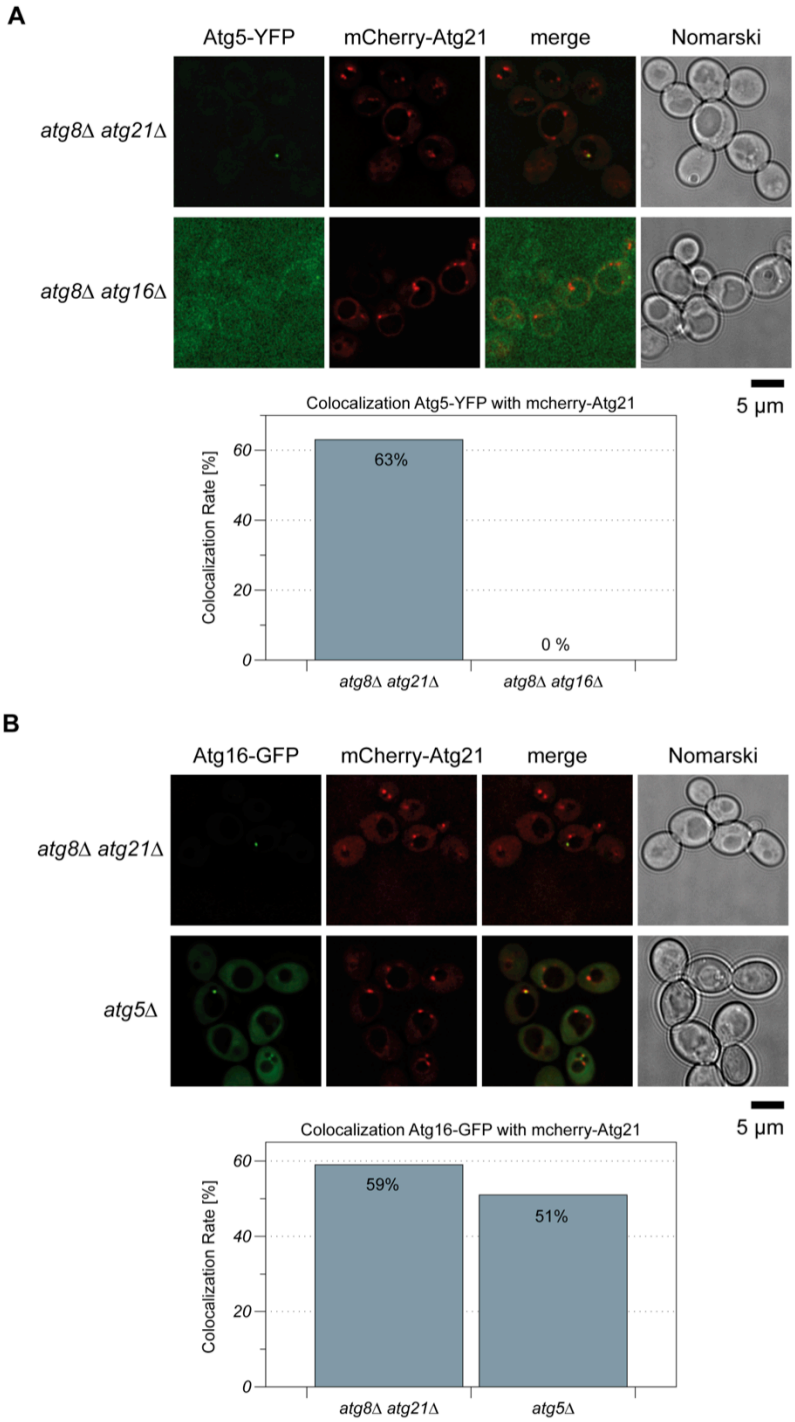

Figure 32: Atg16 and Atg21 colocalize in the absence of Atg5

(A) *atg8Δ atg21Δ* and *atg8Δ atg16Δ* cells expressing Atg5-YFP and mCherry-Atg21 were grown to mid-log phase in the presence of 0.3 mM methionine and visualized using a DeltaVision Deconvolution microscope equipped with YFP and mCherry filter sets. Pictures were deconvoluted using SoftWoRx (Applied Precision) software. The percentage of Atg5-YFP colocalized with mCherry-Atg21 was determined. **(B)** *atg8Δ atg21Δ* and *atg5Δ* cells expressing Atg16-GFP and mCherry-Atg21 were grown to log phase in the presence of 0.3 mM methionine and visualized using a DeltaVision Deconvolution microscope equipped with GFP and mCherry

filter sets. Pictures were deconvoluted using SoftWoRx (Applied Precision) software. The percentage of Atg16-GFP colocalized with mCherry-Atg21 was determined.

In mid-log *atg8Δ atg21Δ* cells 63% of the perivacuolar Atg5-YFP puncta and 59% of the perivacuolar Atg16-GFP puncta were colocalized with mCherry-Atg21 (Figure 32 A+B). mCherry-Atg21 most likely colocalized with both proteins at the PAS, because all of the Atg16-GFP and nearly all of the Atg5-YFP dots was located at the PAS under the same conditions (Figure 31). Atg16 links the Atg12-Atg5/Atg16 complex to the PAS (Matsushita et al., 2007). Therefore, Atg5-YFP was completely cytosolic in mid-log *atg8Δ atg16Δ* cells (Figure 32 A). Importantly, the colocalization rate of Atg16-GFP and mCherry-Atg21 did not change in the absence of Atg5 (Figure 32 B).

4.3.6.3 Interaction studies of Atg16 and Atg21 using pull down and GFP-TRAP® analysis

To further confirm a potential interaction of Atg21 and Atg16, pull down and GFP-TRAP® analysis were performed using chromosomally tagged Atg16-HA (cAtg16-HA). cAtg16-HA was still able to mature ApeI under growing conditions, indicating that it was functional (Figure 33 A).

For pull down experiments, recombinant 6xHis-SUMO-Atg21 and 6xHis-SUMO alone as a control were purified using Ni-NTA beads and subsequently incubated with crude extract of growing cAtg16-HA cells. After extended washing, the isolated proteins were eluted from the beads by adding Laemmli buffer containing 100 mM DTT. cAtg16-HA bound specifically to 6xHis-SUMO-Atg21 but not to 6xHis-SUMO alone (see Figure 33 B).

For GFP-TRAP® analysis, growing cAtg16-HA cells expressing GFP-Atg21 or GFP alone as negative control, were lysed using the mild cell lysis procedure. The cell lysates were subjected to GFP-TRAP® beads. After extended washing, the purified proteins were eluted by the addition of Laemmli buffer. cAtg16-HA was specifically co-isolated by GFP-Atg21, but not by GFP alone (Figure 33 C). Atg16 is a member of the E3-like enzyme complex crucial for the lipidation of Atg8. As shown before, Atg21 interacted with Atg8 in the split-ubiquitin assay (see chapter 4.3.5). To exclude the possibility, that Atg16 was co-precipitated by a bridging interaction of Atg8, a GFP-TRAP® analysis was performed with cell

lysate of cAtg16-HA *atg8Δ* cells expressing GFP-Atg21 or GFP alone as negative control. Indeed, also in the absence of Atg8, cAtg16-HA was specifically co-isolated by GFP-Atg21, but not by GFP alone (Figure 33 C).

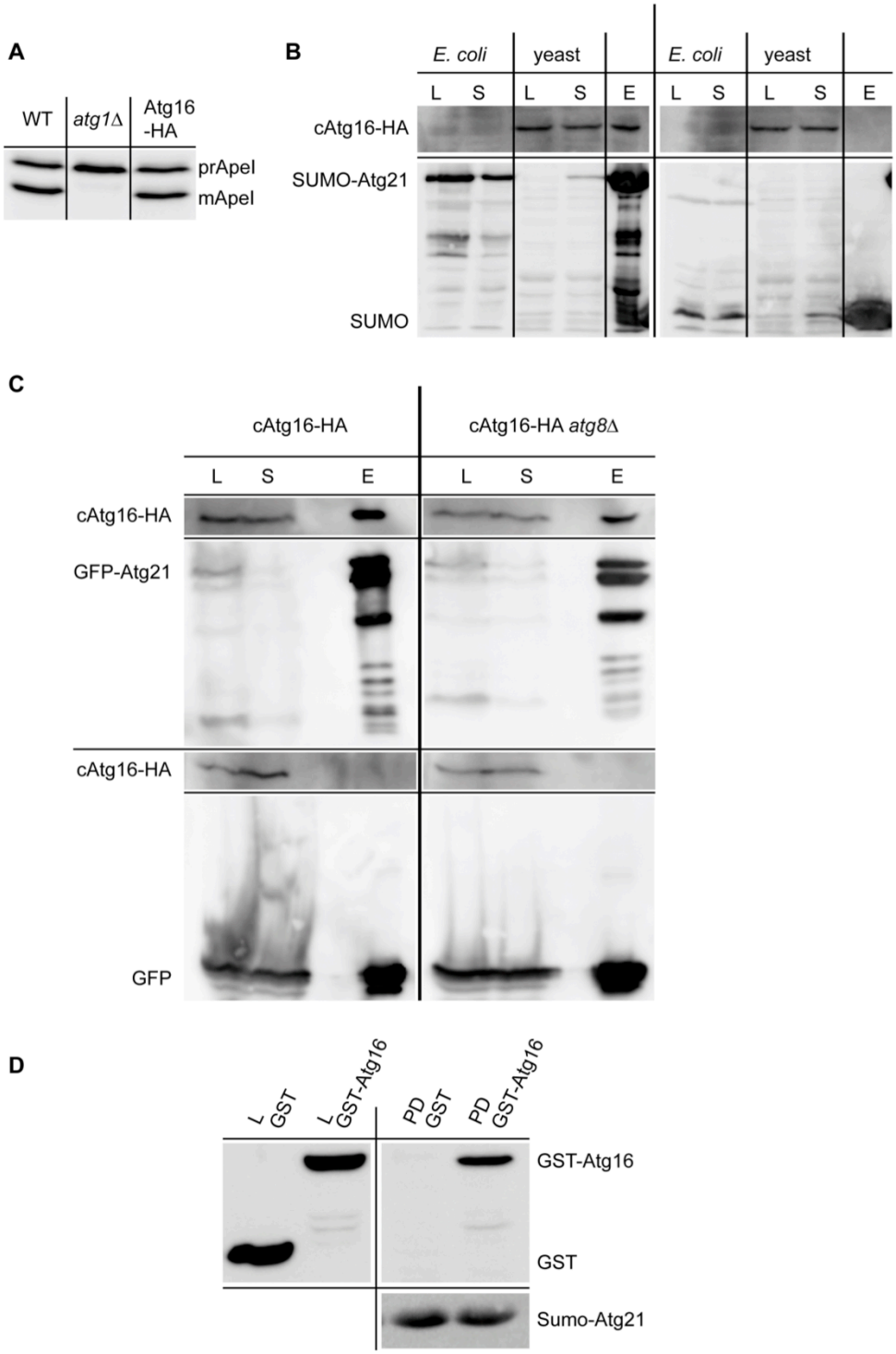

Figure 33: Interaction studies of Atg16 and Atg21 using GFP-TRAP® and pull down experiments

(A) Complementation study of chromosomally tagged Atg16-HA (cAtg16-HA) by monitoring the maturation of ApeI. Samples from growing WT, *atg1Δ* and cAtg16-HA cells were alkaline lysed and immunoblotted. Precursor (prApeI) and matured (mApeI) ApeI were detected using an anti-

ApeI antibody. **(B)** Recombinant 6xHis-SUMO-Atg21 and 6xHis-SUMO alone as a negative control were purified using Ni-NTA beads and incubated with crude extract of growing cAtg16-HA cells. Samples from the respective *E. coli* and yeast cell lysates (L), cleared lysate (*E. coli* S), unbound fraction (yeast S) and the purified proteins (E) were analyzed by immunoblotting using anti-HA and anti-His antibodies. **(C)** Growing cAtg16-HA cells or cAtg16-HA *atg8Δ* cells expressing GFP-Atg21 or GFP as negative control were lysed using the mild cell lysis procedure and subjected to GFP-TRAP® analysis. Samples from the cell lysate (L), the unbound fraction (S) and from the purified proteins (E) were analyzed by immunoblotting using anti-HA and anti-GFP antibodies. **(D)** Immobilized recombinant 6xHis-SUMO-Atg21 was incubated with purified recombinant GST and GST-Atg16. Samples from purified GST-Atg16 and GST (L) and samples from the eluted proteins (PD) were immunoblotted and detected using anti-GST and anti-His antibodies.

To further confirm a direct interaction of Atg16 and Atg21, a direct pull down experiment using purified recombinant 6xHis-SUMO-Atg21 and GST-Atg16 were performed. For this purpose, recombinant GST-Atg16 and GST alone as a negative control were purified using glutathione sepharose. After extended washing, GST and GST-Atg16 were eluted by addition of glutathione. Twice the amount was incubated with immobilized 6xHis-SUMO-Atg21. After extended washing, the bound proteins were eluated by adding Laemmli buffer and analyzed by immunoblot (Figure 33 D). In fact, GST-Atg16 bound specifically to 6xHis-SUMO-Atg21, whereas GST alone did not.
In conclusion, Atg21 probably directly interacts with Atg16.

4.3.6.4 Determination of the Atg21- interacting domain of Atg16

Atg16 consists of 150 amino acids. Amino acids 22 to 46 are predicted to constitute the Atg5-binding region, followed by a short linker region. Amino acids 58 to 119 form a coiled-coil domain, which mediates dimerization of Atg16 ((Fujioka et al., 2010);Figure 34 A).
To identify the Atg21-interacting domain of Atg16, truncated GST-Atg16 versions were constructed and tested for an interaction with 6xHis-SUMO-Atg21 in direct pull down experiments as described before. For this purpose, recombinant GST-Atg16 lacking the coiled-coil domain (GST-Atg16^{aa1-57}), lacking the extreme C-terminal end (GST-Atg16$^{aa1-119}$), which is not required for the coiled-coil formation or lacking the Atg5-binding domain and the following linker region (GST-Atg16$^{aa58-150}$) were purified and incubated with recombinant

6xHis-SUMO-Atg21. GST-Atg16 and GST-Atg16$^{aa58-150}$ bound specifically to 6xHis-SUMO-Atg21, whereas GST alone, GST-Atg16^{aa1-57} and GST-Atg16$^{aa1-119}$ did not (Figure 34 B).

The same truncated versions of Atg16 were created as Atg16-HA constructs and cloned into a pRS313 vector under the control of a *CUP1* promoter. Wild type Atg16-HA and the truncated Atg16-HA versions were co-expressed with GFP-Atg21 or GFP alone as negative control in *atg16Δ* cells. The amount of Atg16$^{1-119}$-HA and Atg16$^{58-150}$-HA or Atg16$^{1-57}$-HA was adjusted by addition of 25 µM $CuSO_4$ or 50 µM $CuSO_4$ to the selective medium over night (approximately 12 hours), respectively. Cells were grown to mid-log phase, lysed under mild conditions and subjected to GFP-TRAP® analysis (Figure 34 C).

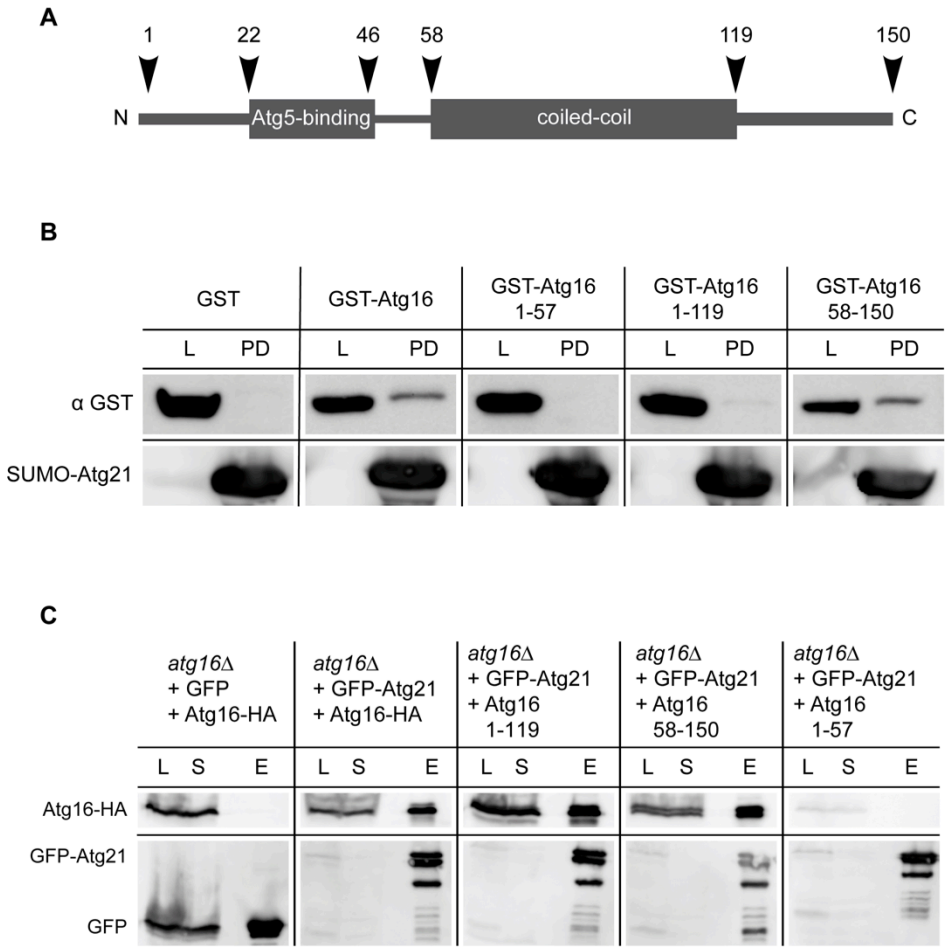

Figure 34: Atg21 interacts with the coiled-coil domain of Atg16

(A) Predicted domain structure of Atg16. Numbers indicate the respective amino acid position. It can not be excluded that the coiled-coil domain might be longer than proposed (Fujioka et al., 2010) **(B)** Immobilized recombinant 6xHis-SUMO-Atg21 was incubated with purified

recombinant GST, GST-Atg16 or the indicated truncated versions of GST-Atg16. Samples of the purified GST and GST-Atg16 versions (L) and the eluted proteins (PD) were immunoblotted and analyzed using anti-GST and anti-His antibodies. **(C)** Growing *atg16Δ* cells expressing GFP-Atg21 or GFP alone as negative control and the indicated Atg16-HA version were lysed using the mild cell lysis procedure and subjected to GFP-TRAP® analysis. Expression of Atg16$^{1-119}$–HA and Atg16$^{58-150}$-HA or Atg16$^{1-57}$-HA was adjusted by addition of 25 µM $CuSO_4$ or 50 µM $CuSO_4$ to the selective medium for approximately 12 h, respectively. Samples of the cell lysate (L), the unbound fraction (S) and the purified proteins (E) were analyzed by immunoblotting using anti-HA and anti-GFP antibodies.

Atg16-HA was specifically purified with GFP-Atg21 but not with GFP alone. Interestingly, Atg16$^{1-119}$-HA and Atg16$^{58-150}$-HA bound specifically to GFP-Atg21. Atg16$^{1-57}$-HA was rather unstable and therefore hardly detectable on the immunoblot. However, even overexposed, no co-precipitated Atg16$^{1-57}$-HA could be detected.

Altogether, these data suggested, that the Atg21-binding region might be positioned within the coiled-coil domain of Atg16. Fujioka *et al.* (2010) defined highly conserved surface residues within the coiled-coil domain of Atg16 that are required for its autophagic function. They measured ApeI maturation and macroautophagy (ALP assay) of a set of mutants under growing and starvation conditions. Mutation to alanine of the aspartic acid at position 101 (D101) and glutamic acid at position 102 (E102) caused strong defects in both pathways when mutated alone or in concert. Hypothetically, Atg16 and Atg21 might have to interact with each other for proper autophagic function. Loss of the interaction by the mentioned mutations in Atg16 might therefore lead to impaired autophagic activity. To test this hypothesis, Atg16-GFP mutants were constructed, that contained mutations of the aspartic acid at position 101 (D101A) and the glutamic acid at position 102 (E102A) either individual or in combination, and observed in direct fluorescence microscopy. *atg8Δ atg16Δ* cells expressing mCherry-Atg21 and the respective Atg16-GFP mutant were grown to log phase in the presence of 0.3 mM methionine to induce endogenous mCherry-Atg21 expression and imaged using a DeltaVision Deconvolution microscope (Figure 35).

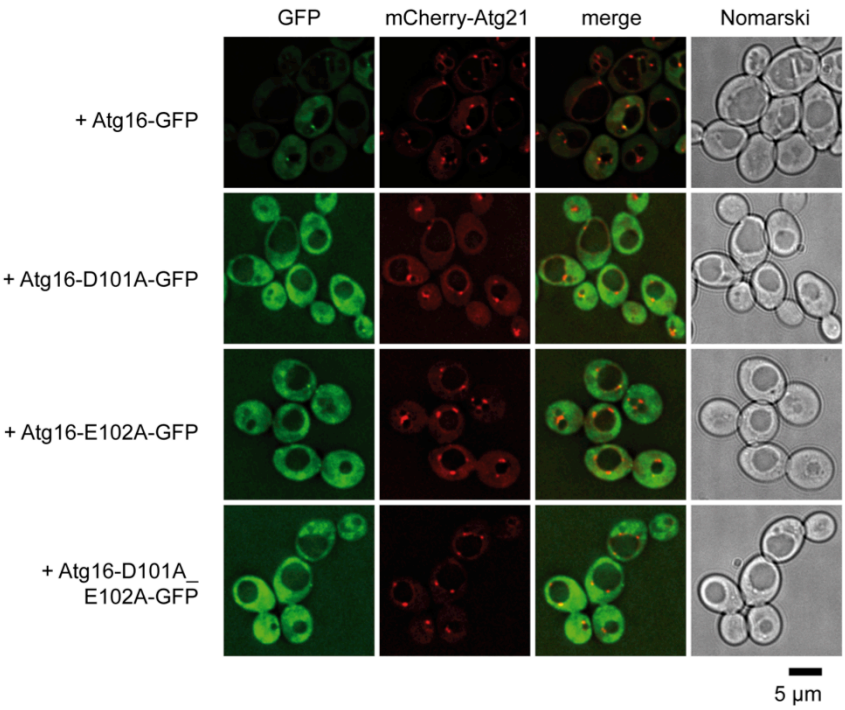

Figure 35: Fluorescence microscopic analysis of the Atg16-GFP point mutants

Growing *atg8Δ atg16Δ* cells expressing mCherry-Atg21 and the indicated Atg16-GFP mutant were grown in the presence of 0.3 mM methionine to log phase and visualized using a DeltaVision Deconvolution microscope equipped with GFP and RFP filter sets. Pictures were deconvoluted using SoftWoRx (Applied Precision) software.

Atg16-GFP formed perivacuolar puncta, which partly colocalized with mCherry-Atg21 as described before. In contrast, Atg16^{D101A}-GFP, Atg16^{E102A}-GFP and Atg16^{D101A_E102A}-GFP were completely cytosolic. Only Atg16^{E102A}-GFP rarely formed faint and hardly detectable perivacuolar puncta. The overall perivacuolar punctate appearance of mCherry-Atg21 did not change in the cells expressing the mutant versions of Atg16-GFP.

Next, Atg16-HA mutants were constructed, that contained mutations of the aspartic acid at position 101 (D101A) and the glutamic acid at position 102 (E102A) either individual or in combination. These mutants were subsequently tested for an interaction with Atg21. As a control, Atg16-HA mutants were used, where the lysine at position 95 (K94A) or glutamic acid at position 97 (E97A) were exchanged by alanine, since these mutants exhibited wild type-like autophagic activity (Fujioka et al., 2010). All residues were predicted to have no influence on the formation of the parallel coiled-coil domain conformation. Based

on the structure, published from Fujioka *et al.* (2010), the mentioned amino acids are located on the surface of the coiled-coil domain, facing the cytosol (Figure 36 A). Nevertheless it was confirmed, that the mutated residues did not change the overall structure of Atg16, which could be another explanation for impaired autophagic function. The coiled-coil domain of Atg16 mediates its dimerization as a prerequisite for the formation of the Atg12-Atg5/Atg16 complex essential for autophagy (Mizushima et al., 1999). In the GFP-TRAP® analysis, Atg16-GFP could only interact and therefore co-precipitate Atg16-HA, if its coiled-coil domain was properly formed. For this purpose, cell lysates of growing *atg16Δ* cells expressing Atg16-GFP, Atg16^{D101A_E102A}-GFP, Atg16^{K94A}-GFP or GFP alone as control were mixed with the respective cell lysate of growing *atg16Δ* cells expressing Atg16-HA, Atg16^{D101A_E102A}-HA or Atg16^{K94A}-HA. The mixture was subjected to GFP-TRAP® analysis and evaluated by immunoblot (Figure 36 B).

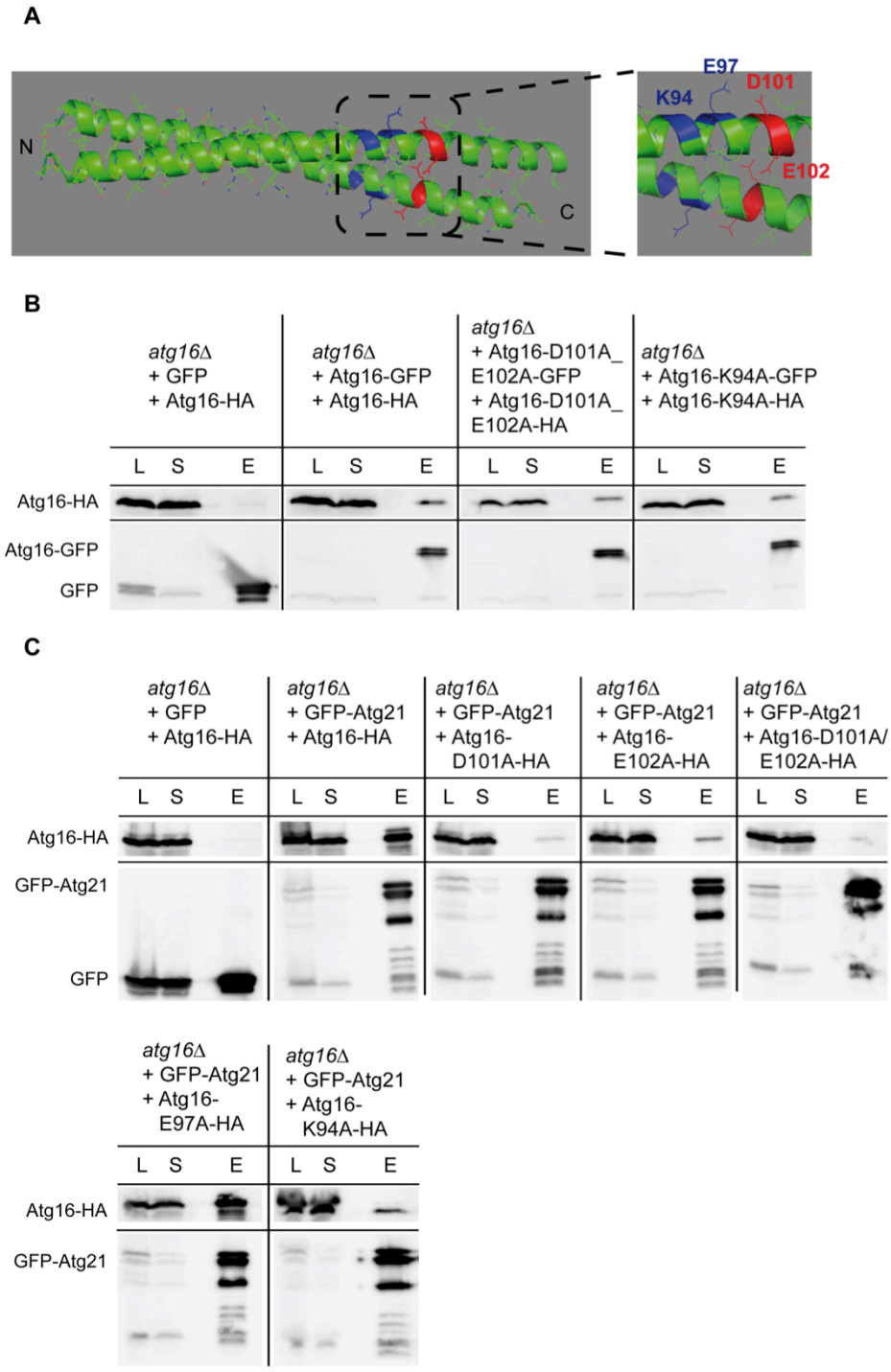

Figure 36: Amino acids D101 and E102 of Atg16 mediate the interaction with Atg21

(A) Ribbon diagram of the dimerized coiled-coil domain of Atg16. The amino acids lysine at position 94 (K94) and glutamic acid at position 97 (E97) are colored blue; aspartic acid at position 101 (D101) and glutamic acid at position 102 (E102) are colored red. The structural model was prepared based on the structural data reported by Fujioka *et al.* (Fujioka et al., 2010). N: N-Terminus; C: C-terminus **(B)** Cell lysate of growing *atg16Δ* cells expressing GFP as negative control or the indicated Atg16-GFP construct was mixed with cell lysate of growing *atg16Δ* cells expressing the indicated Atg16-HA construct. The mixture was subjected to GFP-TRAP® analysis.

Samples of the cell lysate (L), the unbound fraction (S) and the purified proteins (E) were analyzed by immunoblotting using anti-HA and anti-GFP antibodies. **(C)** Growing *atg16Δ* cells expressing GFP-Atg21 or GFP as negative control and the indicated Atg16-HA version were lysed using the mild cell lysis procedure and subjected to GFP-TRAP® analysis. Evaluation was performed as described in (B).

Atg16-GFP specifically co-precipitated Atg16-HA, whereas GFP alone did not. Atg16^{D101A_E102A}-GFP specifically co-precipitated Atg16^{D101A_E102A}-HA. The same was observed for Atg16^{K94A}-GFP and Atg16^{K94A}-HA. In conclusion, the formation of their coiled-coil domain was most likely not affected as the GFP-tagged wild type and mutants were all able to co-precipitate their HA-tagged counterparts.
Next, *atg16Δ* cells expressing GFP-Atg21 or GFP alone as control and the respective Atg16-HA construct were grown to mid-log phase and lysed in a mild way. The cell lysates were subjected to GFP-TRAP® analysis and evaluated by immunoblotting (Figure 36 C). Atg16-HA bound specifically to GFP-Atg21, but not to GFP alone. Interestingly, the binding of Atg16^{E102A}-HA and Atg16^{K94A}-HA to GFP-Atg21 was severely impaired, whereas the binding of Atg16^{D101A}-HA and Atg16^{D101A_E102A}-HA was nearly completely abolished. Atg16^{E97A}-HA bound to GFP-Atg21 in a wild type-like manner.

Both proteins, Atg21 and Atg16, play a crucial role in the ubiquitin-like conjugation of Atg8 to PE. If the interaction of Atg21 and Atg16 is needed for proper Atg8 lipidation, the Atg8-PE formation should be affected in the Atg21-binding defective Atg16 mutants. Therefore, the Atg8-PE formation in the presence of the Atg21-binding defective Atg16 mutants was tested. WT, *atg1Δ*, *atg3Δ*, *atg8Δ*, *atg16Δ* and *atg21Δ* cells expressing the empty vector were used as controls. *atg16Δ* cells expressing Atg16-HA or the indicated either truncated or mutated Atg16-HA version from the *CUP1* promoter were grown to mid-log phase. Samples were lysed using a mild glass bead lysis protocol and prepared for SDS-PAGE as described in Suzuki *et al.* (Suzuki et al., 2001). To adjust the expression level of the Atg16-HA versions, the expression of Atg16$^{1-57}$-HA, Atg16$^{1-119}$-HA and Atg16$^{58-150}$-HA was adjusted by the addition of 50 µM, 10 µM or 25 µM $CuSO_4$ to the selective medium, respectively. The samples were separated on a 15% SDS-PAGE containing 6 M urea to distinguish between Atg8

and Atg8-PE. The SDS-PAGE was subsequently immunoblotted and analyzed by several antibodies (Figure 37). As a loading control, the immunoblot was decorated with anti-PGK antibody, confirming similar protein amounts in all samples.

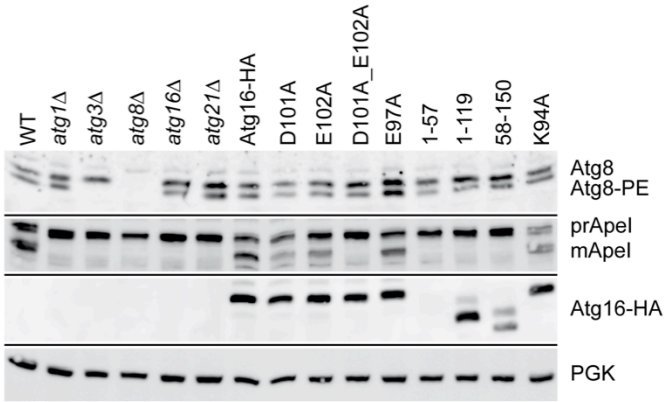

Figure 37: Functional analysis of the Atg16 point mutants

WT, *atg1Δ*, *atg3Δ*, *atg8Δ*, *atg16Δ*, *atg21Δ* cells carrying the empty vector or *atg16Δ* cells expressing the indicated Atg16-HA version were lysed in mid-log phase using a mild glass beads lysis protocol described in Suzuki *et al.* (2001). The expression of Atg16$^{1-57}$-HA, Atg16$^{1-119}$-HA and Atg16$^{58-150}$-HA was adjusted by the addition of 50 µM, 10 µM or 25 µM $CuSO_4$ to the selective medium over night (12 h), respectively. Samples were subjected to SDS-PAGE containing 6 M urea to separate Atg8 and Atg8-PE, immunoblotted and analyzed using anti-Atg8, anti-ApeI, anti-HA and anti-PGK antibodies.

In WT and *atg1Δ* cells, where the lipidation of Atg8 is unaffected, approximately 50% of Atg8 was conjugated to PE. In *atg3Δ* cells, defective in Atg8 lipidation, Atg8 was present solely in its unconjugated form. In *atg16Δ* and *atg21Δ* cells, the lipidation of Atg8 is severely impaired, so that most of Atg8 was present in its unlipidated form. Atg16-HA completely complemented the *atg16Δ* phenotype, as Atg8-PE was formed in a wild type-like manner. The same was observed in *atg16Δ* cells expressing Atg16^{E97A}-HA. In contrast, Atg8-PE formation was severely impaired in *atg16Δ* cells expressing Atg16^{D101A}-HA, Atg16^{E102A}-HA, Atg16^{D101A_E102A}-HA, Atg16^{K94A}-HA Atg16$^{1-57}$-HA, Atg16$^{1-119}$-HA and Atg16$^{58-150}$-HA comparable to *atg16Δ* or *atg21Δ* cells. Except of Atg16$^{1-57}$-HA, all Atg16-HA versions were present in comparable amounts.

The immunoblot was in addition decorated with an anti-ApeI antibody to monitor the autophagic activity. In WT cells, about half of ApeI was present in

the matured form. As expected, the maturation of ApeI was completely blocked in *atg1Δ*, *atg3Δ*, *atg8Δ*, *atg16Δ* and *atg21Δ* cells. Atg16-HA fully complemented ApeI maturation when expressed in *atg16Δ* cells. The same was observed for Atg16^{E97A}-HA and Atg16^{K94A}-HA. ApeI maturation was severely impaired in *atg16Δ* cells expressing Atg16^{D101A}-HA and Atg16^{E102A}-HA mutants. In *atg16Δ* cells expressing Atg16^{D101A_E102A}-HA, Atg16$^{1-57}$-HA, Atg16$^{1-119}$-HA or Atg16$^{58-150}$-HA the maturation of ApeI was completely blocked.

In conclusion, Atg16 interacted directly with Atg21 most likely via its coiled-coil domain. The conserved surface residues, E102 and more important D101, were identified to mediate proper interaction of both proteins. Atg21 and Atg16 interaction was a prerequisite for proper Atg8 lipidation and autophagic function.

5 Discussion

Autophagy is an important cellular degradation and recycling process. It is characterized by the formation of double membrane layered transport vesicles, the autophagosomes. In yeast, the formation of these autophagosomes starts at the pre-autophagosomal structure (PAS) as a cup shaped isolation membrane (phagophore) that expands and thereby encloses cytoplasm and organelles. The autophagosome finally fuses with the vacuolar membrane to release a still one membrane layered vesicle (autophagic body) into the vacuole lumen, where it is lysed. The contents are degraded and finally recycled. There are also several selective types of autophagy like the Cvt pathway in yeast. During this pathway the vacuole hydrolases aminopeptidase I, α-mannosidase and aspartyl aminopeptidase are constitutively transported from the cytoplasm to the vacuole (see chapter 2.2).

In this study, the localization and function of Atg21, one of the proteins essentially required for the Cvt pathway, were investigated using the model organism *Saccharomyces cerevisiae*. Autophagy is highly conserved among all eukaryotes. Therefore, most of the autophagy-related proteins are conserved from yeast to mammals. This conservation includes their function and recruitment hierarchy to the autophagosome formation site (Itakura and Mizushima, 2010). Thus, information obtained in yeast can often be transferred to higher eukaryotes.

Atg21 and its yeast homologues Atg18 and Hsv2 are members of the family of β-propellers that bind polyphosphoinositides (PROPPINs). They are WD40 repeat propellers and contain two lipid binding pockets, that preferential bind to PI3P and PI(3.5)P_2 (Baskaran et al., 2012; Krick et al., 2012; Watanabe et al., 2012). Atg21 and its homologues are highly conserved, but required for different variants of autophagy. While macroautophagy is only significantly reduced in *atg21Δ* cells, Atg21 is required for selective types of autophagy like the Cvt pathway (Barth et al., 2002). Selective types of autophagy require the very same core autophagy proteins involved in bulk autophagy. Therefore, information

obtained in the selective variants can often be transferred to other types of autophagy.

Mammals contain four PROPPIN orthologs, termed WIPIs. Based on phylogenetic tree analysis, WIPI-1 and WIPI-2 were assigned to Atg18 and WIPI-3 and WIPI-4 to Hsv2 (Krick et al., 2012; Polson et al., 2010), whereas Atg21 orthologs have been only found in yeast species so far (Meijer et al., 2007). However, WIPI-1 seems to be involved in LC3 lipidation (Polson et al., 2010; Proikas-Cezanne et al., 2004). In addition, WIPI-2 was reported to positively regulate the lipidation of the mammalian Atg8 ortholog LC3 (Polson et al., 2010). A similar function has been observed specifically for yeast Atg21 (Meiling-Wesse et al., 2004; Stromhaug et al., 2004), suggesting that not the protein itself, but its elementary function in the autophagic process might be conserved in higher eukaryotes.

In addition to the efficient lipidation of Atg8, Atg21 is required for recruitment of Atg8 and Atg5 to the PAS (Meiling-Wesse et al., 2004; Stromhaug et al., 2004). Therefore, no Cvt vesicles are formed in the absence of Atg21, suggesting an elementary role for Atg21 in the PAS assembly especially in selective types of autophagy. Thus, Atg21 has not been detected at the PAS so far.

5.1 Part of Atg21 localizes to the PAS

In this study, a potential PAS localization of Atg21 was investigated using direct fluorescence microscopy. Therefore, *atg21Δ* cells expressing Atg21-YFP from its endogenous promoter and the PAS marker ApeI-RFP were imaged. Cells were analyzed under growing conditions, as Atg21 is strictly required for the constitutive Cvt pathway acting under those conditions.

Usually, Atg8 is used as a PAS marker in Atg protein localization studies. In this study, ApeI-RFP was used as a PAS marker for two reasons. First, the expression of Atg8 is upregulated at autophagy-inducing conditions, but under growing conditions the amount of Atg8 is significantly smaller (Huang et al., 2000). Therefore, the part of Atg8 at the PAS is hardly detectable in fluorescence microscopy and not suitable for PAS rate determination under these conditions. Second, in this study Atg8 was identified as a potential interaction partner of Atg21 (see chapter 5.6). Therefore, Atg21 and Atg8 could form a complex in the cytosol that is subsequently recruited to the PAS. This has been reported for the

Atg21 homologue Atg18 and its interaction partner Atg2 (Obara et al., 2008b). A cytosolic Atg21-Atg8 complex would mimick a colocalization at the PAS. Therefore, the PAS marker ApeI-RFP was used as an alternative. In addition, ApeI is selectively transported to the PAS via the Cvt pathway, where Atg21 is active.

The percentage of ApeI-RFP dots that colocalized with Atg21-YFP was determined (Colocalization rate). In fact, a considerable number of ApeI-RFP respectively PAS dots (49%) colocalized with Atg21-YFP, indicating that indeed a part of Atg21 is present at the PAS (see Figure 11). That is the first time that a part of Atg21 has been detected at the PAS.

Atg19 is the Cvt cargo receptor and directs the ApeI complex to the PAS by binding to Atg11 and Atg8 (Kim and Klionsky, 2000; Shintani et al., 2002). The colocalization rate in *atg19Δ* cells was determined to exclude an interaction of Atg21 and ApeI. As expected, the colocalization rate of Atg21-YFP and perivacuolar ApeI-RFP dots was significantly reduced in *atg19Δ* cells (16%) compared to the wild type (*atg21Δ*=49%). Hence, ApeI-RFP is a suitable PAS marker for colocalization studies with Atg21-YFP under the selected conditions.

Atg11 is a component of the Atg1 kinase complex and acts as a scaffold for PAS assembly for selective types of autophagy. In addition, it acts in cargo recognition via direct binding of receptor proteins like Atg19 in the Cvt pathway. Consequently, the Cvt complex is not directed to the PAS, although Atg19 can still bind to the ApeI complex (Shintani et al., 2002). Indeed, the colocalization rate of Atg21-YFP and ApeI-RFP was significantly reduced in the absence of Atg11 (31%). Unexpectedly, the colocalization rate was only slightly reduced compared to *atg19Δ* cells (16%), though both deletions should result in the absence of ApeI-RFP from the PAS. Atg11 might be partially replaced by Atg17 that adapts the Atg11 scaffold function in the Atg1 kinase complex under autophagy-inducing conditions (Cheong et al., 2008; Suzuki and Ohsumi, 2007; Suzuki et al., 2007). However, it is not known, if all proteins are simultaneous present in the Atg1 kinase complex or if there are subcomplexes, that vary dependent on nutrient conditions. The amount of Atg11, Atg17 and Atg19 at the PAS are proposed to be the same under both growing and starvation conditions (Geng et al., 2008). Furthermore, though bulk autophagy is dramatically induced under

stress conditions, it occurs also at a basal level under normal growth conditions (Parzych and Klionsky, 2013; Yorimitsu and Klionsky, 2005). Therefore, *atg11Δ atg17Δ* double mutants are usually used to completely block autophagosome formation. Speculatively, the lack of Atg11 could be partially complemented by Atg17 even under nutrient-rich conditions. This would result in a PAS formation at a low frequency and Atg19 would still be able to direct the ApeI complex to the PAS by binding to Atg8. In contrast, in the absence of the receptor Atg19, the ApeI complex is not able to bind to any PAS component. This could explain, why the deletion of *ATG19* has a more severe effect than the deletion of *ATG11*. To prove this hypothesis, the colocalization rate of Atg21-YFP and ApeI-RFP should be further determined in *atg11Δ atg17Δ* cells.

Atg21 is peripherally membrane associated by binding to PI3P and/or PI(3,5)P_2 (Krick et al., 2006). Yeast has only one phosphoinositide 3-kinase, Vps34, which is present in two complexes. Each complex contains in addition to the core components a unique factor, that links the kinase complex to a specific site and therefore to a specific cellular function. Vps38, the unique subunit of complex II, recruits the kinase complex to endosomes (Kihara et al., 2001; Obara et al., 2006). Atg21-YFP formed one to six perivacuolar dots within the cell. Some of those have been colocalized earlier with endosomal marker proteins as FYVE-RFP or Snf7-RFP (Krick et al., 2008a). The localization of Atg21 at endosomal compartments is dependent on Vps38 and therefore on the endosome-specific PI3P pool (Krick et al., 2008a). The autophagy-specific Vps34 complex I at the PAS specifically contains Atg38 and Atg14 (Araki et al., 2013; Obara et al., 2006). In the absence of Atg14 respectively the PAS-specific PI3P pool, Atg21 should be also absent from the PAS. Indeed, the colocalization rate of Atg21-YFP and ApeI-RFP was significantly reduced in *atg14Δ* cells (22%) compared to wild type cells (49%), confirming that the PAS localization of Atg21 is PI3P-dependent. In contrast to *vps38Δ* cells, where Atg21 seems to be nearly completely released to the cytosol (Krick et al., 2008a), the deletion of *ATG14* did not lead to a change in the overall punctate appearance of Atg21-YFP. Under growing conditions, the majority of PI3P have been reported to locate at endosomes and the vacuolar membrane, whereas only a minor amount has been found at the PAS (Obara et al., 2008a). Therefore, probably only a small part of Atg21-YFP is located at the

PAS, whereas the major part is located at other sites as endosomes. That might also be a reason why Atg21 has not been detected at the PAS before. Stromhaug *et al.* (2004) have explicitly monitored cells expressing chromosomally tagged Atg21-GFP and prApeI-RFP as PAS marker and observed, that these two proteins did not colocalize. The endogenous expression level of Atg21 is quite low leading to a weak fluorescence signal. The Atg21-YFP construct used in this study was also expressed from its endogenous promoter, but a higher resolution microscopy has been used for analysis. Therefore, that Atg21 has not been detected at the PAS before could be due to a difference in the microscope sensitivity. Furthermore, the PAS localization of Atg21 was not immediately obvious. Though the Cvt pathway is highly active under the elected conditions, only 35% of the cells averaged a perivacuolar ApeI-RFP respectively PAS dot. In addition, Atg21-YFP forms approximately three to six dots within the cell. For the quantification of the Atg21 PAS localization, it was necessary to determine the ApeI-RFP and Atg21-YFP dots in a high number of cells to validate the results.

As shown for the Atg21 homologue Atg18, proper membrane association is mediated by two components, the PIP binding and an additional protein interaction partner like Atg2 (Obara et al., 2008b; Rieter et al., 2013). The PAS localization of the Atg18-Atg2 complex additionally requires the membrane protein Atg9 (Reggiori et al., 2004). Atg9 forms a trimeric complex with Atg23 and Atg27. All three proteins cycle between the PAS and a non-PAS pool and the PAS recruitment of all three proteins depends on the presence of each other. In contrast, the retrograde transport of Atg9 from the PAS to its non-PAS pool is independent of Atg23 and Atg27 but dependent on the Atg2-Atg18 complex (Legakis et al., 2007). It has been already shown by two independent approaches that the PIP binding is required for proper Atg21 localization. First, Atg21 is not present at the PAS in the absence of PI3P (see above). Second, mutations within the lipid binding domain of Atg21 result into release of the protein into the cytosol (Krick et al., 2006). In order to find the additional protein component required for proper PAS localization of Atg21, further deletion strains were tested for a loss of the Atg21 PAS localization (see Figure 11+Figure 12).

In the absence of Atg9, the PAS localization of Atg21-YFP was significantly reduced (26%), pointing to a potential influence of Atg9 on the Atg21 PAS localization. In contrast, further split ubiquitin approaches did not detect an interaction of Atg21 and Atg9 (see chapter 5.5). Thus, the effect of Atg9 is probably indirect, because Atg9 is required for the recruitment of Atg14 to the PAS and therefore for the generation of the PAS-specific PI3P pool (Suzuki et al., 2007). The absence of Atg2 or Atg27 had only a slight effect on the PAS localization of Atg21-YFP (34% respectively 38%), whereas the deletion of *ATG23* did not change the colocalization rate of Atg21-YFP (48%). The Atg2-Atg18 complex is required for efficient retrograde transport of Atg9 from the PAS (Reggiori et al., 2004). Therefore, the loss of Atg2 could have a rather indirect effect on the Atg21 PAS localization. Similarly, also Atg27 and Atg23 are required for the transport of Atg9 to the PAS (Legakis et al., 2007). Nonetheless, the loss of Atg27 but not of Atg23 slightly affected the Atg21 PAS localization. In addition, split-ubiquitin approaches detected a potential interaction of Atg27 and Atg21 (see Figure 21), pointing to a stabilizing role for Atg27 in Atg21 PAS localization. However, a potential interaction of Atg21 and Atg27 was analyzed in further experiments and are discussed in more detail below (see chapter 5.5).

As mentioned before, Atg21 is required for the recruitment of Atg8 and Atg5 to the PAS (Meiling-Wesse et al., 2004; Stromhaug et al., 2004). Atg8 is conjugated to PE in a ubiquitin-like manner, where the Atg12-Atg5/Atg16 complex functions as an E3-like enzyme ((Nakatogawa, 2013), see chapter 2.2.4.4). Both, Atg8 and Atg12-Atg5/Atg16 are among the last components, that are recruited to the PAS (Suzuki et al., 2007). Furthermore, Atg16 mediates the PAS localization of the Atg12-Atg5/Atg16 complex (Hanada et al., 2007; Suzuki et al., 2001). The loss of Atg8 did not affect the PAS localization of Atg21-YFP, whereas the Atg21 PAS localization was slightly reduced in the absence of Atg16 (Colocalization rate: 52% respectively 34%). Therefore, the Atg21 PAS localization is most likely independent on Atg8, but stabilized by Atg16. As discussed below, this study revealed that Atg21 and Atg16 interact directly with each other. Furthermore, two surface residues within the coiled-coil domain were identified to specifically bind to Atg21 (see chapter 4.3.6.4). The Atg12-Atg5/Atg16 complex is proposed to be dimeric mediated by the coiled-coil domain of Atg16 (Fujioka et al., 2010;

Kuma et al., 2002). Therefore, one Atg12-Atg5/Atg16 complex exhibits two Atg16 molecules and thus two potential Atg21 binding sites. It could be possible, that Atg16 bridges two Atg21 molecules resulting in a dimeric Atg21-Atg16 respectively Atg21-Atg16/Atg5-Atg12 complex. The Atg21 dimerization would further stabilize the PI3P-dependent membrane association of Atg21. Consequently, the Atg21 PAS localization could be destabilized in the absence of Atg16 as observed in this study. This hypothesis is further supported by the observation, that Atg5 is not required for the colocalization of Atg16-GFP and mCherry-Atg21 at the PAS (see chapter 4.3.6.2 and Figure 32). Dimerization of Atg16 is independent of Atg5 and Atg12 (Mizushima et al., 1999). Thus, Atg16 alone would be sufficient to bridge Atg21 and thus stabilize the membrane association of Atg21 at the PAS. This model would also not exclude a potential additional interaction with the membrane protein Atg27 to stabilize membrane association. As mentioned above, the Atg21 homologue Atg18 binds to the cytosolic protein Atg2, and both proteins are recruited to the PAS by additional interaction with the membrane protein Atg9 (Reggiori et al., 2004). Similarly, interaction with the membrane protein Atg27 in addition to the cytosolic Atg16 could enhance the Atg21 PAS localization. However, this model has to be proven by further Atg21 localization studies. The PAS localization of Atg21 should be determined in *atg5Δ* and *atg12Δ* cells to exclude an influence of the remaining components of the Atg12-Atg5/Atg16 complex on the Atg21 PAS localization. Importantly, the deletion of Atg16 or Atg27 had only a slight effect on the Atg21 PAS localization, suggesting that more than one component might stabilize the Atg21 PAS localization. This implies that the simultaneous deletion of two or more components should result in a more severe defect in Atg21 PAS localization. Therefore, the determination of the Atg21 PAS localization in *atg14Δ atg16Δ, atg14Δ atg27Δ* or *atg16Δ atg27Δ* cells should be further determined to prove the hypothesis.

In conclusion, part of Atg21 clearly localizes at the PAS in a PI3P-dependent manner. As mentioned before, the assembly of the PAS and the recruitment of the Atg proteins is a quite dynamic process and occurs in a specific hierarchy. Based on the results obtained from the PAS localization analysis of Atg21-YFP in this study, Atg21 is most likely recruited to the PAS after localization of the

Atg14-containing Vps34 kinase complex and therefore after the generation of the PAS-specific PI3P pool, but before recruitment of Atg8 and its E3-like enzyme, the Atg12-Atg5/Atg16 complex.

5.2 Atg21 is located on the outer autophagosomal membrane

Atg21 is peripherally membrane associated at the PAS via binding of PI3P (see Figure 11). In the current model, the PAS assembles through hierarchical interactions between Atg proteins and generates the phagophore, which expands to become an autophagosome. The specific localization of each protein at the PAS seems to correspond directly to its respective function (Suzuki et al., 2013).

A more detailed insight into the Atg protein distribution at the PAS and across the phagophore membrane, was reported by Suzuki *et al.* (2013). By high overexpression of prApeI, a giant prApeI complex is generated, that is too large to be packed into a Cvt vesicle or even in an autophagosome. Instead, the expansion of the phagophore arrests at its maximum length, resulting in a cup-shaped like structure associated with both the giant prApeI complex and the vacuolar membrane. Moreover, the distribution pattern of the Atg proteins across the phagophore and the PAS is also arrested and can be visualized by direct fluorescence microscopy. Unfortunately, the distribution of Atg21 was not monitored, probably because it has not been detected at the PAS so far. However, the Atg21 homologue Atg18 and its interaction partner Atg2 localize to the edges of the expanding phagophore (Suzuki et al., 2013). As discussed before, in contrast to Atg18, Atg2 most likely only indirectly affects the PAS localization of Atg21. Therefore, the localization pattern of Atg18 can probably not be transferred to Atg21.

Atg8 is distributed evenly across the outer and inner membrane of the expanding phagophore, whereas the Atg12-Atg5/Atg16 complex is restricted to the outer membrane (Kirisako et al., 2000; Mizushima et al., 2001; Suzuki et al., 2001; Suzuki et al., 2013). As discussed below in more detail, Atg21 probably interacts with Atg8 and the Atg12-Atg5/Atg16 complex (see chapter 5.6+5.7). At least the interaction with the Atg12-Atg5/Atg16 complex occurs at the PAS. Furthermore, Atg21 probably mediates membrane association of the Atg12-Atg5/Atg16 complex by direct binding of Atg16 (see chapter 5.7), suggesting that

Atg21 and the Atg12-Atg5/Atg16 complex share the same localization pattern on the forming autophagosome. In contrast, PI3P that mediates the peripheral membrane association of Atg21, is distributed across the inner and outer autophagosomal membrane (Obara and Ohsumi, 2008). But among the autophagy-related proteins only those on the inner membrane of the expanding phagophore are trapped inside the matured autophagosome and transported into the vacuole. Using direct fluorescence microscopy, a potential transport of mCherry-Atg21 into the vacuole was tested in growing *atg21Δ pep4Δ* cells (see Figure 14). mCherry-Atg21 is most probably not transported into the vacuole. Therefore, as the Atg12-Atg5/Atg16 complex, Atg21 is most likely restricted to the outer membrane of the expanding phagophore and dissociates from that structure immediately before or after completion of the autophagosome as it was suggested for the Atg12-Atg5 complex before (Suzuki et al., 2001). Nevertheless, using the above-mentioned giant ApeI complex approach, the localization of Atg21 across the autophagosomal membranes should be determined in further experiments. Electron microscopy could be additionally used to prove a potential restriction of Atg21 to the outer autophagosomal membrane. Up to now, a transport of the Atg21 homologue Atg18 into the vacuole has also not been reported, probably because Atg18 is not located across the expanding membranes but at the edges of the phagophore (Suzuki et al., 2013).

Maturation and/or fusion of the autophagosomes with the vacuolar membrane require the dissociation of the autophagic machinery. The covalent anchored Atg8 is cleaved off by Atg4 (Kirisako et al., 2000), whereas the major part of the autophagic machinery is probably released by the degradation of PI3P via the phosphatase Ymr1 (Cebollero et al., 2012). As shown for Atg18, proper membrane association is mediated by two components, the PIP binding and an additional protein interaction partner. The degradation of PI3P leads to its dissociation from the membrane (Cebollero et al., 2012). If this was also true for Atg21, Atg21 should remain associated with autophagosomes in the absence of Ymr1 as shown for its homologue Atg18. Since those autophagosomes are not able to fuse with the vacuole (Cebollero et al., 2012), the deletion of *YMR1* would result in an increased colocalization of Atg21-YFP and the Cvt vesicle marker ApeI-RFP in fluorescence microscopy. Therefore, the influence of Ymr1

respectively clearance of PI3P on the dissociation of Atg21 from the autophagosome should be further tested by determination of the colocalization rate of Atg21-YFP and ApeI-RFP as described before (see chapter 4.2.1).

Phosphorylation of the PIP binding site of Atg18 from *Pichia pastoris* regulates its ability to bind to PI(3,5)P_2 at the vacuolar membrane (Tamura et al., 2013), pointing to an additional regulatory mechanism for PROPPIN dissociation. Along this line, the serine/threonine kinase activity of Atg1 is suggested to specifically function in the regulation of Atg protein localization at the PAS (Cheong et al., 2008). Atg21 has originally been identified as a target of the Atg1 kinase (Ptacek et al., 2005). That led to the idea, that Atg1 could regulate the Atg21 PAS localization via phosphorylation. Nevertheless, a potential influence of Atg1 on the PAS localization of Atg21 is highly speculative and has to be carefully analyzed further.

The respective interaction partner could represent another regulatory level for membrane dissociation. Recently, a potential posttranslational modification site was identified within Atg18, which could contribute to the regulation of the Atg18-Atg2 interaction or other functions of Atg18 (Rieter et al., 2013). Therefore, identification of the interaction partner of Atg21 at the PAS or endosomes could give more hints for a regulation of the Atg21 localization within the cell.

In contrast to Atg21 and Atg18, two of the mammalian PROPPIN orthologs, WIPI-1 and WIPI-2 are located on the inner and outer membrane of generated autophagosomes (Proikas-Cezanne et al., 2011), suggesting a different sorting mechanism in mammals and/or a function different from their yeast counterparts.

5.3 Atg21 is part of a high molecular weight complex

Atg21 was detected as a part of a high molecular weight complex of ≥ 670 kDa using gelfiltration chromatography and density gradient centrifugation (see Figure 16+Figure 18). This high molecular weight Atg21 complex was highly sensitive to the cell lysis and buffer conditions (see chapter 4.3.1). In this study, a mild cell lysis procedure was established that keeps the sensible complex intact

as a prerequisite not only for further analysis of the complex but also for the identification and verification of potential Atg21 interacting proteins.

Sorbitol density gradient centrifugation was used to further analyze the high molecular weight Atg21 complex in depicted mutant strains (see chapter 4.3.1.2). Atg21 is required for the Cvt pathway, which describes the selective transport of ApeI to the vacuole. ApeI forms large dodecamers. One dodecamer has a high molecular weight (~670 kDa) and was therefore used as a size marker in gelfiltration chromatography and density gradient centrifugation. Otherwise, it would be also possible that the ApeI complex is part of the high molecular weight Atg21 complex. That would also explain the co-elution respectively –sedimentation in gelfiltration respectively sorbitol gradient centrifugation. However, neither the absence of the cargo receptor Atg19 (see Figure 18) nor the absence of ApeI itself (data not shown) did influence the assembly of the high molecular weight Atg21 complex in this study, suggesting that ApeI is probably not part of that complex.

The type I membrane protein Atg27 is, similar to Atg21, required for the Cvt pathway, but only affects macroautophagy (Yen and Klionsky, 2007). Therefore, Atg27 would be a good candidate for an interaction partner of Atg21. However, the deletion of *ATG27* did not influence the assembly of the high molecular weight Atg21 complex. Furthermore, the loss of the kinase Atg1 did also not affect the assembly of the Atg21 complex (see Figure 18). However, it cannot be excluded, that one of the tested proteins is a component of the Atg21 complex anyway. Due to their low molecular weight, a change in the distribution pattern of the Atg21 complex within the sorbitol density gradient centrifugation would only be visible if one of the tested proteins was a stoichiometric component of the complex. It can only be concluded, that none of the tested proteins had an effect on the formation of the high molecular weight Atg21 complex.

Hypothetically, the high molecular weight Atg21 complex could constitute an assembly of Atg18 family members in a large scaffold structure. This hypothesis is supported by the finding that Atg21 interacts with itself and its homologues Atg18 and Hsv2 (split-ubiquitin assay data not shown and (Nair et al., 2010)).

As discussed below, 6xHis-SUMO-Atg21 specifically co-precipitated all members of the TOR complex 1 (TORC1) in pull down experiments (see chapter 5.4).

TORC1 is a huge dimeric complex with a predicted molecular size of ~ 2 MDa, estimated by gelfiltration chromatography (Loewith and Hall, 2011). The high molecular weight Atg21 complex was partly present in fractions corresponding to a much higher molecular weight as the ApeI complex (670 kDa) (see Figure 16+Figure 18). Therefore, TORC1 or part of it could represent another candidate for the high molecular weight Atg21 complex. However, this is highly speculative. For determination of the Atg21 complex components, the amount of the complex should be scaled up to identify the respective proteins by mass spectrometry. The formation of the complex was independent of Atg1 (see Figure 18). In general, the loss of Atg1 results in an arrest of most of the autophagy-related proteins at the PAS. If the Atg21 complex was formed or at least partially present at the PAS, *atg1Δ* cells could be used to enrich the amount of the Atg21 complex. However, identification of its components would contribute to elucidate the molecular function of Atg21.

5.4 Identification of Atg21 interaction partner

The pull down approach was used to further identify Atg21 interaction partner. Recombinant 6xHis-SUMO-Atg21 and 6xHis-SUMO alone as negative control were purified and incubated with yeast crude cell extract. The co-precipitated proteins were analyzed by both immunoblotting and mass spectrometry (see Figure 19). Curiously, no Atg protein has been identified in mass spectrometry, although mCherry-Atg19 was clearly detected by the anti-Red antibody in immunoblotting. The samples tested by immunoblot were the same that were subsequently subjected to mass spectrometry analysis, excluding differences in the pull down procedure. Based on the immunoblot signal, the amount of mCherry-Atg19 should be above the critical detection level for mass spectrometry. Furthermore, prediction programs did not propose any secondary modifications that would complicate an identification of Atg19 in mass spectrometry analysis. For the mass spectrometry analysis, the samples were first separated by SDS-PAGE. After Coomassie staining, the gel was cut into slices and the protein content of each slice was determined. mCherry-Atg19 has a molecular weight of about 75 kDa corresponding approximately to the molecular weight of 6xHis-SUMO-Atg21 (70 kDa). Therefore, mCherry-Atg19 was probably

present in the same slice as at least part of 6xHis-SUMO-Atg21. The amount of 6xHis-SUMO-Atg21 was much higher than the amount of mCherry-Atg19 (see Figure 19). This could have resulted in a masking and therefore non-detection of mCherry-Atg19 in mass spectrometry analysis. Along this line, the huge amount of 6xHis-SUMO-Atg21 probably also shifted adjacent proteins when loaded on SDS-PAGE, explaining the slight molecular shift of mCherry-Atg19 in the bound fraction in immunoblotting (see Figure 19).

Surprisingly, all components of the target of rapamycin complex I (TORC1) were specifically co-precipitated by 6xHis-SUMO-Atg21 (see Figure 19). TORC1 consists of Tco89, Kog1, Lst8 and the serine/threonine kinase Tor1 or Tor2 and is most likely dimeric (Loewith and Hall, 2011). Its large size (~ 2 MDa) would make it a good candidate as component of the high molecular weight Atg21 complex detected in gelfiltration chromatography and density gradient centrifugation (see chapter 5.3). TORC1 has a central role in several cellular processes that regulate cell growth in response to nutrients and growth factors. In general, TORC1 is active under growing conditions and is regulated by the availability of nutrients such as nitrogen and carbon (Loewith and Hall, 2011). TORC1 also acts as a negative regulator of autophagy. In yeast, it directly phosphorylates Atg13 (Kamada et al., 2010), which most likely regulates Atg1-kinase activity. Under autophagy-inducing conditions, Atg13 is dephosphorylated and autophagy is induced. TORC1 is highly conserved in mammals. Recent studies revealed, that the Atg18 ortholog WIPI-1 specifically regulates TORC1 signaling in melanosome formation by an unknown mechanism, that is distinct from the regulation of autophagosome formation (Ho et al., 2011).

However, at this point, it is highly speculative that Atg21 might regulate TORC1 activity as it was proposed for the PROPPIN ortholog WIPI-1 or that Atg21 is conversely regulated via phosphorylation by TORC1 as Atg13. Further characterization of a potential interaction should clarify, if Atg21 interacts directly with one of the TORC1 components or if Atg21 and TORC1 are simultaneously present in the same complex. Thereby, a potential functional role of this interaction could be proposed.

5.5 Interaction studies of Atg21 and Atg27

The membrane protein Atg27 forms a trimeric complex with the second membrane protein Atg9 and the cytosolic protein Atg23 with Atg9 bridging both. All three proteins cycle between the PAS and a peripheral site. The cycling of each protein to the PAS is dependent on the presence of the other complex components (Legakis et al., 2007). Recent studies revealed that Atg9 resides on peripheral vesicular structures, which directly contributes to the formation of the phagophore upon autophagy induction (Kakuta et al., 2012; Mari et al., 2010; Yamamoto et al., 2012). At least Atg27 is present on the Atg9-containing vesicles, suggesting that the trimeric complex is required for membrane delivery to the PAS (Kakuta et al., 2012). Atg9 is required for this process under both growing and starvation conditions, whereas Atg27 is only required for efficient formation of Cvt vesicles. Therefore, Atg27 has the same autophagy phenotype as Atg21 and could be an appropriate protein interaction partner of Atg21. Indeed, an interaction of both proteins was detected in the split-ubiquitin assay (see Figure 21). Furthermore, Atg21 specifically interacted with Atg27 but not with Atg9 or Atg23. Atg27 contains 271 amino acids and is a type I membrane protein. Therefore, it has one transmembrane domain (residues 199-221) and its C-terminus faces the cytosol, whereas the N-terminus extends into the lumen (Yen et al., 2007) (see Figure 22). Nui-Atg27, where the Nui part was facing the lumen, did not interact with Atg21-Cub. Atg27 contains a N-terminal signal sequence, which is cleaved off after membrane insertion (Yen et al., 2007). In the Nui-Atg27 construct, the Nui part is N-terminally fused to Atg27. This could either result in a masking of the signal sequence and therefore in a mislocalization of Nui-Atg27 or in a cleavage of the Nui part together with the signal sequence. This would also explain why an indirect binding of Atg27-Cub and Nui-Atg23 but not of Atg23-Cub and Nui-Atg27 was detected in the split-ubiquitin assay (see Figure 21 B). However, Nui-Atg21 and Atg27-Cub, where the Cub part faces the cytosol, did clearly interact with each other, suggesting that Atg21 probably interacts with Atg27 on the cytosolic site. Atg9 is a multispanning membrane protein and both termini extend into the cytosol, whereas Atg23 is a cytoplasmic protein, which binds to Atg9 on the cytoplasmic site (Legakis et al., 2007). Atg9 interacts directly with Atg27 and served therefore as positive control for Atg27-Cub.

Atg23 is a cytosolic protein and interacts indirectly with Atg27 via Atg9. Therefore, Atg23 served as control how an indirect interaction looks like in the split-ubiquitin system (see Figure 21). The interaction of Atg21 with the C-terminal part of Atg27 was indirectly confirmed by truncated versions of Atg27 in the split-ubiquitin assay (see Figure 22). Due to the N-terminal signal sequence only C-terminal truncated versions of Atg27 have been tested. Atg27$^{1-198}$-Cub remained most likely cytosolic, because it was lacking its transmembrane domain. In contrast, neither Atg9 as positive control nor Atg21 interacted with Atg27$^{1-221}$-Cub. This construct was lacking the C-terminus, but still contained the transmembrane domain, supporting an interaction of Atg21 with the C-terminus of Atg27 on the cytosolic site. This would indicate that Atg27 serves as a protein interaction partner to mediate proper membrane association of Atg21. But in fluorescence microscopy the PAS localization of Atg21-YFP had been only slightly influenced by the deletion of *ATG27* (see Figure 12). As already explained in more detail, Atg27 could alternatively mediate the PAS localization of Atg21 together with an additional component. Only the simultaneous deletion of both components would then disturb the Atg21 PAS localization (see chapter 5.1).

Furthermore, the colocalization of cAtg27-GFP and mCherry-Atg21 was analyzed in direct fluorescence microscopy to support a potential interaction of both proteins (see Figure 23). Indeed, in more than half of the cells at least 50% of the mCherry-Atg21 dots colocalized with cAtg27-GFP. This colocalization rate corresponds perfectly to the colocalization rate obtained for Atg27 and Atg9 respectively Atg23 in previous studies (Legakis et al., 2007), supporting a potential interaction of Atg21 and Atg27. Atg1 is required for the retrograde movement of the all three proteins Atg9, Atg23 and Atg27 from the PAS to a peripheral site. Thus all three proteins should be restricted to the PAS by the loss of Atg1 (Legakis et al., 2007; Yen et al., 2007). The colocalization of cAtg27-GFP and mCherry-Atg21 was obtained in *atg1Δ* cells to test if both proteins colocalized at the PAS (data not shown). Surprisingly, cAtg27-GFP still formed several dots within the cell comparable to wild type cells. The successful deletion of *ATG1* was verified by control PCR analysis and ApeI maturation defect (data not shown). In addition, cAtg27-GFP was completely functional (Figure 23 A),

excluding a mislocalization of cAtg27-GFP. This discrepancy in the localization pattern might be caused by improved microscope sensitivity.

Yeast cells commonly exhibit only one PAS. However, in several cells, all or at least most of the mCherry-Atg21 dots colocalized with cAtg27-GFP (see Figure 23), suggesting that both proteins probably colocalized at multiple sites within the cell. It has to be clarified if one of these sites corresponds to the PAS. A colocalization respectively interaction of both proteins at a site different from the PAS would also explain, why the deletion of *ATG27* had only a slight effect on the PAS localization of Atg21-YFP (see Figure 12).

However, Atg27 cycles between the PAS, Golgi and Mitochondria (Kakuta et al., 2012; Yen and Klionsky, 2007), whereas Atg21 localizes to endosomes, the vertices of vacuolar junctions and the PAS (Krick et al., 2008a; Meiling-Wesse et al., 2004)(this study). Determination of the colocalization site of Atg21 and Atg27 could give further information about a potential interaction of both and its physiological relevance. As mentioned before, Atg9-containing vesicles probably directly contribute to the formation of the phagophore (Mari et al., 2010; Yamamoto et al., 2012). Atg27 is required for the anterograde movement of Atg9 to the PAS and vice versa. Thus, Atg27 is also present on the Atg9-containing vesicles and therefore probably involved in the membrane delivery to the PAS at least under nutrient-rich conditions (Kakuta et al., 2012). Moreover, the retrograde moving of Atg9 and Atg27 from the PAS to their peripheral sites occurs independently from each other, suggesting that these proteins may not necessarily cycle together (Legakis et al., 2007). In addition to the Atg1-Atg13 complex, which is needed for the retrograde moving of both Atg9 and Atg27, the Atg21 homologue Atg18 and its interaction partner Atg2 are required for the retrograde moving of Atg9, but not of Atg27 (Yen et al., 2007). Cycling of Atg27 is required for its proper function in Cvt formation. This led to the idea that Atg21 might be involved in the retrograde cycling of Atg27. The loss of Atg21 would lead to a defect of Atg27 cycling and therefore of the membrane delivery under growing conditions resulting in a defect in Cvt vesicle formation, a phenotype that is observed for both proteins. However, this is highly speculative and should be further analyzed. The aspect that Atg27 cycling is independent of Atg14 (Yen et al., 2007), which is in turn needed for proper Atg21 PAS localization (see

4.2.1), argues against that hypothesis. A localization study of Atg27 in the absence of Atg21 will shed light on this question. As a next step, the potential interaction of both proteins, suggested by the split-ubiquitin assay and the fluorescence microscopy, should be confirmed. In this study, pull down or GFP-TRAP® analysis failed to detect a potential interaction of Atg27 and Atg21 (see Figure 24). Atg27 is a membrane protein. Thus, it is possible, that Atg27 was not properly solubilized under the chosen conditions. The cell lysis procedure could be improved and different detergents could be tested to detect a potential interaction with Atg21 as a prerequisite for further functional studies.

5.6 Interaction studies of Atg21 and Atg8

The small ubiquitin-like protein Atg8 represents one of the core autophagy proteins and plays dual roles in autophagy. It is required for the expansion of the phagophore. In addition, Atg8 links the cargo to the forming autophagosome by binding to the receptor protein and helps therefore in cargo recognition during selective types of autophagy. To fulfill its function, Atg8 has to be lipidated to PE in a series of conjugation reactions similar to protein ubiquitination (Nakatogawa, 2013) (see chapter 2.2.4.4). Atg21 is required for efficient lipidation of Atg8 and for its recruitment to the PAS, but the underlying mechanism remains elusive (Meiling-Wesse et al., 2004; Stromhaug et al., 2004).
In this study, a potential interaction of Atg21 and Atg8 was detected in the split-ubiquitin assay (see Figure 25). Bimolecular Fluorescence Complementation (BiFC) was used to further verify a potential interaction of both proteins. As a positive control, cells expressing N-YN Atg8 and its processing enzyme N-YC Atg4 were used. Unfortunately, the resulting eYFP-Atg8-Atg4 complex completely located to the nucleus (see Figure 26 C). Since none of the proteins has been detected in the nucleus before, they were probably completely mislocated. Both constructs were expressed from a constitutive *ADH* promoter and therefore highly overexpressed, which may have caused the mislocalization of eYFP-Atg4-Atg8. In contrast, the expression of N-YN Atg8 and Atg21 C-YC resulted in perivacuolar dots, which colocalized with the PAS marker ApeI-RFP in a high frequency (60%) (see Figure 26 E). This suggests a potential interaction of Atg21 and Atg8 at the PAS. Cells expressing Atg21 C-YC and N-YN alone were

used as a negative control. Surprisingly, those cells also showed a perivacuolar dot similar to cells expressing both proteins (see Figure 26 E). The formation of those false-positive signals did not change even after improvement of the expression conditions. Taken together, all cells expressing Atg21 C-YC showed a false-positive signal independent of expression partner, level or duration. During BiFC, the assembly of the two halves of eYFP is irreversible and results in a significant stabilization of the eYFP-protein complex. One advantage of this method is the visualization of only weak and therefore hardly detectable interactions (Skarp et al., 2008). In the negative control cells, N-YN alone was most likely evenly distributed throughout the cytosol. In addition, the amount of N-YN was much higher compared to the amount of N-YN Atg8. Thereby, N-YN might have colocalized by chance close enough to Atg21 C-YC so that the eYFP-Atg21 complex could reassemble. Due to the irreversible assembly of both eYFP halves, those complexes would be stabilized and detected by fluorescence microscopy as false positive signals. To avoid incidental eYFP-Atg21 complex formation and therefore false-positive signals, N-YN could be fused to a protein with a defined localization that does not interact with Atg21. Cells expressing that fusion protein and Atg21 C-YC should be further analyzed by fluorescence microcopy to prove if they could serve as a suitable negative control.

The split-ubiquitin assay and BiFC are quite similar methods. BiFC directly monitors the reassembly of eYFP, whereas split-ubiquitin indirectly evaluates the reassembly of two ubiquitin halves. In the split-ubiquitin assay, the empty vector was used as negative control. Therefore, it has never been tested, if one half of ubiquitin expressed alone led to a false-positive interaction signal as the YN part in BiFC. In the split-ubiquitin approach, even the difference between direct and indirect interaction is clearly detectable and was therefore used as an internal control (see Figure 21+Figure 30). This increases the reliability of the method. Moreover, a potential interaction detected in split-ubiquitin was only taken as a hint and confirmed by further approaches.

Surprisingly, the initial functionality test of the BiFC constructs revealed a slight ApeI maturation defect in *atg8Δ* cells simultaneously expressing both N-YN Atg8 and Atg21 C-YC (see Figure 26 D). In contrast, N-YN Atg8 alone complemented the ApeI maturation defect of *atg8Δ* cells. Fluorescence microscopy confirmed

the reassembly of the two halves of eYFP to an Atg8-Atg21-eYFP complex (see Figure 26 E). As mentioned above, the assembly of eYFP results in an irreversible formation of the Atg8-Atg21-eYFP complex. These data led to the idea that both proteins would have to dissociate at some point to fulfill their function. It could be possible, that a necessary interaction with further Atg proteins is sterically blocked. PI3P clearance by Ymr1 and therefore dissociation of the autophagic machinery from autophagosomal membranes is required for the maturation of the autophagosome (Cebollero et al., 2012). Furthermore, the Atg8 part present on the outer autophagosomal membrane has to be cleaved off by Atg4 as a prerequisite for the maturation into a fusion-capable autophagosome (Nair et al., 2012; Yu et al., 2012). Nair *et al*. (2010) speculated, that Atg21 and Atg18 might prevent premature cleavage of Atg8 from PE by regulating the access to Atg8. Due to the irreversible assembly of the eYFP-Atg8-Atg21 complex, the dissociation of Atg21, that would otherwise allow Atg4 to cleave its substrate Atg8, could be blocked. Therefore, the outer part of Atg8 could not be cleaved off, resulting in an at least delay of the Cvt vesicle maturation and therefore ApeI maturation. However, since the effect on the ApeI maturation obtained in this study is quite small, this hypothesis should be further analyzed.

In conclusion, a potential interaction of Atg21 and Atg8 was detected in the split-ubiquitin assay. The interaction was also detected in *atg4Δ* and *atg5Δ* cells, where the lipidation of Atg8 is blocked (Figure 25). This pointed to a specific interaction of Atg21 with unlipidated Atg8. Furthermore, recent studies identified WD40 propeller as a new class of ubiquitin binding proteins (Pashkova et al., 2010), supporting an interaction of Atg21 with the ubiquitin-like Atg8. Atg21 is required for efficient lipidation of Atg8 and its recruitment to the PAS by an unknown mechanism (Meiling-Wesse et al., 2004; Stromhaug et al., 2004). The fact that Atg21 interacted with unlipidated Atg8 in the split-ubiquitin assay improves a potential recruitment function for Atg21 in Atg8 lipidation. Nevertheless, as a prerequisite for further functional studies, an interaction of both proteins has to be confirmed by further approaches as pull down or GFP-TRAP®s. Almost all Atg8-interacting proteins contain a specific WXXL motif, called Atg8-interacting motif (AIM). This binding motif is specific for Atg8 homologues, since the side chains of the tryptophan and the lysine within the

AIM bind to hydrophobic pockets in Atg8. These pockets are conserved among all Atg8 homologues but not among other ubiquitin-like proteins (Noda et al., 2010). In addition, Atg8 contains a N-terminal helical domain (NHD) that is absent in ubiquitin. This NHD is required for efficient autophagy, since truncation or deletion of this domain affects autophagy (Nakatogawa et al., 2007). Furthermore, the residues phenylalanine at position 5 and lysine at position 6 within the NHD are essential for binding of at least one interaction partner, Shp1 (Krick et al., 2010). However, it would be interesting to further elucidate, if Atg21 contains an AIM or if the interaction of both proteins is mediated by the NHD as it was shown for interaction with Shp1.

5.7 Interaction studies of Atg21 and Atg16

Atg16 is a small coiled-coil protein, which forms a complex with the Atg12-Atg5 conjugate via non-covalently binding to Atg5. This complex plays a crucial role as an E3-like enzyme in the ubiquitin-like conjugation reaction of Atg8 to PE. Most likely, Atg12 directly binds and activates the E2 enzyme Atg3. Therefore, Atg12-Atg5/Atg16 probably acts as a platform to bring the Atg8-carrying Atg3 into close proximity to the substrate PE (see chapter 2.2.4.4). The Atg12-Atg5 conjugate was shown to accelerate the Atg8-PE conjugation *in vitro*, revealing that Atg16 is dispensable for the E3-like function of the Atg12-Atg5 conjugate (Hanada et al., 2007). *In vitro* Atg5 seems to be able to bind to lipids, but it fails to recruit the Atg12-Atg5 conjugate to the autophagic membranes *in vivo* (Romanov et al., 2012). Consequently, *in vivo* Atg16 is required for the membrane recruitment of the Atg12-Atg5/Atg16 complex. In addition, the lipidation of Atg8 is severely impaired in *atg16Δ* cells, suggesting that the membrane recruitment of the complex by Atg16 is crucial for its E3-like function (Hanada et al., 2007). The Atg16-mediated PAS localization is dependent on Atg14 and therefore on the PAS-specific PI3P pool. But Atg16 does not contain an obvious PI3P binding motif (Cebollero et al., 2012; Matsushita et al., 2007; Suzuki et al., 2001). Therefore, the underlying mechanism for Atg16 mediated membrane association remains elusive.

The Atg12-Atg5/Atg16 complex is only transiently located at the PAS. For detection via fluorescence microscopy, its PAS localization has to be enriched by

gene deletions that affect the autophagic flux (Stromhaug et al., 2004). Stromhaug *et al*. (2004) showed, that the PAS localization of Atg5-YFP in such an Atg8 deletion strain is prevented by the additional loss of Atg21 under growing conditions. In addition, it was reported previously, that the perivacuolar puncta formation of Atg16-GFP was significantly decreased in *atg18Δ atg21Δ* cells under starvation conditions (Nair et al., 2010). In this study, growing *atg8Δ* cells and *atg8Δ atg21Δ* cells expressing Atg16-GFP and ApeI-RFP were analyzed using direct fluorescence microscopy to test, if Atg21 had also an influence on the Atg16 PAS localization under growth conditions (see Figure 31), since Atg21 is required for the Cvt pathway. Indeed, the absence of Atg21 led to a significant reduction in the Atg16-GFP PAS rate, that was comparable to the reduction in the Atg5-YFP PAS rate. These results suggest that the Atg16 PAS localization is also dependent on Atg21 under growing conditions (see Figure 31). Furthermore, mCherry-Atg21 colocalized with both Atg16-GFP and Atg5-YFP. All of the Atg16-GFP dots and almost all of the Atg5-YFP dots colocalized with the PAS marker ApeI-RFP under those conditions, suggesting that their colocalization with mCherry-Atg21 occured at the PAS (see Figure 32). The colocalization of mCherry-Atg21 and Atg5-YFP was abolished in the absence of Atg16, whereas the colocalization of mCherry-Atg21 and Atg16-GFP was independent on the absence of Atg5. Taken together, the PAS localization of Atg5 depends on both, Atg21 and Atg16 as reported before (Suzuki et al., 2001; Stromhaug et al., 2004), whereas the presence of Atg16 at the PAS depends on Atg21. These data suggests that Atg21 mediates the membrane association of the Atg12-Atg5/Atg16 complex under growing conditions. In this study, it was already shown, that part of Atg21 localizes to the PAS by binding to PI3P (see chapter 5.1). Therefore, the recruitment of the Atg12-Atg5/Atg16 complex to the PAS mediated by binding of Atg16 to Atg21 would explain both, the dependence on Atg21 and on Atg14 respectively the PAS-specific PI3P pool for proper Atg12-Atg5/Atg16 complex localization. Therefore, a potential interaction of Atg21 and Atg16 was analyzed via additional approaches. Pull down experiments using purified recombinant 6xHis-SUMO-Atg21 incubated with yeast crude cell extract further supported an interaction of Atg21 and Atg16. In this approach, 6xHis-SUMO-Atg21, but not 6xSUMO alone, specifically co-precipitated Atg16-HA (see

Figure 33 B). Furthermore, Atg16-HA specifically bound to GFP-Atg21 but not to GFP alone in GFP-TRAP®s (see Figure 33 C). Within the E3-like complex Atg12 interacts with the E2 enzyme Atg3 (Noda et al., 2012). In this study, a potential interaction of Atg21 and Atg8 was already shown. Therefore, it could be possible, that Atg16 is co-precipitated via the bridging protein Atg8. That possibility was excluded in a GFP-TRAP® performed with the crude cell extract of *atg8Δ* cells. Atg16-HA still specifically interacted with GFP-Atg21, supporting a direct interaction (see Figure 33 C). The split-ubiquitin assay detected an interaction of Atg21 with Atg16 (see Figure 30). In contrast, Atg21 interacted neither with Atg5 nor Atg12, supporting an exclusive binding to Atg16. Finally, direct pull down experiments using recombinant proteins were performed to confirm a direct interaction of both proteins. Indeed, purified GST-Atg16 bound specifically to purified 6xHis-SUMO-Atg21, whereas GST alone did not (see Figure 33 D). Taken together, Atg16 most likely binds directly to Atg21.

Atg16 consists of a N-terminal Atg5 binding region that is followed by a short linker region and a C-terminal coiled-coil domain (Fujioka et al., 2010) (see Figure 34 A). Analysis of truncated versions of Atg16 revealed in pull down and GFP-TRAP®s that the coiled-coil domain of Atg16 is required for the interaction with Atg21 (see Figure 34 C). In GFP-TRAP®s, both Atg16 lacking the Atg5-binding region (Atg16$^{58-150}$-HA) or the extreme C-terminus (Atg16$^{1-119}$-HA), that is not required for the coiled-coil formation, still bound to GFP-Atg21. Atg16$^{1-57}$-HA was rather unstable and therefore hardly detectable on the immunoblot. However, even overexposed, no bound Atg16$^{1-57}$-HA could be detected. These results suggest a specific Atg21 binding region within the coiled-coil domain of Atg16. Pull down experiments in principle supported those findings (see Figure 34 B). In contrast to Atg16$^{1-119}$-HA in the GFP-TRAP®s, GST-Atg16$^{1-119}$ did not bind to 6xHis-SUMO-Atg21. It cannot be excluded, that the coiled-coil domain might be longer than proposed (Fujioka et al., 2010). Therefore, the heterologous expression of GST-Atg16$^{1-119}$ in *E. coli* might lead to an incorrect folding of the protein fragment. However, the direct interaction of Atg16 and Atg21 is probably mediated by a region in the C-terminal coiled-coil domain of Atg16.

The coiled-coil domain is crucial for dimerization respectively formation of the Atg12-Atg5/Atg16 complex and is therefore required for its autophagic function

(Kuma et al., 2002). Moreover, Fujioka *et al.* (2010) identified conserved surface residues within the coiled-coil domain of Atg16, that are dispensable for the formation of the coiled-coil structure, but are strictly required for the Cvt pathway and macroautophagy under both growing and starvation conditions. As mentioned before, the PAS recruitment of the Atg12-Atg5/Atg16 complex is a prerequisite for its E3-like function in autophagy (Hanada et al., 2007). Results from this study propose that the PAS recruitment of the complex is probably mediated by binding of Atg21 to the coiled-coil domain of Atg16. Therefore, the conserved residues in the coiled-coil domain of Atg16 that are crucial for autophagy, could mediate the interaction with Atg21. Two conserved Atg16 residues, the aspartic acid at position 101 (D101) and the glutamic acid at position 102 (E102) were mutated either alone or in concert to alanine and the interaction with Atg21 was tested (see Figure 36). Indeed, both amino acid substitutions severely affected the interaction with GFP-Atg21 in GFP-TRAP®s. Interestingly, the interaction of Atg16^{E102A}-HA with GFP-Atg21 was significantly reduced, whereas the binding of Atg16^{D101A}-HA and Atg16^{D101A_E102A}-HA was completely abolished, suggesting a stricter requirement of amino acid D101 for the interaction with Atg21. Consequently, Atg21-binding deficient Atg16-GFP mutants were not longer able to localize to the PAS and were completely cytosolic in fluorescence microscopy (see Figure 35). Interestingly, only Atg16^{E102A}-GFP showed a rare and very faint perivacuolar dot in the same cells, supporting a stricter requirement of D101 for the Atg21 interaction than E102. The possibility, that the mutations of these amino acids disturb the structure of the Atg16 coiled-coil domain leading to a misfolded protein unable to bind Atg21, could be excluded for two reasons. First, the coiled-coil domain of Atg16 mediates dimerization of Atg16 and the ability of the Atg16 mutants to dimerize was verified in GFP-TRAP®s (see Figure 36 B). Second, Fujioka *et al.* (2010) used the Atg16^{D101A_E102A} mutant to crystalize the coiled-coil domain of Atg16. This would have been impossible with mutations in Atg16 that affect the coiled-coil formation.

Taken together, the conserved surface residues E102 and more important D101 in the coiled-coil domain of Atg16 mediate the interaction with Atg21. Mutations of these residues disturb the binding to Atg21 and result in a severe Cvt pathway

and autophagy defect (this study,(Fujioka et al., 2010)), indicating that the interaction with Atg21 is needed for the autophagic function of Atg16. In detail, the autophagic function of Atg16 is represented by its role in the E3-like Atg12-Atg5/Atg16 complex during lipidation of Atg8. Therefore, the ability of the E3 complex containing the Atg21-binding deficient Atg16 mutants to efficiently conjugate Atg8 to PE was tested under growing conditions (see Figure 37). Indeed, the lipidation of Atg8 was significantly retarded in *atg16Δ* cells expressing the Atg21-binding defective mutants (Atg16^{D101A}-HA, Atg16^{E102A}-HA or Atg16^{D101A_E102A}-HA). The retardation is comparable to *atg21Δ* or *atg16Δ* cells. It can be excluded, that the HA-tag influenced the functionality of Atg16-HA, since the Atg16 wild type construct fully complemented both the ApeI maturation and Atg8 lipidation defect in *atg16Δ* cells. Consequently, the Atg21-binding deficient Atg16 mutants showed an additional ApeI maturation defect as previously described by Fujioka *et al.* (2010). Interestingly, D101A had a stronger effect on the ApeI maturation as E102A, supporting a stronger requirement for the interaction with Atg21. In contrast to the GFP-TRAP® results, the double mutation D101A_E102A exhibited the strongest effect and caused a complete block in ApeI maturation. This further supports that both amino acids contribute to the interaction with Atg21 *in vivo*.

Atg8 lipidation and ApeI maturation were also tested in *atg16Δ* cells expressing the truncated versions of Atg16 (see Figure 37). Atg8 lipidation and ApeI maturation was abolished in cells expressing Atg16$^{1-57}$-HA, most likely because this construct was not stable in yeast cells resulting in an *atg16Δ* phenotype. Furthermore, Atg8 lipidation was impaired in *atg16Δ* cells expressing Atg16$^{58-150}$-HA. This truncated Atg16 version is still able to bind to Atg21 as seen in GFP-TRAP®s, but the Atg5-binding domain is lacking. Therefore, the E3-like Atg12-Atg5/Atg16 complex could not be formed resulting in an Atg8 lipidation and ApeI maturation defect. *atg16Δ* cells expressing Atg16$^{1-119}$-HA exhibited an ApeI maturation defect as described before (Fujioka et al., 2010). Interestingly, those cells additionally showed an impaired Atg8 lipidation. This construct is able to bind to Atg21 as seen in GFP-TRAP®s (see Figure 34) and still contains the Atg5-binding region, suggesting that the extreme C-terminal domain of Atg16

might be involved in Atg8 lipidation and autophagy in a mechanism independent on formation of the Atg12-Atg5/Atg16 complex and binding to Atg21.

Taken together, the interaction of Atg16 and Atg21 mediated by the residues D101 and E102 within the coiled-coil region in Atg16 is required for efficient Atg8 lipidation and therefore efficient ApeI transport.

One of the control mutants Atg16^{K94A}-HA showed an unexpected autophagic activity under Cvt conditions in these studies. Originally, it was reported, that K94 and E97 have no influence on the autophagic activity of Atg16 (Fujioka et al., 2010). Therefore, mutations to alanine of both residues were selected as negative controls. Interestingly, the interaction of Atg16^{K94A}-HA and Atg21 was severely impaired in GFP-TRAP®s, comparable to the defect seen with Atg21 and Atg16^{E102A}-HA (see Figure 36 C). Consequently, as interaction of Atg21 and Atg16 is proposed to be essential for Atg8 lipidation reaction, the formation of Atg8-PE was significantly retarded in *atg16Δ* cells expressing Atg16^{K94A}-HA (see Figure 37). Surprisingly, the ApeI maturation occurred normally in these cells, corresponding to results from Fujioka *et al.* (2010). In addition, the ability of Atg16^{K94A} to dimerize was confirmed by GFP-TRAP®s (see Figure 36 B), excluding a structural defect of the mutant. Taken together, these cells exhibited normal Cvt pathway independent on lipidated Atg8. The lipidation of Atg8 was not completely blocked in these cells (see Figure 37), suggesting that the residual amount of Atg8-PE might be sufficient for Cvt vesicle formation. However, the amount of lipidated Atg8 was comparable to that of other Atg21-binding deficient Atg16 mutants, where ApeI maturation is blocked (see Figure 37). The mechanism that allows ApeI maturation without proper Atg8 lipidation in cells expressing Atg16^{K94A}-HA remains to be elucidated.

Proposed model:

One elementary result of this study represents the detection of Atg21 at the PAS under growing conditions. This is the first time that Atg21 has been detected at the PAS (see Figure 11). The Atg21 PAS localization is dependent on Atg14 and thus on the PAS-specific PI3P pool. Importantly, Atg21 recruits the Atg12-Atg5/Atg16 complex to the PAS via direct interaction with the coiled-coil region of Atg16 (see chapter 4.3.6.4). Thereby the underlying mechanism of PI3P-

dependent plus Atg16-mediated recruitment of the Atg12-Atg5/Atg16 complex to autophagosomal membranes has been elucidated in this study. More importantly, the interaction of Atg21 and Atg16 is not only a prerequisite for the proper PAS localization of the Atg12-Atg5/Atg16 complex but also for its autophagic function (see chapter 5.7). Consequently, interaction of Atg16 and Atg21 is needed for efficient Atg8 lipidation (see Figure 37), providing a reasonable explanation for the proposed function of Atg21 in Atg8 lipidation (Meiling-Wesse et al., 2004; Stromhaug et al., 2004).
Interestingly, also Atg21 and Atg8 probably interact with each other (chapter 5.6). This interaction occurs even if Atg8 is unlipidated. Taken together, these data suggest, that Atg21 not only mediates the membrane association of the E3 enzyme Atg12-Atg5/Atg16, but also acts as a scaffold for the Atg8 lipidation reaction by mediating interaction of activated Atg8 and its E3-enzyme Atg12-Atg5/Atg16. Importantly, this model provides a reasonable explanation for the fundamental role of Atg21 in Cvt vesicle formation.

The Atg12-Atg5/Atg16 complex was proposed to specify the lipidation site of Atg8 via association with Atg8-carrying Atg3 and autophagosomal membranes (Hanada et al., 2007). However, it was unclear how Atg16 mediates the membrane association of the E3-like complex to determine the site of Atg8 lipidation. Regarding the proposed model, Atg21 represents the missing link that mediates PI3P-dependent membrane association of the lipidation machinery by recruiting the activated substrate Atg8 and the E3 enzyme required for the last step of Atg8 lipidation. Thereby, Atg21 might represent the key factor to specify the lipidation site.
In the absence of Atg8, Atg21 and the otherwise hardly detectable Atg12-Atg5/Atg16 complex colocalize at the PAS (see Figure 32), suggesting that the lack of Atg8 leads to the accumulation of both proteins. This would however indicate that Atg8 is lipidated at the PAS. In fact, it is still highly under debate, where the Atg8 lipidation occurs within the cell. Recent studies suggest, that Atg8 lipidation does not only occur at the PAS or the phagophore in response to autophagy-inducing signals but in addition constitutively and non-selectively at other sites in the cell (Nair et al., 2012; Nakatogawa et al., 2012; Yu et al., 2012).

These results have been obtained in a strain lacking Atg4, leading to an artificial situation, where Atg8 cannot be delipidated. Furthermore, a model has been proposed, where Atg4 should subsequently deconjugate the Atg8-PE on inappropriate membranes, but not from the PAS, where it is protected against delipidation. This should maintain a cytoplasmic pool of unlipidated Atg8 that can undergo lipidation and participate in autophagosome formation at the PAS (Nakatogawa et al., 2012). The mechanism that should restrict and regulate Atg4 activity is not known. As mentioned before, Nair *et al.* (2010) speculated that both, Atg18 and Atg21, prevent premature cleavage of Atg8 from PE via regulating the access to Atg8. It remains to be determined, if Atg21 and Atg12-Atg5/Atg16 were involved in the lipidation of Atg8 at another site than the PAS or if they were involved in the protection of Atg8 from cleavage by Atg4 as discussed before (see chapter 5.6). However, results from this study question the proposed model of a ubiquitous Atg8 lipidation within the cell. In the absence of Atg8, the Atg12-Atg5/Atg16 complex was restricted specifically to the PAS and no other site in the cell.

As already mentioned, recent studies revealed that Atg5 alone is capable to bind membranes *in vitro*. Fractionation experiments using different yeast deletion strains supported that Atg5 partially mediates membrane binding also *in vivo* (Romanov et al., 2012). Surprisingly, this membrane binding is inhibited by Atg12 alone, but recovered upon binding of Atg16 to the Atg12-Atg5 conjugate, indicating that Atg16 regulates association of the Atg12-Atg5 conjugate with membranes *in vivo* (Romanov et al., 2012). This study now revealed that the Atg12-Atg5/Atg16 membrane association is mediated via interaction of Atg16 with Atg21 (see chapter 5.7). The formation of the Atg12-Atg5 conjugate seems unaffected in *atg21Δ* cells (Stromhaug et al., 2004). Atg16 and the Atg12-Atg5 conjugate could either form a complex in the cytosol, which is subsequently recruited to the PAS or Atg16 localizes independently to the PAS via binding to Atg21 and subsequently recruits the Atg12-Atg5 conjugate to that site. In the latter case, the binding of Atg21 to Atg16 would have to stimulate its interaction with the Atg12-Atg5 conjugate by an unknown mechanism to preserve the Atg12-Atg5/Atg16 complex formation in the cytosol. In another model, it is also possible, that Atg21 as a WD40 propeller facilitates the Atg12-Atg5/Atg16

complex formation by binding both, Atg16 and the Atg12-Atg5 conjugate. As mentioned above, WD40 propeller were identified to bind to ubiquitin-like proteins (Pashkova et al., 2010). Atg12 contains one (Suzuki et al., 2005), whereas Atg5 exhibits two ubiquitin-like folds (Matsushita et al., 2007). As already shown before, Atg21 probably binds to Atg8, supporting the ability of Atg21 to bind to ubiquitin-like proteins. In contrast, the split-ubiquitin assay detected a specific interaction of Atg21 with Atg16, but neither with Atg12 nor Atg5 (see Figure 30), arguing against a potential additional interaction with Atg5 and/or Atg12. Anyhow, an interaction of Atg21 with Atg5 or Atg12 should be analyzed by further approaches like pull down or GFP-TRAP®s. Furthermore, the formation of the Atg12-Atg5/Atg16 complex can be visualized by gelfiltration chromatography as an approximately 350 kDa complex (Kuma et al., 2002). The complex is most likely dimeric mediated by Atg16 (Fujioka et al., 2010). In the absence of Atg16, the Atg12-Atg5 conjugate remains monomeric and would be easily distinguishable from the Atg12-Atg5/Atg16 complex in gelfiltration chromatography. Therefore, determining the molecular weight range of the Atg12-Atg5 conjugate in *atg21Δ* cells by gelfiltration chromatography, should reveal an influence of Atg21 on the formation of the Atg12-Atg5/Atg16 complex.
Furthermore, the Atg16- and Atg8-interacting site within the WD40 propeller Atg21 should be identified. WD40 propeller are commonly known to serve as a large interaction platform to mediate protein-protein interactions. Mapping of the Atg16- and Atg8-interacting site within Atg21 would elucidate the constitution of the proposed Atg8 lipidation complex. It is possible, that Atg21 recruits additional proteins of the Atg8 conjugation machinery in order to further facilitates the lipidation reaction. A candidate for additional interaction with Atg21 would be at least the E2 enzyme Atg3, which carries the activated Atg8. Atg12 directly binds and most likely activates Atg3 (Hanada et al., 2007; Sakoh-Nakatogawa et al., 2013). Thereby, Atg8 and Atg16 are already indirectly connected via the Atg12-Atg5 conjugate bound to Atg3. It can not be excluded that a simultaneous binding of Atg8 and Atg16 is not possible due to steric hinderance. As mentioned above, Atg5 is able to partially mediate membrane association after initial recruitment of Atg16 to autophagosomal membranes (Romanov et al., 2012). Therefore, it could be speculated, that Atg21 is only

needed for the initial recruitment of the Atg12-Atg5/Atg16 complex to the autophagosomal membranes. Afterwards the complex would be able to remain membrane associated mediated by Atg5 and a simultaneous binding of Atg21 to Atg16 and Atg8 would not be absolutely necessary. However, identification of the Atg16- and Atg8-interacting site within Atg21 should shed light on this question. Chopping Atg21 in pieces, that could be used as Atg21 versions in GFP-TRAP®s or pull downs, is not possible, because of the rigid propeller fold. Alternatively, competition of short Atg21 peptides representing potential binding sites with full length Atg21 in pull down experiments with Atg8 or Atg16 could elucidate the binding site within Atg21.

In this study, the conserved surface residues D101 and E102 within the coiled-coil region of Atg16 were identified to bind Atg21 (see Figure 36). These residues originate from a set of mutants, that Fujioka *et al*. (2010) have tested for a defect in the Cvt pathway and autophagy. In addition to D101 and E102, mutation of the isoleucines at position 104 and 108 (I104 and I108) alone or in concert caused strong defects in both pathways. It would be interesting to test if these residues were additionally required for an interaction with Atg21. Results from this study and observations from Fujioka *et al.* (2010) revealed that the extreme C-terminus of Atg16, that is not required for the coiled-coil formation, might have a crucial but yet unidentified role in autophagy independent of Atg21 (see above). Similarly, it could be possible, that the I104 and I108 have a different role than binding to Atg21. Interaction studies with Atg16 mutants using GFP-TRAP®s or further approaches should shed light on this question.

Atg21 is required for the Cvt pathway. All approaches in this study were therefore performed under growing conditions. Bulk autophagy is also severely affected in the absence of Atg21 under autophagy-inducing conditions, but not completely blocked (Barth et al., 2002; Stromhaug et al., 2004). Similar, Atg21 is required for the PAS recruitment of Atg8 only under growing conditions, but *atg21Δ* cells accumulate unlipidated Atg8 even after 4 h of nitrogen starvation (Stromhaug et al., 2004). The lipidation is not completely blocked, but severely delayed. The amount of Atg8 is highly upregulated under autophagy-inducing conditions, suggesting that the small part of Atg8, that is lipidated in the absence of Atg21, is sufficient to be detected at the PAS and to maintain a particular level

of bulk autophagy. However, the fact that Atg8 lipidation is impaired in the absence of Atg21 even under starvation, suggests that Atg21 is also needed for the recruitment of the Atg12-Atg5/Atg16 complex under those conditions. In contrast, Nair *et al.* (2010) observed perivacuolar Atg16-GFP puncta formation after 4 h starvation in wild type and *atg21Δ* / *atg18Δ* single or *atg21Δ atg18Δ* double deletion cells. Only the simultaneous loss of both Atg18 and Atg21 resulted in a significant reduction in the Atg16-GFP PAS localization (Nair et al., 2010), suggesting that both proteins are required in concert for the Atg12-Atg5/Atg16 recruitment under starvation conditions. However, this finding seems to disagree with the observation that the loss of Atg18 has no effect on the Atg8 recruitment to the PAS or its lipidation, neither under growing nor under starvation conditions (Stromhaug et al., 2004; Suzuki et al., 2007). Further investigation on the specific role of each homologue under both growing and starvation conditions should shed light on these discrepancies.

6 Bibliography

Alemu, E. A., Lamark, T., Torgersen, K. M., Birgisdottir, A. B., Larsen, K. B., et al. (2012). ATG8 family proteins act as scaffolds for assembly of the ULK complex: sequence requirements for LC3-interacting region (LIR) motifs. *Journal of Biological Chemistry* **287**, 39275–39290.

Araki, Y., Ku, W. C., Akioka, M., May, A. I., Hayashi, Y., Arisaka, F., Ishihama, Y. and Ohsumi, Y. (2013). Atg38 is required for autophagy-specific phosphatidylinositol 3-kinase complex integrity. *J Cell Biol* **203**, 299–313.

Baba, M., Takeshige, K., Baba, N. and Ohsumi, Y. (1994). Ultrastructural analysis of the autophagic process in yeast: detection of autophagosomes and their characterization. *J Cell Biol* **124**, 903–913.

Barth, H., Meiling-Wesse, K., Epple, U. D. and Thumm, M. (2001). Autophagy and the cytoplasm to vacuole targeting pathway both require Aut10p. *FEBS Letters* **508**, 23–28.

Barth, H., Meiling-Wesse, K., Epple, U. D. and Thumm, M. (2002). Mai1p is essential for maturation of proaminopeptidase I but not for autophagy. *FEBS Letters* **512**, 173–179.

Baskaran, S., Ragusa, M. J. and Hurley, J. H. (2012). How Atg18 and the WIPIs sense phosphatidylinositol 3-phosphate. *Autophagy* **8**, 1851–1852.

Budovskaya, Y., Stephan, J., Deminoff, S. and Herman, P. (2005). An evolutionary proteomics approach identifies substrates of the cAMP-dependent protein kinase. *Proc Natl Acad Sci U S A* **102**, 13933–13938.

Cebollero, E., der Vaart, van, A., Zhao, M., Rieter, E., Klionsky, D. J., Helms, J. B. and Reggiori, F. (2012). Phosphatidylinositol-3-phosphate clearance plays a key role in autophagosome completion. *Curr Biol* **22**, 1545–1553.

Chang, C.-Y. C. and Huang, W.-P. W. (2007). Atg19 mediates a dual interaction cargo sorting mechanism in selective autophagy. *Mol Biol Cell* **18**, 919–929.

Chen, Y. and Klionsky, D. J. (2011). The regulation of autophagy - unanswered questions. *J Cell Sci* **124**, 161–170.

Cheong, H., Nair, U., Geng, J. and Klionsky, D. J. (2008). The Atg1 kinase complex is involved in the regulation of protein recruitment to initiate sequestering vesicle formation for nonspecific autophagy in Saccharomyces cerevisiae. *Mol Biol Cell* **19**, 668–681.

Chew, L. H., Setiaputra, D., Klionsky, D. J. and Yip, C. K. (2013). Structural characterization of the Saccharomyces cerevisiae autophagy regulatory complex Atg17-Atg31-Atg29. *Autophagy* **9**.

Choi, A. M. K., Ryter, S. W. and Levine, B. (2013). Autophagy in human health and disease. *N. Engl. J. Med.* **368**, 1845–1846.

Dove, S. K., Dong, K., Kobayashi, T., Williams, F. K. and Michell, R. H. (2009). Phosphatidylinositol 3,5-bisphosphate and Fab1p/PIKfyve underPPIn endo-lysosome function. *Biochem J* **419**, 1.

Dove, S., Piper, R., McEwen, R., Yu, J., King, M., Hughes, D., Thuring, J., Holmes, A., Cooke, F., Michell, R., et al. (2004). Svp1p defines a family of phosphatidylinositol 3,5-bisphosphate effectors. *EMBO J* **23**, 1922–1933.

Efe, J., Botelho, R. and Emr, S. (2007). Atg18 regulates organelle morphology and Fab1 kinase activity independent of its membrane recruitment by phosphatidylinositol 3,5-bisphosphate. *Mol Biol Cell* **18**, 4232–4244.

Fujioka, Y., Noda, N. N., Nakatogawa, H., Ohsumi, Y. and Inagaki, F. (2010). Dimeric coiled-coil structure of Saccharomyces cerevisiae Atg16 and its functional significance in autophagy. *Journal of Biological Chemistry* **285**, 1508–1515.

Fujita, N., Itoh, T., Omori, H., Fukuda, M., Noda, T. and Yoshimori, T. (2008). The Atg16L complex specifies the site of LC3 lipidation for membrane biogenesis in autophagy. *Mol Biol Cell* **19**, 2092–2100.

Geng, J., Baba, M., Nair, U. and Klionsky, D. J. (2008). Quantitative analysis of autophagy-related protein stoichiometry by fluorescence microscopy. *J Cell Biol* **182**, 129–140.

Gillooly, D. J., Morrow, I. C., Lindsay, M., Gould, R., Bryant, N. J., Gaullier, J. M., Parton, R. G. and Stenmark, H. (2000). Localization of phosphatidylinositol 3-phosphate in yeast and mammalian cells. *EMBO J* **19**, 4577–4588.

Goffeau, A., Barrell, B., Bussey, H., Davis, R., Dujon, B., Feldmann, H., Galibert, F., Hoheisel, J., Jacq, C., Johnston, M., et al. (1996). Life with 6000 Genes. *Science* 1–7.

Guan, J., Stromhaug, P., George, M., Habibzadegah-Tari, P., Bevan, A., Dunn, W. and Klionsky, D. (2001). Cvt18/Gsa12 is required for cytoplasm-to-vacuole transport, pexophagy, and autophagy in Saccharomyces cerevisiae and Pichia pastoris. *Mol Biol Cell* **12**, 3821–3838.

Hanada, T., Noda, N. N., Satomi, Y., Ichimura, Y., Fujioka, Y., Takao, T., Inagaki, F. and Ohsumi, Y. (2007). The Atg12-Atg5 conjugate has a novel E3-like activity for protein lipidation in autophagy. *J Biol Chem* **282**, 37298–37302.

Hanahan, D. (1983). Studies on Transformation of *Escherichia coli* with Plasmids. *J Mol Biol* **166**, 557–580.

Harding, T., Morano, K., Scott, S. and Klionsky, D. (1995). Isolation and characterization of yeast mutants in the cytoplasm to vacuole protein targeting pathway. *J Cell Biol* **131**, 591–602.

He, C. and Klionsky, D. J. (2009). Regulation mechanisms and signaling pathways of autophagy. *Annu Rev Genet* **43**, 67–93.

He, C., Song, H., Yorimitsu, T., Monastyrska, I., Yen, W.-L., Legakis, J. E. and Klionsky, D. J. (2006). Recruitment of Atg9 to the preautophagosomal structure by Atg11 is essential for selective autophagy in budding yeast. *J Cell Biol* **175**, 925–935.

Ho, H., Ogawa, M., Kapadia, R., Yoshikawa, Y., Al-Tahan, S., Kobayashi, T., Ahmad, S., Mimuro, H., Ganesan, A. K., Fukumatsu, M., et al. (2011). WIPI1 coordinates melanogenic gene transcription and melanosome formation via TORC1 inhibition. *Journal of Biological Chemistry* **286**, 12509–12523.

Huang, W. P., Scott, S. V., Kim, J. and Klionsky, D. J. (2000). The itinerary of a vesicle component, Aut7p/Cvt5p, terminates in the yeast vacuole via the autophagy/Cvt pathways. *J Biol Chem* **275**, 5845–5851.

Hutchins, M. and Klionsky, D. (2001). Vacuolar localization of oligomeric alpha-mannosidase requires the cytoplasm to vacuole targeting and autophagy pathway components in Saccharomyces cerevisiae. *J Biol Chem* **276**, 20491–20498.

Ichimura, Y., Kirisako, T., Takao, T., Satomi, Y., Shimonishi, Y., Ishihara, N., Mizushima, N.,

Tanida, I., Kominami, E., Ohsumi, M., et al. (2000). A ubiquitin-like system mediates protein lipidation. *Nature* **408**, 488–492.

Inoue, Y. and Klionsky, D. J. (2010). Regulation of macroautophagy in Saccharomyces cerevisiae. *Semin Cell Dev Biol* **21**, 664–670.

Ishihara, N., Hamasaki, M., Yokota, S., Suzuki, K., Kamada, Y., Kihara, A., Yoshimori, T., Noda, T. and Ohsumi, Y. (2001). Autophagosome requires specific early Sec proteins for its formation and NSF/SNARE for vacuolar fusion. *Mol Biol Cell* **12**, 3690–3702.

Itakura, E. and Mizushima, N. (2010). Characterization of autophagosome formation site by a hierarchical analysis of mammalian Atg proteins. *Autophagy* **6**, 764–776.

Janke, C., Magiera, M., Rathfelder, N., Taxis, C., Reber, S., Maekawa, H., Moreno-Borchart, A., Doenges, G., Schwob, E., Schiebel, E., et al. (2004). A versatile toolbox for PCR-based tagging of yeast genes: new fluorescent proteins, more markers and promoter substitution cassettes. *Yeast* **21**, 947–962.

Jao, C. C., Ragusa, M. J., Stanley, R. E. and Hurley, J. H. (2013). A HORMA domain in Atg13 mediates PI 3-kinase recruitment in autophagy. *Proc Natl Acad Sci U S A* **110**, 5486–5491.

Jeffries, T., Dove, S., Michell, R. and Parker, P. (2004). PtdIns-specific MPR pathway association of a novel WD40 repeat protein, WIPI49. *Mol Biol Cell* **15**, 2652–2663.

Jin, N., Chow, C. Y., Liu, L., Zolov, S. N., Bronson, R., Davisson, M., Petersen, J. L., Zhang, Y., Park, S., Duex, J. E., et al. (2008). VAC14 nucleates a protein complex essential for the acute interconversion of PI3P and PI(3,5)P(2) in yeast and mouse. *EMBO J* **27**, 3221–3234.

Kabeya, Y., Mizushima, N., Ueno, T., Yamamoto, A., Kirisako, T., Noda, T., Kominami, E., Ohsumi, Y. and Yoshimori, T. (2000). LC3, a mammalian homologue of yeast Apg8p, is localized in autophagosome membranes after processing. *EMBO J* **19**, 5720–5728.

Kabeya, Y., Noda, N. N., Fujioka, Y., Suzuki, K., Inagaki, F. and Ohsumi, Y. (2009). Characterization of the Atg17-Atg29-Atg31 complex specifically required for starvation-induced autophagy in Saccharomyces cerevisiae. *Biochem Biophys Res Commun* **389**, 612–615.

Kakuta, S., Yamamoto, H., Negishi, L., Kondo-Kakuta, C., Hayashi, N. and Ohsumi, Y. (2012). Atg9 vesicles recruit vesicle-tethering proteins Trs85 and Ypt1 to the autophagosome formation site. *Journal of Biological Chemistry* **287**, 44261–44269.

Kamada, Y., Funakoshi, T., Shintani, T., Nagano, K., Ohsumi, M. and Ohsumi, Y. (2000). Tor-mediated induction of autophagy via an Apg1 protein kinase complex. *J Cell Biol* **150**, 1507–1513.

Kamada, Y., Yoshino, K. I., Kondo, C., Kawamata, T., Oshiro, N., Yonezawa, K. and Ohsumi, Y. (2010). Tor Directly Controls the Atg1 Kinase Complex To Regulate Autophagy. *Mol Cell Biol* **30**, 1049–1058.

Kawamata, T., Kamada, Y., Kabeya, Y., Sekito, T. and Ohsumi, Y. (2008). Organization of the pre-autophagosomal structure responsible for autophagosome formation. *Mol Biol Cell* **19**, 2039–2050.

Kihara, A., Noda, T., Ishihara, N. and Ohsumi, Y. (2001). Two Distinct Vps34 Phosphatidylinositol 3-Kinase Complexes Function in Autophagy and Carboxypeptidase Y Sorting in Saccharomyces cerevisiae. *J Cell Biol* **152**, 519–530.

Kim, J. and Klionsky, D. (2000). Autophagy, cytoplasm-to-vacuole targeting pathway, and pexophagy in yeast and mammalian cells. *Annu Rev Biochem* **69**, 303–342.

Kim, J., Dalton, V., Eggerton, K., Scott, S. and Klionsky, D. (1999). Apg7p/Cvt2p is required for the cytoplasm-to-vacuole targeting, macroautophagy, and peroxisome degradation pathways. *Mol Biol Cell* **10**, 1337–1351.

Kirisako, T., Baba, M., Ishihara, N., Miyazawa, K., Ohsumi, M., Yoshimori, T., Noda, T. and Ohsumi, Y. (1999). Formation process of autophagosome is traced with Apg8/Aut7p in yeast. *J Cell Biol* **147**, 435–446.

Kirisako, T., Ichimura, Y., Okada, H., Kabeya, Y., Mizushima, N., Yoshimori, T., Ohsumi, M., Takao, T., Noda, T. and Ohsumi, Y. (2000). The reversible modification regulates the membrane-binding state of Apg8/Aut7 essential for autophagy and the cytoplasm to vacuole targeting pathway. *J Cell Biol* **151**, 263–276.

Klionsky, D. J., Cregg, J. M., Dunn, W. A., Emr, S. D., Sakai, Y., Sandoval, I. V., Sibirny, A., Subramani, S., Thumm, M., Veenhuis, M., et al. (2003). A unified nomenclature for yeast autophagy-related genes. *Developmental Cell* **5**, 539–545.

Klionsky, D., Cueva, R. and Yaver, D. (1992). Aminopeptidase I of Saccharomyces cerevisiae is localized to the vacuole independent of the secretory pathway. *J Cell Biol* **119**, 287–299.

Knop, M., Siegers, K., Pereira, G., Zachariae, W., Winsor, B., Nasmyth, K. and Schiebel, E. (1999). Epitope tagging of yeast genes using a PCR-based strategy: more tags and improved practical routines. *Yeast* **15**, 963–972.

Kraft, C., Kijanska, M., Kalie, E., Siergiejuk, E., Lee, S. S., Semplicio, G., Stoffel, I., Brezovich, A., Verma, M., Hansmann, I., et al. (2012). Binding of the Atg1/ULK1 kinase to the ubiquitin-like protein Atg8 regulates autophagy. *EMBO J* **31**, 3691–3703.

Krick, R., Bremer, S., Welter, E., Schlotterhose, P., Muehe, Y., Eskelinen, E.-L. and Thumm, M. (2010). Cdc48/p97 and Shp1/p47 regulate autophagosome biogenesis in concert with ubiquitin-like Atg8. *J Cell Biol* **190**, 965–973.

Krick, R., Busse, R. A., Scacioc, A., Stephan, M., Janshoff, A., Thumm, M. and Kühnel, K. (2012). Structural and functional characterization of the two phosphoinositide binding sites of PROPPINs, a β-propeller protein family. *Proc Natl Acad Sci U S A* **109**, E2042–9.

Krick, R., Henke, S., Tolstrup, J. and Thumm, M. (2008a). Dissecting the localization and function of Atg18, Atg21 and Ygr223c. *Autophagy* **4**, 896–910.

Krick, R., Muehe, Y., Prick, T., Bremer, S., Schlotterhose, P., Eskelinen, E.-L., Millen, J., Goldfarb, D. S. and Thumm, M. (2008b). Piecemeal microautophagy of the nucleus requires the core macroautophagy genes. *Mol Biol Cell* **19**, 4492–4505.

Krick, R., Tolstrup, J., Appelles, A., Henke, S. and Thumm, M. (2006). The relevance of the phosphatidylinositolphosphat-binding motif FRRGT of Atg18 and Atg21 for the Cvt pathway and autophagy. *FEBS Letters* **580**, 4632–4638.

Kuma, A., Mizushima, N., Ishihara, N. and Ohsumi, Y. (2002). Formation of the approximately 350-kDa Apg12-Apg5.Apg16 multimeric complex, mediated by Apg16 oligomerization, is essential for autophagy in yeast. *J Biol Chem* **277**, 18619–18625.

Kvam, E. and Goldfarb, D. (2007). Nucleus-vacuole junctions and piecemeal microautophagy of the nucleus in S. cerevisiae. *Autophagy* **3**, 85–92.

Laemmli, U.K. (1970). Cleavage of structural proteins during the assembly of the head of bacteriophage T4. *Nature* **227**, 680-685.

Lang, T., Schaeffeler, E., Bernreuther, D., Bredschneider, M., Wolf, D. H. and Thumm, M. (1998). Aut2p and Aut7p, two novel microtubule-associated proteins are essential for

delivery of autophagic vesicles to the vacuole. *EMBO J* **17**, 3597–3607.

Laser, H., Bongards, C., Schuller, J., Heck, S., Johnsson, N. and Lehming, N. (2000). A new screen for protein interactions reveals that the Saccharomyces cerevisiae high mobility group proteins Nhp6A/B are involved in the regulation of the GAL1 promoter. *Proc Natl Acad Sci U S A* **97**, 13732–13737.

Legakis, J. E., Yen, W.-L. and Klionsky, D. J. (2007). A cycling protein complex required for selective autophagy. *Autophagy* **3**, 422–432.

Lipatova, Z., Belogortseva, N., Zhang, X. Q., Kim, J., Taussig, D. and Segev, N. (2012). Regulation of selective autophagy onset by a Ypt/Rab GTPase module. *Proc Natl Acad Sci U S A* **109**, 6981–6986.

Loewith, R. and Hall, M. N. (2011). Target of Rapamycin (TOR) in Nutrient Signaling and Growth Control. *Genetics* **189**, 1177–1201.

Longtine, M., McKenzie, A., Demarini, D., Shah, N., Wach, A., Brachat, A., Philippsen, P. and Pringle, J. (1998). Additional modules for versatile and economical PCR-based gene deletion and modification in Saccharomyces cerevisiae. *Yeast* **14**, 953–961.

Lynch-Day, M. A. and Klionsky, D. J. (2010). The Cvt pathway as a model for selective autophagy. *FEBS Letters* **584**, 1359–1366.

Lynch-Day, M. A., Bhandari, D., Menon, S., Huang, J., Cai, H., Bartholomew, C. R., Brumell, J. H., Ferro-Novick, S. and Klionsky, D. J. (2010). Trs85 directs a Ypt1 GEF, TRAPPIII, to the phagophore to promote autophagy. *Proc Natl Acad Sci U S A* **107**, 7811–7816.

Mari, M., Griffith, J., Rieter, E., Krishnappa, L., Klionsky, D. J. and Reggiori, F. (2010). An Atg9-containing compartment that functions in the early steps of autophagosome biogenesis. *J Cell Biol* **190**, 1005–1022.

Matsushita, M., Suzuki, N. N., Obara, K., Fujioka, Y., Ohsumi, Y. and Inagaki, F. (2007). Structure of Atg5.Atg16, a complex essential for autophagy. *J Biol Chem* **282**, 6763–6772.

Matsuura, A., Tsukada, M., Wada, Y. and Ohsumi, Y. (1997). Apg1p, a novel protein kinase required for the autophagic process in Saccharomyces cerevisiae. *Gene* **192**, 245–250.

Meijer, W. H., der Klei, van, I. J., Veenhuis, M. and Kiel, J. A. K. W. (2007). ATG genes involved in non-selective autophagy are conserved from yeast to man, but the selective Cvt and pexophagy pathways also require organism-specific genes. *Autophagy* **3**, 106–116.

Meiling-Wesse, K., Barth, H., Voss, C., Eskelinen, E.-L., Epple, U. D. and Thumm, M. (2004). Atg21 is required for effective recruitment of Atg8 to the preautophagosomal structure during the Cvt pathway. *J Biol Chem* **279**, 37741–37750.

Michell, R. H. and Dove, S. K. (2009). A protein complex that regulates PtdIns(3,5)P2 levels. *EMBO J* **28**, 86–87.

Michell, R. H., Heath, V. L., Lemmon, M. A. and Dove, S. K. (2006). Phosphatidylinositol 3,5-bisphosphate: metabolism and cellular functions. *Trends Biochem Sci* **31**, 52–63.

Mijaljica, D., Nazarko, T. Y., Brumell, J. H., Huang, W.-P., Komatsu, M., Prescott, M., Simonsen, A., Yamamoto, A., Zhang, H., Klionsky, D. J., et al. (2012). Receptor protein complexes are in control of autophagy. *Autophagy* **8**.

Mizushima, N., Noda, T. and Ohsumi, Y. (1999). Apg16p is required for the function of the Apg12p-Apg5p conjugate in the yeast autophagy pathway. *EMBO J* **18**, 3888–3896.

Mizushima, N., Noda, T., Yoshimori, T., Tanaka, Y., Ishii, T., George, M. D., Klionsky, D. J., Ohsumi, M. and Ohsumi, Y. (1998). A protein conjugation system essential for autophagy. *Nature* **395**, 395–398.

Mizushima, N., Yamamoto, A., Hatano, M., Kobayashi, Y., Kabeya, Y., Suzuki, K., Tokuhisa, T., Ohsumi, Y. and Yoshimori, T. (2001). Dissection of autophagosome formation using Apg5-deficient mouse embryonic stem cells. *J Cell Biol* **152**, 657–68.

Morales Quinones, M., Winston, J. T. and Stromhaug, P. E. (2012). Propeptide of Aminopeptidase 1 Protein Mediates Aggregation and Vesicle Formation in Cytoplasm-to-Vacuole Targeting Pathway. *Journal of Biological Chemistry* **287**, 10121–10133.

Motley, A. M., Nuttall, J. M. and Hettema, E. H. (2012). Pex3-anchored Atg36 tags peroxisomes for degradation in Saccharomyces cerevisiae. *EMBO J* **31**, 2852–2868.

Mülhardt, Cornel: Der Experimentator Molekularbiologie/Genomics; 5. Auflage, München 2006, Seite 136

Mumberg, D., Muller, R. and Funk, M. (1995). Yeast vectors for the controlled expression of heterologous proteins in different genetic backgrounds. *Gene* **156**, 119–122.

Müller, J. and Johnsson, N. (2008). Split-ubiquitin and the split-protein sensors: chessman for the endgame. *ChemBioChem* **9**, 2029–2038.

Nair, U., Cao, Y., Xie, Z. and Klionsky, D. J. (2010). Roles of the lipid-binding motifs of Atg18 and Atg21 in the cytoplasm to vacuole targeting pathway and autophagy. *Journal of Biological Chemistry* **285**, 11476–11488.

Nair, U., Yen, W.-L., Mari, M., Cao, Y., Xie, Z., Baba, M., Reggiori, F. and Klionsky, D. J. (2012). A role for Atg8–PE deconjugation in autophagosome biogenesis. *Autophagy* **8**, 780–793.

Nakatogawa, H. (2013). Two ubiquitin-like conjugation systems that mediate membrane formation during autophagy. *Essays Biochem.* **55**, 39–50.

Nakatogawa, H., Ichimura, Y. and Ohsumi, Y. (2007). Atg8, a ubiquitin-like protein required for autophagosome formation, mediates membrane tethering and hemifusion. *Cell* **130**, 165–178.

Nakatogawa, H., Ishii, J., Asai, E. and Ohsumi, Y. (2012). Atg4 recycles inappropriately lipidated Atg8 to promote autophagosome biogenesis. *Autophagy* **8**, 177–186.

Noda, N. N., Fujioka, Y., Hanada, T., Ohsumi, Y. and Inagaki, F. (2012). Structure of the Atg12-Atg5 conjugate reveals a platform for stimulating Atg8-PE conjugation. *EMBO Rep*.

Noda, N. N., Kumeta, H., Nakatogawa, H., Satoo, K., Adachi, W., Ishii, J., Fujioka, Y., Ohsumi, Y. and Inagaki, F. (2008). Structural basis of target recognition by Atg8/LC3 during selective autophagy. *Genes Cells* **13**, 1211–1218.

Noda, N. N., Ohsumi, Y. and Inagaki, F. (2009). ATG systems from the protein structural point of view. *Chem. Rev.* **109**, 1587–1598.

Noda, N. N., Ohsumi, Y. and Inagaki, F. (2010). Atg8-family interacting motif crucial for selective autophagy. *FEBS Letters* **584**, 1379–1385.

Obara, K. and Ohsumi, Y. (2008). Dynamics and function of PtdIns(3)P in autophagy. *Autophagy* **4**, 952–954.

Obara, K., Noda, T., Niimi, K. and Ohsumi, Y. (2008a). Transport of phosphatidylinositol 3-phosphate into the vacuole via autophagic membranes in Saccharomyces cerevisiae. *Genes*

Cells **13**, 537–547.

Obara, K. and Ohsumi, Y. (2011). Atg14: a key player in orchestrating autophagy. *International Journal of Cell Biology* **2011**, 713435.

Obara, K., Sekito, T. and Ohsumi, Y. (2006). Assortment of phosphatidylinositol 3-kinase complexes--Atg14p directs association of complex I to the pre-autophagosomal structure in Saccharomyces cerevisiae. *Mol Biol Cell* **17**, 1527–1539.

Obara, K., Sekito, T., Niimi, K. and Ohsumi, Y. (2008b). The Atg18-Atg2 complex is recruited to autophagic membranes via phosphatidylinositol 3-phosphate and exerts an essential function. *J Biol Chem* **283**, 23972–23980.

Ohashi, Y. and Munro, S. (2010). Membrane delivery to the yeast autophagosome from the Golgi-endosomal system. *Mol Biol Cell* **21**, 3998–4008.

Pan, X., Roberts, P., Chen, Y., Kvam, E., Shulga, N., Huang, K., Lemmon, S. and Goldfarb, D. (2000). Nucleus-vacuole junctions in Saccharomyces cerevisiae are formed through the direct interaction of Vac8p with Nvj1p. *Mol Biol Cell* **11**, 2445–2457.

Parzych, K. R. and Klionsky, D. (2013). An overview of autophagy: Morphology, mechanism and regulation. *Antioxid Redox Signal*.

Pashkova, N., Gakhar, L., Winistorfer, S. C., Yu, L., Ramaswamy, S. and Piper, R. C. (2010). WD40 repeat propellers define a ubiquitin-binding domain that regulates turnover of F box proteins. *Mol Cell* **40**, 433–443.

Polson, H. E. J., De Lartigue, J., Rigden, D. J., Reedijk, M., Urbé, S., Clague, M. J. and Tooze, S. A. (2010). Mammalian Atg18 (WIPI2) localizes to omegasome-anchored phagophores and positively regulates LC3 lipidation. *Autophagy* **6**.

Proikas-Cezanne, T. and Robenek, H. (2011). Freeze-fracture replica immunolabelling reveals human WIPI-1 and WIPI-2 as membrane proteins of autophagosomes. *J. Cell. Mol. Med.* **15**, 2007–2010.

Proikas-Cezanne, T., Waddell, S., Gaugel, A., Frickey, T., Lupas, A. and Nordheim, A. (2004). WIPI-1alpha (WIPI49), a member of the novel 7-bladed WIPI protein family, is aberrantly expressed in human cancer and is linked to starvation-induced autophagy. *Oncogene* **23**, 9314–9325.

Ptacek, J., Devgan, G., Michaud, G., Zhu, H., Zhu, X., Fasolo, J., Guo, H., Jona, G., Breitkreutz, A., Sopko, R., et al. (2005). Global analysis of protein phosphorylation in yeast. *Nature* **438**, 679–684.

Ragusa, M. J., Ragusa, M. J., Stanley, R. E., Stanley, R. E., Hurley, J. H. and Hurley, J. H. (2012). Architecture of the Atg17 Complex as a Scaffold for Autophagosome Biogenesis. *Cell*.

Reggiori, F. and Klionsky, D. J. (2013). Autophagic Processes in Yeast: Mechanism, Machinery and Regulation. *Genetics* **194**, 341–361.

Reggiori, F., Tucker, K., Stromhaug, P. and Klionsky, D. (2004). The Atg1-Atg13 complex regulates Atg9 and Atg23 retrieval transport from the pre-autophagosomal structure. *Dev Cell* **6**, 79–90.

Rieter, E., Vinke, F., Bakula, D., Cebollero, E., Ungermann, C., et al. (2013). Atg18 function in autophagy is regulated by specific sites within its β-propeller. *J Cell Sci* **126**, 593–604.

Roberts, P., Moshitch-Moshkovitz, S., Kvam, E., O'Toole, E., Winey, M. and Goldfarb, D. (2003). Piecemeal microautophagy of nucleus in Saccharomyces cerevisiae. *Mol Biol Cell* **14**,

129–141.

Romanov, J., Walczak, M., Ibiricu, I., Schüchner, S., Ogris, E., Kraft, C. and Martens, S. (2012). Mechanism and functions of membrane binding by the Atg5-Atg12/Atg16 complex during autophagosome formation. *EMBO J*.

Sakoh-Nakatogawa, M., Matoba, K., Asai, E., Kirisako, H., Ishii, J., Noda, N. N., Inagaki, F., Nakatogawa, H. and Ohsumi, Y. (2013). Atg12-Atg5 conjugate enhances E2 activity of Atg3 by rearranging its catalytic site. *Nat Struct Mol Biol* **20**, 433–439.

Schlumpberger, M., Schaeffeler, E., Straub, M., Bredschneider, M., Wolf, D. H. and Thumm, M. (1997). AUT1, a gene essential for autophagocytosis in the yeast Saccharomyces cerevisiae. *J Bacteriol* **179**, 1068–1076.

Schu, P., Takegawa, K., Fry, M., Stack, J., Waterfield, M. and Emr, S. (1993). Phosphatidylinositol 3-kinase encoded by yeast VPS34 gene essential for protein sorting. *Science* **260**, 88–91.

Scott, S., Baba, M., Ohsumi, Y. and Klionsky, D. (1997). Aminopeptidase I is targeted to the vacuole by a nonclassical vesicular mechanism. *J Cell Biol* **138**, 37–44.

Scott, S., Guan, J., Hutchins, M., Kim, J. and Klionsky, D. (2001). Cvt19 is a receptor for the cytoplasm-to-vacuole targeting pathway. *Mol Cell* **7**, 1131–1141.

Scott, S., Hefner-Gravink, A., Morano, K., Noda, T., Ohsumi, Y. and Klionsky, D. (1996). Cytoplasm-to-vacuole targeting and autophagy employ the same machinery to deliver proteins to the yeast vacuole. *Proceed. Nat. Acad. Sci. USA* **93**, 12304–12308.

Scott, S., Nice, D., Nau, J., Weisman, L., Kamada, Y., Keizer-Gunnink, I., Funakoshi, T., Veenhuis, M., Ohsumi, Y. and Klionsky, D. (2000). Apg13p and Vac8p are part of a complex of phosphoproteins that are required for cytoplasm to vacuole targeting. *J Biol Chem* **275**, 25840–25849.

Sekito, T., Kawamata, T., Ichikawa, R., Suzuki, K. and Ohsumi, Y. (2009). Atg17 recruits Atg9 to organize the pre-autophagosomal structure. *Genes Cells* **14**, 525–538.

Sheng, Y., Mancino, V. and Birren, B. (2005). Transformation of *Escherichia coli* with large DNA molecules by electroporation. *nucleic acids research* **23**, 1–7.

Shintani, T. and Klionsky, D. J. (2004). Cargo proteins facilitate the formation of transport vesicles in the cytoplasm to vacuole targeting pathway. *J Biol Chem* **279**, 29889–29894.

Shintani, T., Huang, W., Stromhaug, P. and Klionsky, D. (2002). Mechanism of cargo selection in the cytoplasm to vacuole targeting pathway. *Dev Cell* **3**, 825–837.

Shintani, T., Mizushima, N., Ogawa, Y., Matsuura, A., Noda, T. and Ohsumi, Y. (1999). Apg10p, a novel protein-conjugating enzyme essential for autophagy in yeast. *EMBO J* **18**, 5234–5241.

Skarp, K.-P., Zhao, X., Weber, M. and Jantti, J. (2008). Use of bimolecular fluorescence complementation in yeast Saccharomyces cerevisiae. *Methods Mol Biol* **457**, 165–175.

Stanley, R. E., Ragusa, M. J. and Hurley, J. H. (2013). The beginning of the end: how scaffolds nucleate autophagosome biogenesis. *Trends Cell Biol*.

Straub, M., Bredschneider, M. and Thumm, M. (1997). AUT3, a serine/threonine kinase gene, is essential for autophagocytosis in Saccharomyces cerevisiae. *J Bacteriol* **179**, 3875–3883.

Stromhaug, P. E., Reggiori, F., Guan, J., Wang, C.-W. and Klionsky, D. J. (2004). Atg21 is a

phosphoinositide binding protein required for efficient lipidation and localization of Atg8 during uptake of aminopeptidase I by selective autophagy. *Mol Biol Cell* **15**, 3553–3566.

Sugawara, K., Suzuki, N., Fujioka, Y., Mizushima, N., Ohsumi, Y. and Inagaki, F. (2004). The crystal structure of microtubule-associated protein light chain 3, a mammalian homologue of Saccharomyces cerevisiae Atg8. *Genes Cells* **9**, 611–618.

Suzuki, K. (2012). Selective autophagy in budding yeast. *Cell Death Differ* –.

Suzuki, K. and Ohsumi, Y. (2007). Molecular machinery of autophagosome formation in yeast, Saccharomyces cerevisiae. *FEBS Letters* **581**, 2156–2161.

Suzuki, K. and Ohsumi, Y. (2010). Current knowledge of the pre-autophagosomal structure (PAS). *FEBS Letters* **584**, 1280–1286.

Suzuki, K., Akioka, M., Kondo-Kakuta, C., Yamamoto, H. and Ohsumi, Y. (2013). Fine mapping of autophagy-related proteins during autophagosome formation in Saccharomyces cerevisiae. *J Cell Sci* **126**, 2534–2544.

Suzuki, K., Kirisako, T., Kamada, Y., Mizushima, N., Noda, T. and Ohsumi, Y. (2001). The pre-autophagosomal structure organized by concerted functions of APG genes is essential for autophagosome formation. *EMBO J* **20**, 5971–5981.

Suzuki, K., Kubota, Y., Sekito, T. and Ohsumi, Y. (2007). Hierarchy of Atg proteins in pre-autophagosomal structure organization. *Genes Cells* **12**, 209–218.

Suzuki, N. N., Yoshimoto, K., Fujioka, Y., Ohsumi, Y. and Inagaki, F. (2005). The crystal structure of plant ATG12 and its biological implication in autophagy. *Autophagy* **1**, 119–126.

Tamura, N., Oku, M., Ito, M., Noda, N. N., Inagaki, F., et al. (2013). Atg18 phosphoregulation controls organellar dynamics by modulating its phosphoinositide-binding activity. *J Cell Biol* **202**, 685–698.

Tanida, I., Mizushima, N., Kiyooka, M., Ohsumi, M., Ueno, T., Ohsumi, Y. and Kominami, E. (1999). Apg7p/Cvt2p: A novel protein-activating enzyme essential for autophagy. *Mol Biol Cell* **10**, 1367–1379.

Taylor, R., Taylor, R., Chen, P.-H., Chen, P.-H., Chou, C.-C., Chou, C.-C., Patel, J., Patel, J., Jin, S. V. and Jin, S. V. (2012). KCS1 deletion in Saccharomyces cerevisiae leads to a defect in translocation of autophagic proteins and reduces autophagosome formation. *Autophagy* **8**, 19–18.

Thumm, M., Egner, R., Koch, B., Schlumpberger, M., Straub, M., Veenhuis, M. and Wolf, D. H. (1994). Isolation of autophagocytosis mutants of Saccharomyces cerevisiae. *FEBS Letters* **349**, 275–280.

Wach, A., Brachat, A., Alberti-Segui, C., Rebischung, C. and Philippsen, P. (1997). Heterologous HIS3 marker and GFP reporter modules for PCR-targeting in Saccharomyces cerevisiae. *Yeast* **13**, 1065–1075.

Wach, A., Brachat, A., Pohlmann, R. and Philippsen, P. (1994). New heterologous modules for classical or PCR-based gene disruptions in Saccharomyces cerevisiae. *Yeast* **10**, 1793–1808.

Watanabe, Y., Kobayashi, T., Yamamoto, H., Hoshida, H., Akada, R., Inagaki, F., Ohsumi, Y. and Noda, N. N. (2012). Structure-based analyses reveal distinct binding sites for Atg2 and phosphoinositides in Atg18. *Journal of Biological Chemistry* **287**, 31681–31690.

Wittke, S., Lewke, N., Müller, S. and Johnsson, N. (1999). Probing the molecular environment of membrane proteins in vivo. *Mol Biol Cell* **10**, 2519–2530.

Xie, Z., Nair, U. and Klionsky, D. J. (2008). Atg8 controls phagophore expansion during autophagosome formation. *Mol Biol Cell* **19**, 3290–3298.

Xu, C. and Min, J. (2011). Structure and function of WD40 domain proteins. *Protein Cell* **2**, 202–214.

Yamaguchi, M., Noda, N. N., Yamamoto, H., Shima, T., Kumeta, H., Kobashigawa, Y., Akada, R., Ohsumi, Y. and Inagaki, F. (2012). Structural insights into Atg10-mediated formation of the autophagy-essential Atg12-Atg5 conjugate. *Structure* **20**, 1244–1254.

Yamamoto, H., Kakuta, S., Watanabe, T. M., Kitamura, A., Sekito, T., Kondo-Kakuta, C., Ichikawa, R., Kinjo, M. and Ohsumi, Y. (2012). Atg9 vesicles are an important membrane source during early steps of autophagosome formation. *J Cell Biol* **198**, 219–233.

Yen, W.-L. and Klionsky, D. J. (2007). Atg27 is a second transmembrane cycling protein. *Autophagy* **3**, 254–256.

Yen, W.-L., Legakis, J. E., Nair, U. and Klionsky, D. J. (2007). Atg27 is required for autophagy-dependent cycling of Atg9. *Mol Biol Cell* **18**, 581–593.

Yorimitsu, T. and Klionsky, D. (2005). Autophagy: molecular machinery for self-eating. *Cell Death Differ* **12 Suppl 2**, 1542–1552.

Yorimitsu, T., He, C., Wang, K. and Klionsky, D. J. (2009). Tap42-associated protein phosphatase type 2A negatively regulates induction of autophagy. *Autophagy* **5**, 616–624.

Yu, Z.-Q., Ni, T., Hong, B., Wang, H.-Y., Jiang, F.-J., Zou, S., Chen, Y., Zheng, X.-L., Klionsky, D. J., Liang, Y., et al. (2012). Dual roles of Atg8–PE deconjugation by Atg4 in autophagy. *Autophagy* **8**, 877–876.

Yuga, M., Gomi, K., Klionsky, D. J. and Shintani, T. (2011). Aspartyl aminopeptidase is imported from the cytoplasm to the vacuole by selective autophagy in Saccharomyces cerevisiae. *Journal of Biological Chemistry* **286**, 13704–13713.

7 Acknowledgement

Ganz besonders möchte ich Herrn Prof. Michael Thumm für die Bereitstellung dieses interessanten Themas, für die Möglichkeit zur Promotion und für die Unterstützung in sämtlichen Bereichen danken!

Prof. Volka Lipka möchte ich für die Übernahme des Zweitgutachtens danken!

Vielen Dank an alle Mitgliedern meines Thesis Committees: Herrn Prof. Thumm, Herrn Prof. Lipka und Frau Dr. Kühnel für alle wissenschaftlichen Ratschläge und wertvolle Anregungen!

Des Weiteren danke ich der Göttinger Graduate School for Neuroscience, Biophysics and Molecular Biosciences (DFG Grants GSC 226/1, GSC 226/2) für die finanzielle Unterstützung während der gesamten Promotionszeit!

Ein besonderer Dank geht an Rosi, die mir jederzeit unterstützend zur Seite stand. Vielen Dank für die vielen hilfreichen Ratschläge und dein offenes Ohr zu jeder Zeit!

Weiterhin möchte ich Klaus Neiffer für die geduldige Durchführung der zahlreichen Gelfiltrationen danken!

Ganz besonders möchte ich auch der gesamten Arbeitsgruppe Thumm: Petra, Rosi, Peter, Marco und auch der Ehemaligen Evelyn für das humorvolle Laborklima, die vielen netten Gespräche in- und außerhalb des Labors und die tolle Zeit bedanken!

Mein großer Dank geht an meinen Freund Benjamin Voß sowie an meine Familie und Freunde, die jederzeit an mich geglaubt haben und mich stets kräftig unterstützt haben!

Vielen Dank!